UNIVERSITAT DE BARCELONA

Connecting RAGE and cell plasticity in triple-negative breast cancer

Mireia Pujals Pruneda

UNIVERSITAT DE BARCELONA

Tesi doctoral

CONNECTING RAGE AND CELL PLASTICITY IN TRIPLE-NEGATIVE BREAST CANCER

Autora: Mireia Pujals Pruneda

Director: Josep Villanueva Cardús

UNIVERSITAT DE BARCELONA

FACULTAT DE MEDICINA

PROGRAMA DE DOCTORAT EN BIOMEDICINA

2021

CONNECTING RAGE AND CELL PLASTICITY IN TRIPLE-NEGATIVE BREAST CANCER

Memòria presentada per:

Mireia Pujals Pruneda

per optar al grau de Doctora per la Universitat de Barcelona

Tesi realitzada al laboratori de Biomarcadors Tumorals de l'Institut d'Oncologia de la Vall d'Hebron (VHIO)

Dr. Josep Villanueva Cardús	Dra. Neus Agell Jane	Mireia Pujals Pruneda
Director	Tutora	Doctoranda

UNIVERSITAT DE BARCELONA

VHIO VALL D'HEBRON Institute of Oncology

AGRAÏMENTS

Per fi ha arribat el GRAN dia! Però tot això no hagués estat possible sense tota la gent que d'alguna manera o altra heu anat passant per la meva vida durant aquests anys.

Primer de tot m'agradaria donar les gràcies a en Josep per haver confiat en mi i donar-me l'oportunitat de realitzar aquesta tesi. També vull agrair-te tot el recolzament que m'has donat tots aquets anys, i haver estat allà sempre que ho he necessitat.

També vull donar les gràcies a totes les persones que han passat pel laboratori durant aquests anys. Gràcies Olga per tot el que m'has ensenyat des del primer minut, i per la paciència que vas tenir quan tot just acabava de sortir de la carrera. Sense tu possiblement no hagés començat aquest camí, gràcies. Chiara moltíssimes gràcies pel teu suport constant, escoltar els meus problemes i ajudar-me a trobar solucions. Gràcies també per les bones estones que hem passat juntes: les cerveses i els cafès al sol amb en Gabriel, les nostres reunions a cultius, la teva energia positiva i tots els riures que hem compartit. José Ángel no puc estar més agraïda per tot el que m'has ajudat en aquesta última etapa, sobretot amb els nostres amiguets. També per preocupar-te en tot moment dels resultats aportant sempre alguna solució. Gràcies també als que ja no hi sou, però que per mi heu sigut igual d'importants. Mercè mil gràcies pel teus consells ja siguin des de Barcelona, Zurich o Ribes han estat sempre de gran ajuda. Has estat un gran pilar des del començament, i ara al final, tot i la distància, encara m'has donat molt bons consells, merci bonica. Marta gràcies per portar al laboratori l'energia! La teva empenta i motivació ens vam fer passar grans moments. Llàstima que fos breu (i amb el COVID encara més), però ara comença la teva aventura i et desitjo el millor. Candi de tu no m'he oblidat. També has sigut un referent des del primer dia i m'has ensenyat que si lluites per un objectiu es pot aconseguir. Així que ara et queda a tu un gran camí per endavant, molta sort! Ah, i gràcies per tots els viatges amb cotxe i les caravanes compartides,

tot i que ets una gran escapista. Carla, has estat una gran sorpresa d'última hora. Mil gràcies! Perquè tot hi haver viscut intensament aquesta última etapa de la tesi sempre has estat disposada a ajudar-me, i això m'ha salvat d'algun que altre mal de cap.

No voldria deixar-me la Nathalie, en Juan, en Gabriel, la Mireia i l'Ana. Gràcies a tots per haver estat allà quan ho he necessitat, però sobretot pels bons moments compartits, els cafès al sol, els dinars al pícnic, els sopars, les cerveses i els coneixements que m'heu transmès en tot moment.

Per descomptat que fora del laboratori també hi ha molta gent a qui he de donar les gràcies. Emanuela sense tu els *in vivo* no haguessin estat possible, grazie mille! Ets una crack i con tu "fuerza y coraje" sempre ets capaç de trobar temps per tothom. Has estat allà en tot moment per resoldre tots els dubtes i en totes les operacions. Estefania gràcies per ajudar-me en els dubtes, la incerteses, les preocupacions, però sobretot gràcies per les estones viscudes fora del lab. Ah, i no vull pas deixar-me als veïns d'Hemato i la infiltrada! Cristina, Dani, Carlota, Júlia i Carlota gràcies pels riures, el suport, la companyia, les cerveses i els sopars. I gràcies a tots els de la 4a planta i molta altra gent del VHIO que sempre esteu disposats a donar un cop de mà i muntar algun que altre sarau.

I no em podria deixar les meves nenes! Sense elles la vida no seria el mateix, sou la meva segona família. Gràcies per està sempre allà, us estimo. I la resta de la colla, perquè uns sense els altres no seria el mateix. A les nenes de la uni, quina gran època la universitat, que bé ens ho vam passar i quins grans moments viscuts. I ara, tot i que cada una a fet el seu camí, sempre sabem trobar una estona per veure'ns i posar-nos al dia. Judit guapa, quina paciència has tingut tot aquest temps en ajudar-me en les correccions de l'anglès tot i no entendre res del que deia, ets un sol.

I diuen que els amics es trien però la família no, però jo he tingut la sort de tenir la millor! Mama, papa i Laura sense vosaltres no seria qui soc ni estaria on soc ara. Sou un gran suport, i tot i la distància, sempre us sento a prop. Sempre us heu preocupat

per mi, per la investigació (encara que no entengueu del que us parlo...), i quan he tingut dubtes sempre m'heu donat el suport i consells que necessitava. Gràcies també a la resta de la família, avis i avies, tietes, tiets i cosins, que bé ens ho passem quan estem tots junts, sou la bomba! Tots vosaltres, des del més petits fins al més gran, sempre us heu interessat per les meves cèl·lules i ratolins. Us estimo.

I a tu Uri, al teu costat em fas créixer com a persona, m'aportes saviesa, coneixements i inquietuds. Gràcies, per la paciència, per aguantar les meves exposicions, escoltar els problemes i saber-me distreure quan em feia falta. I sobretot per aquests últims mesos de bogeria, per donar-me tot el teu suport i haver estat allà en els bons moment i no tant bons. T'estimo.

TABLE OF CONTENTS

LIST OF FIGURES

LIST OF TABLES

LIST OF ABBREVIATIONS

3D	Three dimensional
%	Percentage
ºC	Centigrade degrees
AD	Alzheimer disease
AGEs	Advanced Glycation End-products
ATP	Adenosine triphosphate
BB94	Batimastat
BC	Breast cancer
C1	Constant 1 RAGE domain
C2	Constant 2 RAGE domain
CA	Carbonic anhydrase
CFTR	Cystic fibrosis transmembrane conductance regulator
CO_2	Carbon dioxide
Ct	Cycle threshold
CVD	Cardiovascular disease
DA	Dalton
DAMPs	Damage-associated molecular pattern
dH2O	Distillated water
DIAPH1	Diaphanous-1
DMEM	Dulbecco's Modified Eagle's Medium
DMSO	Dimethyl sulfoxide
DN-RAGE	Dominant-negative of RAGE
DTT	Dithiothreitol
ECM	Extracellular matrix
EDA	Exploratory data analysis
EDTA	Ethylenediaminetetraacetic acid
EMP	Epithelial-mesenchymal plasticity
EMP-TF	Epithelial-mesenchymal plasticity transcription factors
EMT	Epithelial-mesenchymal transition

ER	Estrogen receptor
ERK1/2	Extracellular signal-regulated kinase 1/2
EVs	Extracellular vesicles
FA	Formic acid
FBS	Fetal bovine serum
FDA	Food and Drug Administration
FDR	False discovery rate
FGF2	Fibroblast growth factor 2
FL-RAGE	Full-length of RAGE
GLM	Generalized linear models
h	Hour
HCl	Hydroxide chloride
HEPES	4-(2-hydroxyethyl)-1-piperazineethanesulfonic acid
HER2	Human epidermal growth factor receptor 2
HIF	Hypoxia-inducible factor
HMG	High mobility group
HMGA1	High-mobility group AT-hook 1
HMGB1	High-mobility group box 1
HMGN1	High-mobility group nucleosome-binding domain-containing protein 1
HRE	Hypoxia response elements
IF	Immunofluorescence
IP	Intraperitoneal injection
iTGF-βRII	Inhibitor of the TGF-β receptor II
kDa	Kilodalton
LB	Lysogeny broth
LDHA	Lactate dehydrogenase A
MCT	Monocarboxylate transporter
MET	Mesenchymal-epithelial transition
MGO	Methylglyoxal
min	Minutes

mL	Milliliter
MMP	Matrix metalloprotease
NaCl	Sodium chloride
NaF	Sodium fluoride
NaOH	Sodium hydroxide
NF-kB	Nuclear factor-kappa B
ng	Nanogram
NHE	Na+/H+ exchanger
NK	Natural killer
O_2	Oxygen
O/N	Overnight
PBS	Phosphate-buffered saline
PCA	Principal component analysis
PCR	Polymerase chain reaction
PDK1	Pyruvate dehydrogenase kinase 1
PES	Polyethersulfone
pHe	Extracellular pH
pHi	Intracellular pH
PIPES	Piperazine-N,N'-bis(2-ethanesulfonic acid)
PMSF	Phenylmethanesulfonyl fluoride
ppm	Parts per million
PR	Progesterone receptor
PRR	Pattern recognition receptor
PVDF	Polyvinylidene fluoride
RAGE	Receptor for Advanced Glycation End-product
RNA	Ribonucleic acid
rpm	Revolutions per minute
RT	Room temperature
RT-PCR	Real-time quantitative PCR
s	Second
SDS	Sodium dodecyl sulfate

SDS-PAGE	Sodium dodecyl sulfate-polyacrilamide gel electrophoresis
shRAGE	Short-hairpin RNA
siRNA	Small interfering RNA
spc	Spectral counts
TEMED	Tetramethylethylenediamine
TF	Transcription factors
TGF-β1	Transforming growth factor beta 1
TLR	Toll-like receptor
TNBC	Triple-negative-breast cancer
UPS	Unconventional secretion pathway
V-ATPases	Vacuolar ATPase proton pump
V-domain	Variable RAGE domain
VHIO	Vall d'Hebron Institut d'Oncologia
βA	β amyloid
µg	Microgram
µL	Microliter
µm	Micrometer
µM	Micromolar

Nucleotides

A adenine **T** thymine **G** guanine **C** cytosine

SUMMARY

RAGE is a transmembrane protein of the immunoglobulin family highly expressed during embryonic development but rarely expressed in adult healthy tissues. However, under cellular stress RAGE is re-expressed and mediates inflammatory chronic diseases including diabetes, Alzheimer's and cancer. RAGE is a multi-ligand receptor and its protein ligands, which are unconventionally secreted, are overexpressed under inflammatory conditions, activating RAGE-driven signaling pathways.

The aim of this thesis is to study the involvement of RAGE in Triple Negative Breast Cancer (TNBC) progression. First, we show that breast cancer (BC) cells exposed to different microenvironmental stresses become more migratory and invasive. Under acute acidosis, the secretome of different BC cells is enriched with RAGE ligands. Moreover, acidosis induces an oligomerization of RAGE, which correlates with its signaling activation. In BC cells, ligand binding to RAGE activates NF-kB and/or ERK1/2 pathways promoting breast cancer cell migration and invasion. Both the ablation of RAGE expression and its inhibition using RAGE antagonists block RAGE-mediated signaling and cell migration and invasion in TNBC cells. Furthermore, blocking RAGE in mesenchymal TNBC cells induces a mesenchymal-to-epithelial transition (MET) by down-regulating SNAIL1 expression. TNBC mesenchymal cells under RAGE inhibition gain the expression of several epithelial markers, increase cell adhesions and become less invasive. Furthermore, in a TNBC *in vivo* model, we show that treatment with a RAGE antagonist reduces the incidence of metastasis and increases overall survival. Therefore, this study shows that RAGE drives EMT and tumor cell invasion in mesenchymal TNBC cells, and it shows that RAGE is a new candidate therapeutic target for breast cancer.

INTRODUCTION

1. TRIPLE-NEGATIVE BREAST CANCER

Triple-negative breast cancer (TNBC) is defined by the lack of expression of estrogen receptors (ER), progesterone receptors (PR) and the human epidermal growth factor receptor 2 (HER2) [1]. It is the most aggressive variant of breast cancer (BC) causing higher mortality than other breast cancer types despite it represents less than 15% of all BC [2]. Treatment options for TNBC are limited since the hormonal receptor and HER-2 targeted drugs typically used for other breast cancer types are ineffective. Due to a lack of targeted therapies for TNBC, chemotherapy including platinum salts, anthracyclines and taxanes remain the standard therapeutic approach for this disease [3]. Despite the aggressive nature of TNBC, 35% of patients present a pathologic complete response after chemotherapy [4]. Paradoxically, TNBC patients have also a higher risk to develop distant metastasis within 5 years following the diagnosis. However, after this period the probability for recurrence decreases rapidly (Fig. 1) [1]. TNBC is a heterogenous disease and it has been classified into different subtypes depending on gene expression, clinical characteristics and treatment response [5,6]. The high heterogeneity, where different TNBC subtypes exhibit different sensitivity to therapeutics [7], causes a worse overall survival for this breast cancer subtype. Therefore, it is important to find new strategies to find the appropriate treatment for each patient [5,8]. Recently, new strategies such as antibody–drug conjugates (ADC) which recognize glycoproteins from the plasma membrane over-expressed in cancer cells have been tested in clinical trials [9,10]. Interestingly, last year the anti-Trop-2 ADC was approved by the Food and Drug Administration (FDA) for patients who have received at least two prior therapies for metastatic disease. Immunotherapeutics, PARP inhibitors as well as inhibitors of the PI3K/AKT/mTOR pathway tested as a monotherapy or in combination with chemotherapy are also being used to treat TNBC patients [4,11–15]. Noteworthy, this year, an immune checkpoint inhibitor against programmed cell death protein 1 (PD-1) receptor, called pembrolizumab, in combination with chemotherapy, was

approved by the FDA to treat TNBC patients with early-stage TNBC, locally recurrent unresectable tumor or metastatic TNBC [16,17].

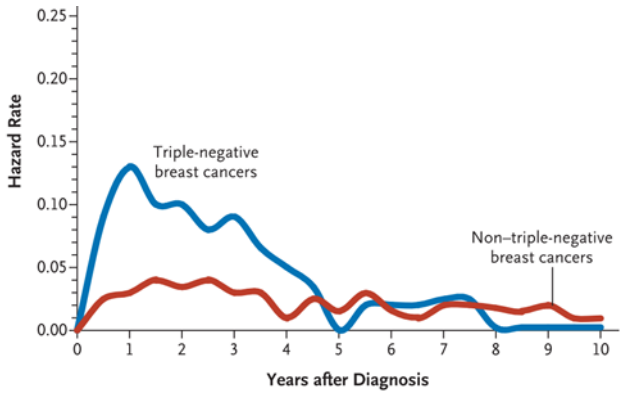

Figure 1. Triple-Negative Breast Cancer recurrence. Comparison of the hazard rate between triple-negative breast cancer and other breast cancers in the development of distant recurrence. Figure extracted from *Foulkes et al., 2010*.

2. TUMOR MICROENVIRONMENT

In the tumor, besides cancer cells, there is an extracellular matrix (ECM) (e.g., collagen, fibronectin, laminin) and other cells including cancer-associated fibroblast, endothelial cells, immune cells and adipocytes which express and secrete different intercellular communicators such as growth factors, cytokines and chemokines that contribute to tumor progression [18–21]. This cell complex around the tumor is known as tumor microenvironment. Furthermore, environmental conditions generated during tumorigenesis including nutrient and oxygen deprivation, as well as extracellular acidosis, also characterize the tumor microenvironment, and play a role in key processes such as tumor dissemination (Fig. 2) [22]. Although in early tumor stages, the tumor microenvironment exerts anti-tumor effects, lastly, in advanced stages it interferes with therapeutic responses [20].

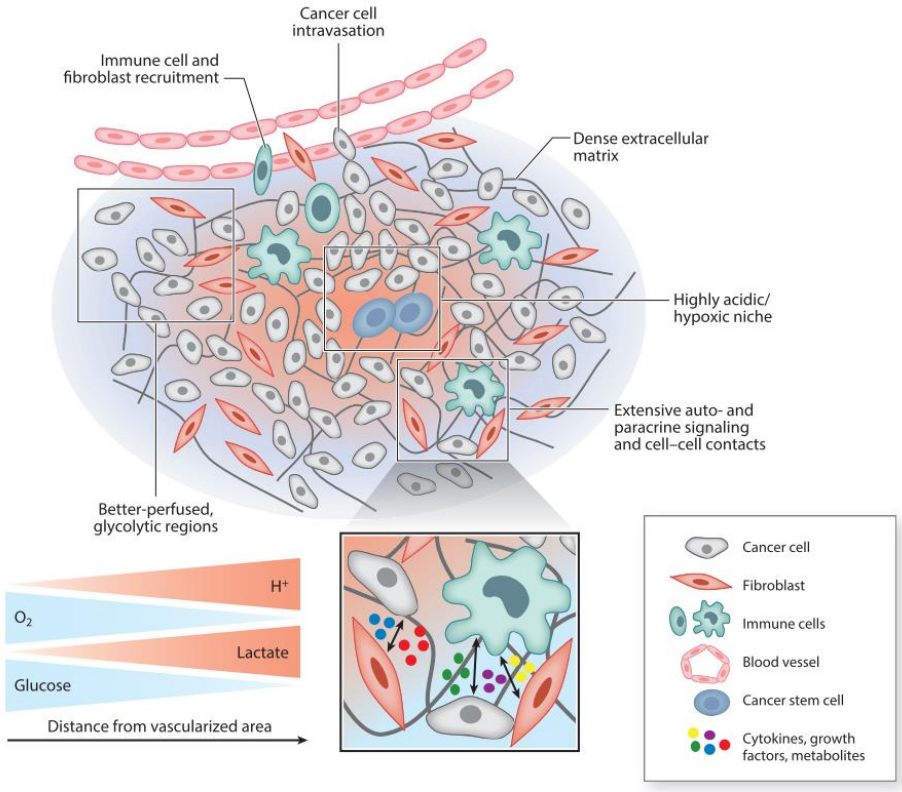

Figure 2: The tumor microenvironment. The tumor microenvironment consists of the extracellular matrix and different stromal cells including fibroblast, vascular and immune cells, and adipocytes. Stromal cells together with cancer cells secret growth factors and cytokines promoting cancer cell invasion and tumor progression. The environmental conditions are different depending on the vasculature distance. Specifically, inside the tumor, the levels of oxygen and glucose decrease, while the levels of lactate and H^+ increase as a consequence of the higher glycolytic activity. Figure extracted from *Boedtkjer, E. et al. 2020.*

2.1. TUMOR MICROENVIRONMENTAL STRESS

In normal conditions, cells metabolize glucose and oxygen into pyruvate, which is then transformed into Acetil-CoA and shuttled into the mitochondria to undergo the Krebs cycle and oxidative phosphorylation [23,24]. This whole metabolic process generates up to 38 ATPs per molecule of glucose. In contrast, generating energy in a tumor is quite different. The high proliferative rate of tumor cells results in an aberrant vasculature and hence in a poor blood perfusion. Therefore, the tumor microenvironment is characterized by oxygen and nutrient deprivation [25,26]. An important consequence of having hypoxic conditions in the tumor

microenvironment is a switch in how tumor cells obtain energy from nutrients, by favoring glycolysis over oxidative phosphorylation [25]. During this process, pyruvate is not transformed to Acetyl-CoA, instead it is reduced to lactate generating only 2 ATPs.

Under hypoxia, the transcription factor (TF) hypoxia-inducible factor (HIF), especially HIF-1α, induces the expression of target genes involved in angiogenesis, tumor progression [27] and glycolytic enzymes to increase glycolysis for ATP production [28,29]. HIF-1 is an heterodimeric complex composed by an oxygen-dependent α-subunit (three different isoforms), and a non-oxygen-dependent β-subunit (two different isoforms) [27,30]. In normal oxygen conditions, HIF-α is polyubiquitinated and degraded by the proteasome in less than 5 minutes, while in the absence of oxygen the half-live of HIF-α increases up to 60 minutes [28] due to the inactivation of HIF enzymes such as FIH and PHDs (Fig. 3). The stability of HIF-α protein induces its translocation into the nucleus where heterodimerize with HIF-β and this complex can bind to the hypoxia response elements (HRE) in the genome such as pyruvate dehydrogenase kinase 1 (PDK1) and lactate dehydrogenase A (LDHA). Therefore, the stabilization of HIF-1α facilitates the metabolic switch from oxidative phosphorylation (OXPHOS) to glycolysis [28–30].

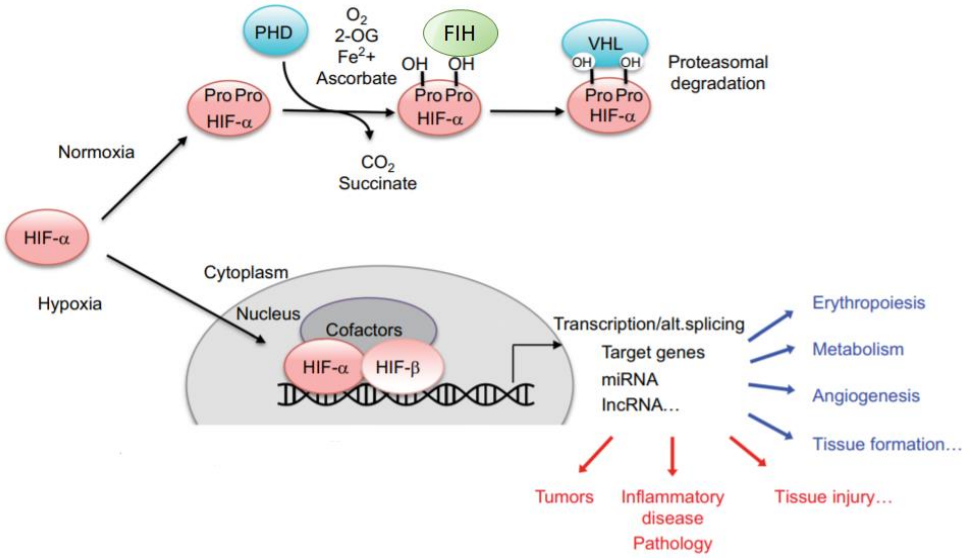

Figure 3. Schematic representation of the hypoxia inducible factor (HIF) pathway. In normoxic conditions, HIF-α is hydroxylated by prolyl hydroxylase domain (PHD) protein and factor inhibiting HIF (FIH). Then, it interacts with the von Hippel–Lindau (VHL) protein enhancing HIF-α ubiquitination and proteasomal degradation. In hypoxic conditions, HIF-α is stabilized and translocated into the nucleus where it dimerizes with HIF-β and other cofactors driving the transcription of genes related with cell survival, metabolism, angiogenesis, cell invasion and metastasis among others. Figure adapted from *Ratcliffe, P. et al. 2017.*

To maintain the ATP production, cells growing in hypoxic conditions increase the rate of glycolysis. However, even in aerobic conditions tumor cells rather than oxidative phosphorylation, they keep producing energy by glycolysis (Fig. 4). This phenomenon, known as the "Warburg effect", is thought to sustain the high proliferation rate of tumor cells although it is not perfectly understood. [24,31–34]. The elevated glycolytic activity increases the levels of lactate, carbonic acid and protons in the cytosol. To survive and proliferate under these conditions, tumor cells increase their membrane transporters [32,33] in order to maintain an adequate intracellular pH (pHi) important for cell survival [35]. The increase in the release of glycolytic byproducts leads to an acidic extracellular microenvironment [28,32,33]. The acidic extracellular pH (pHe= 5.6 to 6.8) and the alkaline intracellular pH (pHi= 7.2 to 7.5) is one of the hallmarks of cancer [28,34,36].

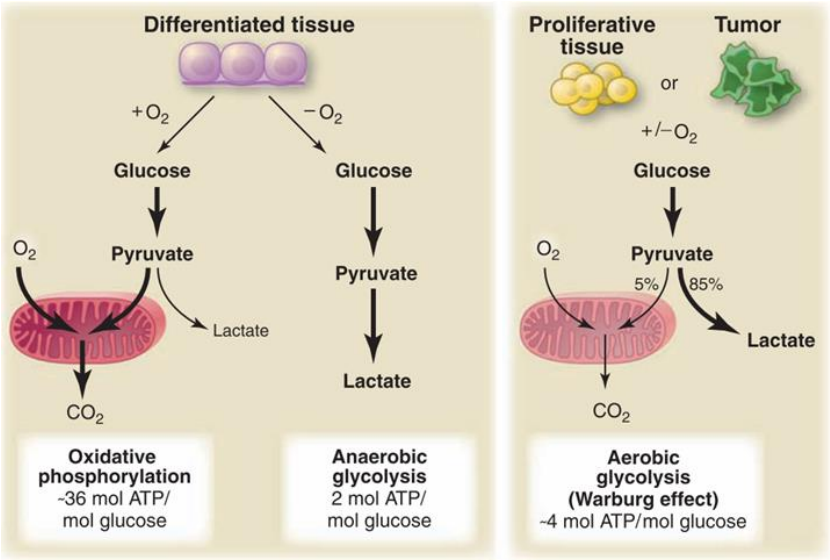

Figure 4: Schematic representation of cancer cell metabolism. Glucose metabolism is oxygen dependent. In the presence of oxygen (normoxia), cells metabolize glucose in the mitochondria using the oxidative phosphorylation. In the absence of oxygen (hypoxia), glucose is metabolized to lactate decreasing the ATP production by anaerobic glycolysis. Tumor cells keep producing energy by aerobic glycolysis even when hypoxia is reversed, a process known as the Warburg effect. Figure extracted from *Vander Heiden, MG. et al. 2009.*

An acidic environment induce apoptosis to healthy cells [37]. However, in cancer cells the acidic extracellular pH is an essential microenvironmental factor contributing to angiogenesis, stress fiber formation, cell migration, tumor invasion and intravasation of malignant cells, which eventually may result in metastasis [28,31,38]. Noteworthy, Rohani and colleagues discovered that acidosis is enriched in the invasive front of tumors [39]. Acidic microenvironment has been related with the induction of different signaling pathways such as NF-kB in breast and prostate cancer [40,41]. The low extracellular pH is also associated to activation of MAPK (ERK1/2 and p38) in prostate and bronchioalveolar carcinoma.

The continuous proliferation in the tumor and its insufficient vascularization ends up inducing a lack of nutrients such as sugars, amino acids and lipids. In order to survive in a nutrient deprived media, cancer cells have developed strategies to acquire nutrients from the tumor microenvironment. For example, tumor cells obtain

substrates for energy production from the extracellular matrix, albumin or by entosis, a process where neighboring cells are engulfed and degraded by lysosomes (Fig. 5) [42–44].

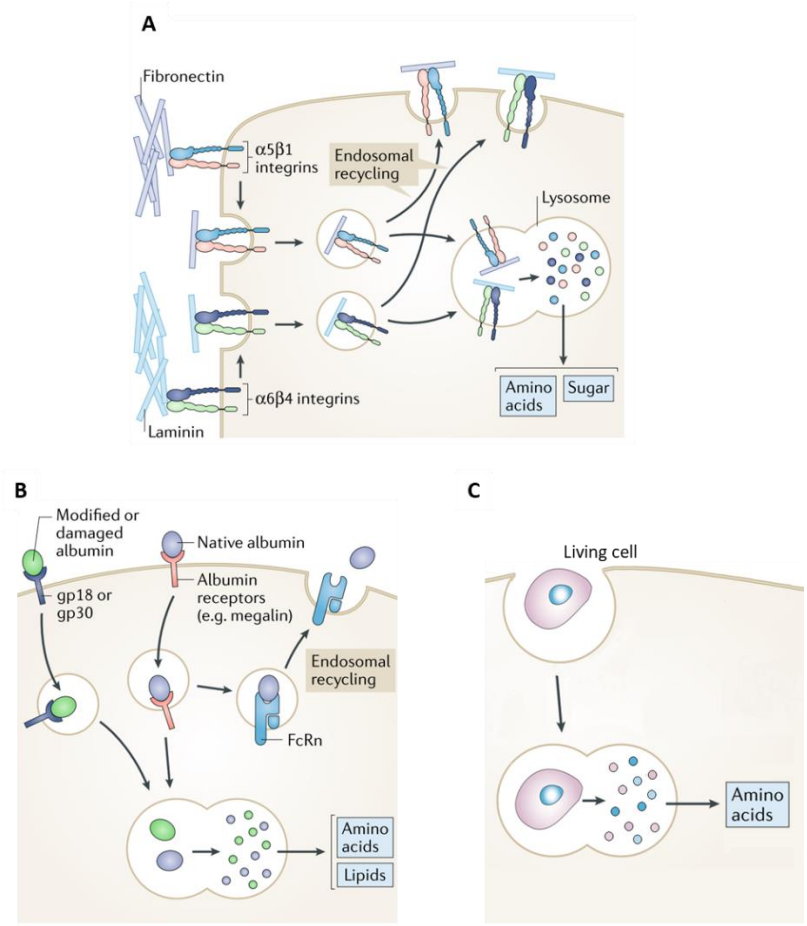

Figure 5. Cell strategies to acquire nutrients in a nutrient-deprived media. In a nutrient-deprived environment, cancer cells acquire nutrients by scavenging macromolecules from the tumor microenvironment to fuel growth and proliferation. Cancer cells acquire amino acids and sugar from the endocytosis of **(A)** Extracellular matrix components such as fibronectin and laminin and **(B)** albumin. **(C)** Entosis of living cells is another strategy used by cancer cells to acquire amino acids. Figure adapted from *Finicle, B. et al. 2018.*

3. EPITHELIAL-MESENCHYMAL TRANSITION

EMT is a cellular process in which epithelial cells acquire a mesenchymal phenotype. During the transition, epithelial cells lose their apical-basal polarity and modify tight

and adherent junctions to allow them to gain motility to migrate and invade [45]. Proteins like E-cadherin and ZO-1, hallmarks of an epithelial phenotype, are down-regulated, while proteins involved in a mesenchymal phenotype such as vimentin, N-cadherin and fibronectins increase their expression. The EMT process can be reversed by the termed mesenchymal-epithelial transition (MET), in which cells re-gain the apical-basal polarization and lose motility [45,46].

3.1. CELL PLASTICITY

EMT plays an essential role during embryonic development by regulating gastrulation and neural crest formation [47]. In adults, EMT plays a key role in the resolution of injuries by participating in the wound healing process. Furthermore, EMT is also involved in some pathological conditions such as fibrosis and cancer [47,48]. During tumorigenesis, EMT plays a role first facilitating local invasion in the primary tumor, and then during metastatic dissemination. Recent research has established that EMT is not a binary (E/M) process, since it involves multiple partial states that give rise to a high degree of cell state plasticity. Therefore, epithelial-mesenchymal plasticity (EMP) rather than EMT is a more accurate definition of this cell fate transition [49]. The intermediary states between epithelial and mesenchymal phenotype are known as partial EMT (pEMT), and therefore, they would acquire/maintain an intermediate phenotype expressing epithelial and mesenchymal markers at the same time (Fig. 6) [47,50–54].

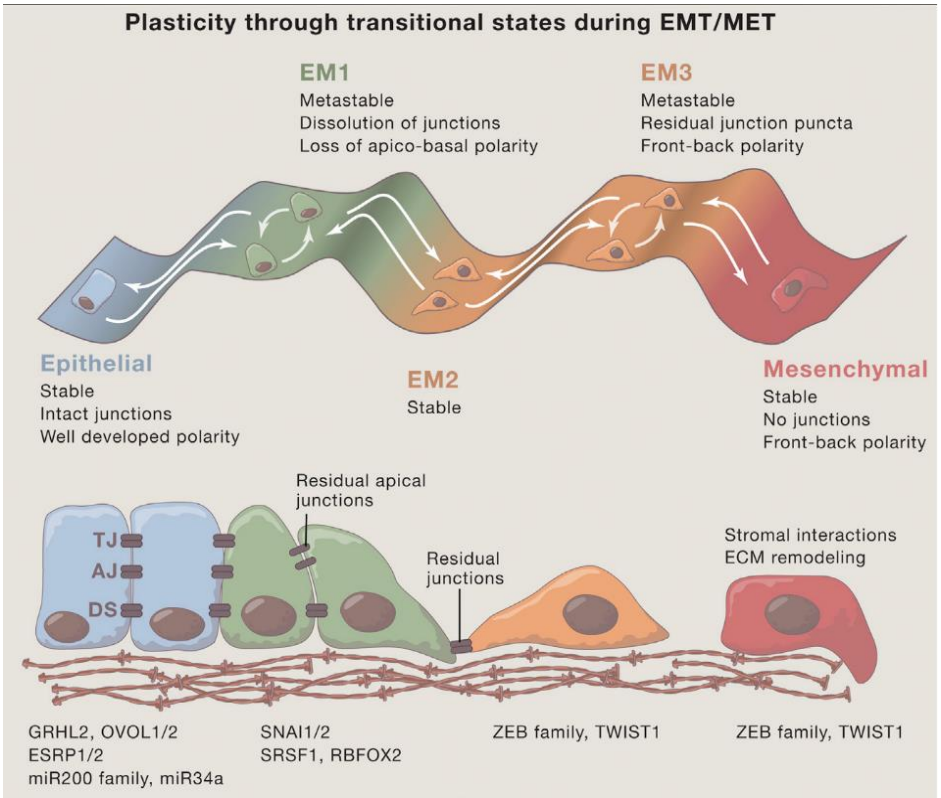

Figure 6. Epithelial-Mesenchymal Plasticity. EMT is a cellular process in which epithelial cells (E) acquire a mesenchymal phenotype (M). Different intermediary phenotypes (EM) that express both epithelial and mesenchymal markers at the same time are generated during this process. During EMT, epithelial cells lose tight junctions (TJ), adherent junctions (AD) and desmosomes (DS) to gain motility. The EMT process can be reverted, and it is known as mesenchymal-epithelial transition (MET). Different transcription factors (EMT-TF) are involved in EMT, including ZEB family, SNAI family, TWIST family, together with miRNAs. Figure extracted from *Nieto M.A. et al. 2016.*

3.2. CELL INVASION AND COLONIZATION

EMP is involved in tumor cell invasion and colonization at distant organs. Both, EMT and MET processes, are required for metastasis dissemination (Fig. 7). EMT is important for cell intra and extravasation, while once in the distant organ MET plays a role in cell proliferation. Furthermore, partial EMT is also detected in cancer cell migration and dissemination including circulating tumor cells (CTCs) of breast cancer patients [55], especially in those cells that migrate in clusters. Two different types of migration are described, single-cell migration and collective migration [56]. For single-

cell migration a complete EMT is required. However, for collective migration the leader cells at the front of migration undergo a partial EMT expressing mesenchymal markers such as N-cadherin to modify their polarity, while also maintaining epithelial characteristics and attachment to their neighbors [56,57]. The rest of the cells from the migratory group keep their apical-basal polarity. *In vitro* studies in lung, ovarian and breast cancer research also demonstrated the existence of intermediary states with co-expression of epithelial and mesenchymal markers [53,58]. Noteworthy, in patients, partial EMT has been associated to poor survival and resistance to therapy [59–62].

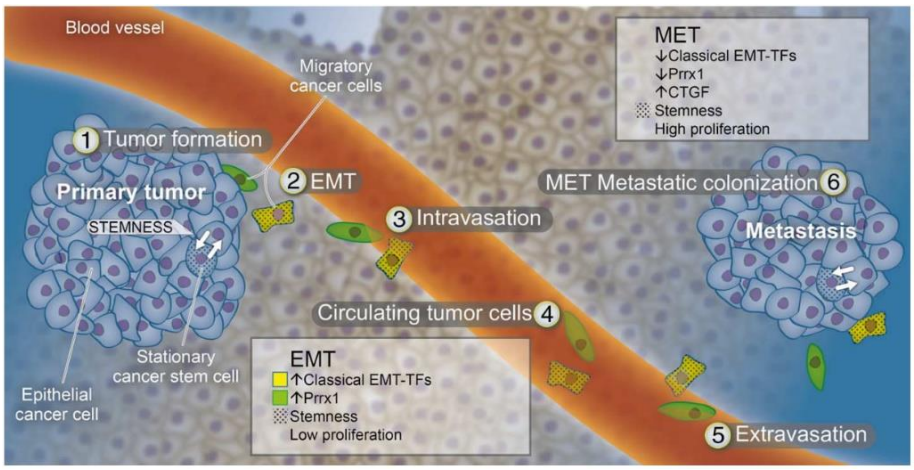

Figure 7. Cell plasticity during the metastatic cascade. Cell plasticity plays an important role during metastatic dissemination. Cells from the primary tumor undergo EMT to escape and intravasate to vessels. Once in circulation, tumor cells colonize distant organs, and cells revert the EMT (MET) to promote metastatic cell proliferation. Figure extracted from *Nieto M.A. 2013.*

3.3. REGULATING CELL PLASTICITY

Different transcription factors (TFs), known as EMT-TFs, are responsible for regulating EMP together with microRNAs (miRNAs), epigenetic modifications and post-translational regulators (Fig. 6). EMT-TF expression is controlled by different signaling pathways, like TGF-β, EGF, FGF, Wnt, Notch and NF-kB pathways [57,63–65]. The expression of EMT-TF also rely on the cell type and the tumor microenvironment [64,66]. The most relevant EMT-TF include the zinc-finger-binding transcription factors (SNAI1 and SNAI2), the basic helix-loop-helix (bHLH) factors (TWIST1 and TWIST2)

and the zinc-finger E-box-binding homeobox factors (ZEB1 and ZEB2) [67]. SNAI1, SNAI2, ZEB1 and ZEB2 are E-cadherin (*CDH1*) repressors that bind directly to the E-box motif in the E-cadherin gen promoter. EMT-TF also repress the expression of genes related with tight junctions and apical-basal polarity. E-cadherin down-regulation enhances cell invasion and metastasis formation, and is also associated with poor prognosis in breast, colon and liver cancer patients [68–70]. The expression of EMT-TF is associated to an increase in cell invasion and metastasis formation. For example, SNAIL1 induces lung metastasis in breast cancer [71,72], and ZEB1 promote breast, pancreas and colon cancer invasion [73–76]. However, in melanoma the TF of ZEB family present opposite functions, acting ZEB2 as a tumor suppressor while ZEB1 promotes melanoma progression [77]. TWIST1 and TWIST2 also induce N-cadherin (*CDH2*) and vimentin expression promoting a mesenchymal phenotype [78]. Other EMT-TF are described such as PRRX1, OVOL1 and OVOL2, being the PRRX1 a mesenchymal promoter, while OVOL1/2 protect the epithelial phenotype [47].

miRNAs are non-coding RNAs that bind to targeted mRNAs inhibiting and destabilizing them. Some examples are the miR-34 and miR-203 targeting SNAI1/2 as well as miR-200 that targets ZEB1/2, which regulate the expression of the EMT-TF producing a negative feed-back loop involved in maintain epithelial homeostasis under normal conditions [47,78,79]. Furthermore, epigenetic modifications as well as post-translational modification also modulate the EMT process [78,80,81].

3.4. EMT AND TUMOR MICROENVIRONMENT

Hypoxia and acidosis are important microenvironmental factors in solid tumors. These factors help cancer cells to invade, degrade the ECM, and eventually promote metastatic dissemination [82–84]. In addition, hypoxia and acidic pH are related to the induction of EMT. Reports in breast cancer melanoma and Lewis lung carcinoma found that acidosis induces EMT [38,85,86] transforming epithelial cells into a more fibroblastic phenotype. Mechanistically, EMT induced by acidosis up-regulates the expression of MMPs, like MMP-9, promoting invasion and ECM degradation [38,39,85].

Hypoxia has been also found to induce EMT in different epithelial cancers such as prostate, ovarian, lung and liver [87–90]. Hypoxia-induced EMT as well as acidosis is characterized by an increase in mesenchymal associated genes and a decrease in epithelial genes regulated by EMT-TF.

3.5. EMT AND THERAPEUTICS

EMT is associated to different aspects of tumorigenesis including tumor progression, tumor stemness, chemoresistance and immune evasion [78,91]. Therefore, strategies are being developed to target and block EMT to avoid its pro-tumorigenic effects and reverse therapeutic resistance. Some drugs targeting EMT have already been approved by the FDA, and several new drugs are under development [92]. Strategies being studied to prevent or reverse EMT include monoclonal antibodies and small molecule inhibitors that block signaling pathways responsible of the EMT activation such as Notch, TGF-β or Wnt, among others [65,92]. Another strategy being studied is targeting miRNAs that control key steps driving EMT [79,93]. Additionally, considering that during EMT cancer cells adapt their metabolism to promote phenotypic changes, different metabolic modulators have been also proposed as EMT inhibitors in cancer [94]. Interestingly, drugs already approved or under clinical trials to treat other human diseases, including salinomycin, metformin and simvastatin, have been proposed to target EMP [93–95]. EMT is also involved in immune evasion by reducing the response to checkpoint inhibitors immunotherapy. Therefore, the combination of immunotherapy with EMT inhibitors have been recently tested to improve tumor immune response [96].

4. SECRETORY PATHWAYS

4.1. CONVENTIONAL SECRETION

Most of the proteins secreted contain a N-terminal signal peptide that allow them to translocate into the endoplasmic reticulum (ER). After protein folding, these proteins leave the ER encapsulated in coat protein complex II (COPII)-coated vesicles that link

them to the Golgi apparatus. Once they reach the Golgi apparatus, they are sorted and re-encapsulated in vesicles that eventually fuse with the plasma membrane for delivery of vesicular cargo into the extracellular space [97]. The ER/Golgi pathway followed by most secreted proteins is known as classical or conventional secretion (Fig. 8). However, other proteins lacking the signal peptide are also transported to the extracellular space through the unconventional protein secretion (UPS).

4.2. UNCONVENTIONAL SECRETION

The unconventional protein secretion (UPS) pathways rely on four different cellular mechanisms to facilitate the secretion of proteins while bypassing the ER/Golgi apparatus (Fig. 8) [98–100]. Type I UPS is defined by proteins that directly translocate across the plasma membrane by them self, the best protein studied is the fibroblast growth factor 2 (FGF2) [101]. For Type II UPS proteins reach the extracellular compartment through ATP-binding cassette transporter (ABC transporters). Examples of Type II UPS are the a-factor in yeasts [102], and m-factor of *Schizosaccharomyces pombe* [103]. Type III UPS is used by hydrophilic proteins that are secreted through vesicles. Those proteins enter into lumen of intracellular vesicles that ultimately fuse with the plasma membrane releasing their cargoes into the extracellular space in a soluble form or they can also be release inside a vesicle, known as extracellular vesicles (EVs) [104]. Two kinds of extracellular vesicles are described, the microvesicles generated by exocytosis of the plasma membrane [105], and the exosomes derived from multivesicular bodies (MVB) when fuse with the plasma membrane [106]. A protein examples of Type III UPS include the two acyl coenzyme A-binding proteins: AcbA (*Dictyostelium discoideum*) [107] and Acb1 (*Saccharomyces cerevisiae*) which are secreted through MVB [108]. Finally, Type IV UPS is used for a group of transmembrane proteins that are synthesized in the ER and reach the plasma membrane by bypassing the Golgi apparatus to be secreted. The best characterized example is the ion channel cystic fibrosis transmembrane conductance regulator (CFTR) [109].

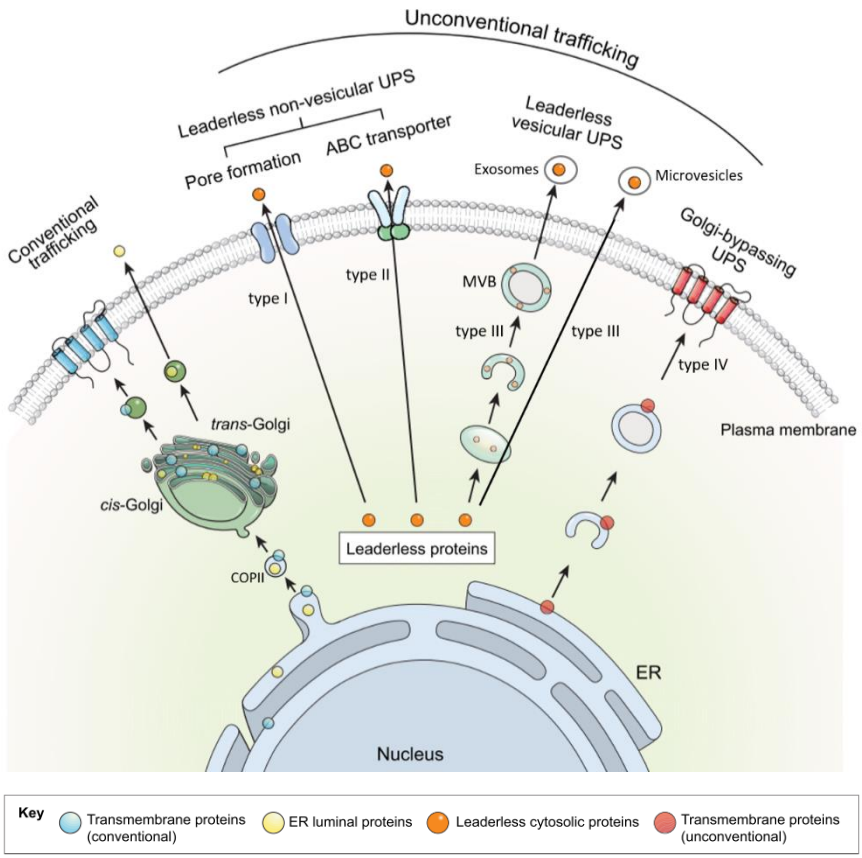

Figure 8. Conventional and Unconventional secretory pathways. Proteins that contain a signal-peptide are secreted by the conventional secretory pathway to the extracellular space or the plasma membrane. These proteins leave the endoplasmic reticulum (ER) to the Golgi encapsulated in coat protein complex II (COPII) vesicles. Once in the Golgi, they are modified and processed to finally be dispatched to the plasma membrane or be secreted. There are four types of unconventional secretory pathways. Type I: proteins able to cross the plasma membrane by themselves. Type II: ABC transporters are used by proteins to be release to the extracellular space. Type III: proteins are secreted through vesicles. Two types of vesicles are described, microvesicles, which are generated by shedding of the plasma membrane, and exosomes, which derive from multivesicular bodies (MVB). Type IV: transmembrane proteins that bypass the Golgi to reach the plasma membrane. Figure adapted from *Jiyoon, K. et al. 2018*

In human biology, inflammation is a common link between UPS and stress. For example, inflammation triggers the secretion of many downstream mediators and unconventionally secreted proteins, including caspase-1 and IL-1β [110,111]. Caspase 1 enzymatically converts the inactive form of IL-1β, pro-IL-1β, to its active form, IL-1β, and the increases in IL-1β are associated with aging and cancer. When pathogens or

tissue damage induces inflammatory stress, the pattern recognition receptors, such as Toll-like receptors, and RAGE, become activated, after which pro-IL-1β is processed by caspase 1 and secreted through UPS [112,113]. Caspase 1 is also required for the unconventional secretion of cytoplasmic proteins, including galectins, the macrophage migration inhibitory factor (MIF), and FGF2 [110,114]. Recent work highlighting inflammation in fostering aberrant growth and precancerous lesions in diverse tissues also implicates UPS proteins in precancerous neoplasia and progression to frank malignancy.

Besides inflammation, the unconventional secreted proteins participate in other biological processes including intercellular communication, invasion, cell proliferation, survival as well as modulation of the immune response [115]. In addition, most of the unconventionally secreted proteins from yeast and mammalian cells mediate signals from environmental stimuli. Different studies demonstrate that microenvironmental stress factors, such as oxidative stress, hypoxia, nutrient deprivation and heat shock, increase the extracellular vesicles release [84,116,117].

The potential role of UPS in tumor biology is further underscored by recent mass spectrometry analyses of secreted proteins which reveal that cancer cells frequently release factors via UPS pathways [118]. While only a handful of UPS proteins have been validated using orthogonal methods, the role of unconventional secretion is emerging as a critical feature of cancer cells that could be modulated in therapy [99,119]. For example, in cancer, EVs contain metalloproteases (MMP2 and MMP9) and urokinase-type plasminogen activator (uPA), that interact with ECM of breast and ovarian cancer inducing matrix degradation and invasion [115,120,121]. Furthermore, exosomes promote invadopodia formation in neck squamous cell carcinoma, and at the same time, invadopodia are key docking sites for exosome secretion [122]. Since metastatic tumor cells encounter different stressors when leaving their primary site to establish a tumor in another tissue, this could coordinate several UPS factors, not only at the primary site, but also within the metastatic niches. Therefore, although

different types of UPS are been described, their inhibition could be interesting to develop therapeutic strategies to avoid cell invasion and metastases.

5. THE RECEPTOR FOR ADVANCED GLYCATION END-PRODUCT

The Receptor for Advanced Glycation End-product (RAGE) is a transmembrane receptor of the immunoglobulin superfamily that was discovered in 1992, when it was isolated from bovine lungs [123]. RAGE is expressed in a wide variety of cells, such as endothelial cells, alveolar type I (AT-1) lung cells, fibroblast, smooth muscle cells, neuronal cells, macrophages, T cells, among others [124–127]. The *RAGE* gene, called *AGER*, is located in the chromosome 6 encoded in the Class III region of the major histocompatibility complex (MHC). The protein was firstly identified as a receptor for AGEs (Advanced Glycation End-products) which gave the name to the receptor. AGEs are produced by the Maillard reaction, a non-enzymatic reaction between reducing sugars and free amino groups of amino acids, lipids and proteins. and their accumulation is detected during aging, diabetes, immunoinflammatory and neurodegenerative diseases [128,129]. Beyond AGEs, RAGE is a multi-ligand receptor, and different proteins unconventionally secreted (see section 5.2) have been described as RAGE ligands including high mobility group proteins (HMG), S100/calgranulins proteins, amyloid beta (Aβ) among others (Fig. 9) [128]. Most of them can be defined as pathogen-associated molecular patterns (PAMPs) or damage-associated molecular pattern (DAMPs), inducing a proinflammatory response.

RAGE is expressed during embryonic development. In spite of the lack of literature, it is known that RAGE is especially expressed in the brain and lungs, and it is implicated in neuronal differentiation and lung development [130–132]. In adult tissue, RAGE expression is mostly repressed [133,134], although it is constitutively expressed in healthy lungs, which suggests that RAGE might have a different function in these organs. Indeed, in lungs, RAGE has a role in cell-cell adhesion, where it promotes the adherence of epithelial cells to the ECM [127,135]. Furthermore, in the alveolar type I (AT1) epithelial cells, RAGE is found in the basolateral plasma membrane

contributing to their spread morphology, essential for gas exchange [127]. Outside lungs, the upregulation of RAGE has been related to different chronic inflammatory diseases such as diabetes [136], Alzheimer disease [137], cardiovascular disease [128], cancer [133,138,139] and retinal disease [135].

5.1. RAGE STRUCTURE

RAGE is glycosylated, and it has a molecular weight of approximately 50 kDa. Its structure consists of three different domains: a large extracellular ligand-binding region (amino acids 23-342), a hydrophobic transmembrane domain (amino acids 343-363) and a small cytoplasmic domain (amino acid 364-404) essential for intracellular signaling [128,140]. The extracellular region is subdivided in three domains: one variable (V) Ig-like domain, and two constant (C1 and C2) Ig-like domains each of which participate in ligand binding. The V (residues 23-116) and C1 (residues 124-221) domains form a net positive charge due to the amount of arginine and lysine residues. The V-C1 positively charged region is the main binding region for ligands, which bind through their negatively charged regions, as demonstrated by X-ray crystallography and NMR spectroscopy [128,140–143]. Due to its ability to recognize different ligands with a similar pattern, RAGE is considered a pattern recognition receptor (PRR) [144]. By contrast with the V-C1 region, the C2 domain is negatively charged, and only the protein S100A6 has been reported to interact with it [145]. Upon ligand binding, RAGE induces a dimerization or even an oligomerization of V-V and C1-C1 RAGE domains [141,146]. Different oligomerizations might explain the specificity and affinity of ligands and the activation of different signaling pathways. The transmembrane domain promotes helix-helix homodimerization, which might also have a role in signal transduction due to the well conserved GxxxG motif [128,147]. The cytoplasmic domain is essential for the interaction with downstream effectors of RAGE, including diaphanous related formin 1 (DIAPH1), ERK1/2, TIRAP and DOCK7 [128,143,148], important to activate different RAGE signaling pathways.

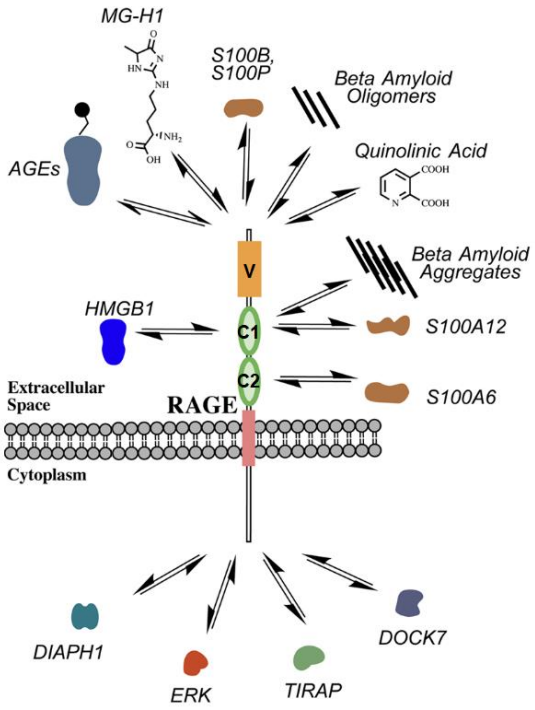

Figure 9. RAGE structure, ligands and signaling pathways. The structure of the full-length RAGE includes an extracellular region containing three different domains (the variable domain (V) and two constant domains (C1 and C2)), a transmembrane region and a cytoplasmic tail. RAGE is activated by different ligands that bind to the extracellular region activating different downstream pathways (DIAPH1, ERK1/2, TIRAP and DOCK7). Figure extracted from *Bongarzone, S. et al. 2017.*

Although RAGE is a transmembrane receptor, different RAGE isoforms are generated either by alternative mRNA splicing, or by proteolytic cleavage of the extracellular domain through the metalloproteinase ADAM10 and MMP9 (Fig. 10) [128,133,149]. These isoforms results into the release of the extracellular domain of RAGE as a soluble isoform (sRAGE) [128,133,149]. A decreased proliferation and invasion has been observed in hepatocellular carcinoma and glioma after sRAGE treatment [150,151]. Therefore, sRAGE would act as a decoy receptor to prevent the cellular responses mediated through RAGE signaling. In fact, the use of sRAGE has been suggested as a potential therapeutic treatment in cancer and inflammatory diseases [152–154]. Furthermore, studies in breast, gastric and lung cancer patients, detected a decrease in sRAGE in cancer patients compared to healthy patients [155–157]. Considering that sRAGE is

positively correlated with good prognosis, the results suggest that sRAGE could be considered as a potential biomarker for early detection of cancer.

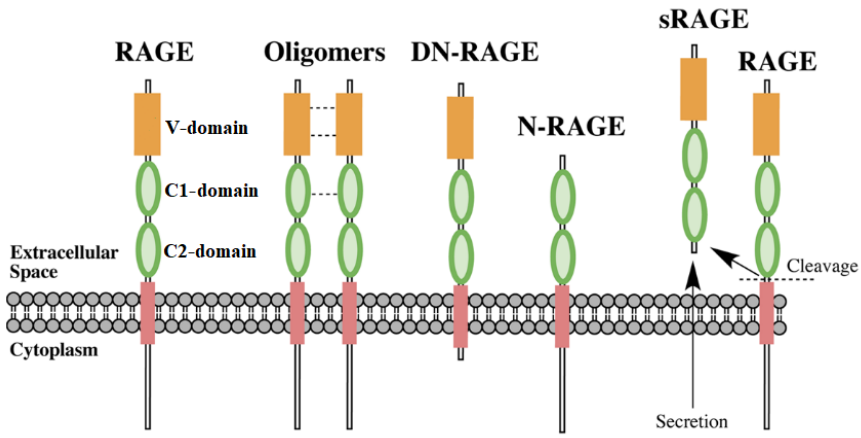

Figure 10. RAGE isoforms. Different RAGE isoforms have been described. From left to right: full-length RAGE (RAGE), oligomers of the full-length RAGE (Oligomers), dominant-negative RAGE (DN-RAGE), N-truncated RAGE (N-RAGE), soluble RAGE (sRAGE). sRAGE is obtained by either cleavage or RNA splicing, inducing its secretion. Figure extracted from *Bongarzone, S. et al. 2017.*

5.2. RAGE LIGANDS

Most of RAGE ligands are proteins unconventionally secreted having dual functions in the intra- and extracellular space. RAGE-ligands activate different signaling pathways depending on the cell type and ligand. The most relevant ligands are described in the following sections:

5.2.1. AGEs

The Advanced Glycation End-products (AGEs), are a group of compounds formed by a non-enzymatic glycosylation reaction between carbonyl groups of reducing sugars and free amino groups of proteins, lipids or nucleic acids [149,158–160]. This process, known as Maillard reaction, was discovered in 1912 [161,162]. The reaction takes place under abundant reducing sugars like in diabetes, although AGEs can also be generated from smoking tobacco and preparing certain foods, in particular those heated [163,164]. Different types of AGEs have been described, such as Nε-carboxy-

methyl-lysine (CML) and Nε-carboxy-ethyl-lysine (CEL) which bind to the V-domain of RAGE [128,160].

AGEs accumulation lead to several pathologies including diabetes, cancer, cardiovascular and neurodegenerative disease, most of them associated with inflammation [129,133,158,165]. Methyl-glyoxal (MGO) is a by-product of glycolysis, involved in AGEs formation. MGO accumulation is involved in diabetes, but is also involved in other chronic inflammatory diseases such as cardiovascular disease and cancer [166,167]. In cancer, MGO is related with progression and metastasis formation, and its inhibition using MGO scavengers, reduces tumor growth [168,169]. However, based on its potent cytotoxic effects, high concentrations of MGO are related with apoptosis [170].

5.2.2. AMYLOID BETA

The amyloid beta peptide (Aβ), is generated from the amyloid precursor, a transmembrane protein that is proteolytically cleaved by the β- and γ-secretases [171]. Aβ monomers generate aggregates including fibrils and oligomers that can bind to different plasma membrane receptors such as RAGE. RAGE is expressed in endothelial, microglia and neuronal cells. When Aβ binds to microglial cells, RAGE triggers an inflammatory response, while in neurons, it induces oxidative stress and Aβ intraneuronal transport [172]. In endothelial cells, RAGE facilitates the transport of Aβ into the brain across the blood-brain barrier (BBB) [173]. Aβ accumulation in the brain correlates with Alzheimer's disease [174,175]. Accordingly, RAGE inhibition decreases Aβ peptide in the brain reducing RAGE activation and suppressing neuroinflammatory responses [176]. Furthermore, an antagonist of RAGE, Azeliragon, was used in clinical trials for patients with Alzheimer's disease reducing disease progression [177]. Unfortunately, in phase III clinical trial Azeliragon failed to meet its primary endpoint [178].

5.2.3. HMG FAMILY

HMG proteins are a family of non-histone chromatin-associate proteins. They are classified intro three families: HMGA, HMGB and HMGN. All HMG proteins are basic, 10–20 kDa proteins which harbor an acidic carboxyl terminus and modulate chromatin structure [179–181]. Each family, however, is distinguished by unique DNA and/or nucleosome binding motifs. The HMGA family includes three isoforms of the HMGA1 (HMGA1a, HMGA1b and HMGA1c), and also the HMGA2. They are characterized by having three AT-hook motifs that mediate binding to the minor groove of B-form DNA at AT-rich regions. HMGA proteins lack an HMG box and appear to bind to DNA with sequence specifically [182,183]. The HMGB family members (HMGB1, HMGB2, HMGB3 and HMGB4) are defined by two DNA-binding box motifs that mediate binding to DNA without sequence specificity [181]. They are the most abundant HMG proteins and were the first HMG proteins to be identified as secreted factors. The HMGN proteins are found only in vertebrates and include five members: HMGN1, HMGN2, HMGN3, HMGN4, HMGN5 [184]. They lack an HMG box, but contain a nucleosome-binding "N" domain that mediate specific binding to nucleosomes [185,186].

HMG proteins were assumed to be nuclear proteins exerting its role in cancer by transcriptionally modulating different signaling pathways. However, members of the three families of HMG proteins have been detected extracellularly, having dual functions arising from dual location [187–189]. Among all of the HMG proteins, only the HMGB1 and HMGA1 have been described as RAGE-ligands, being the HMGB1 the best studied since HMGA1 has been recently described as RAGE ligand [189]. It is described that HMGB1 interacts with RAGE V-domain [128,134,190], whereas HMGA1 still do not know.

HMGB1 is secreted by immune cells like monocytes, neutrophils, NK and endothelial cells triggering inflammatory responses [134,143,150]. HMGB1 can be passively released from necrotic cells by crossing permeabilized membranes once released from the chromatin [191]. It is also actively secreted from damaged cells using an autophagy-

dependent secretion (Type III UPS pathway) [192,193]. HMGB1 is a well-known DAMP protein that can bind to RAGE or to toll-like receptors (TLR2 or TLR4) activating a proinflammatory cascade [128,143]. It is overexpressed in many tumor cells types, such as colon, prostate, pancreatic cancer, hepatocellular carcinoma, and melanoma [150,194]. This overexpression triggers inflammation, regulates migration, and promotes tumor metastases [128,194].

HMGA1 has an essential role during embryonic development, but in adult tissue is absent or barely detectable [119,189,195]. Intracellular HMGA1 becomes aberrantly re-expressed in most aggressive human tumors, where high levels portend poor differentiation status and adverse clinical outcomes [195–198]. While HMGA1 secretion did not appear to be mediated by EVs, the precise UPS pathway employed remains unknown. However, it is known that CK2 is implicated in HMGA1 and HMGB1 secretion [189,199]. Considering that extracellular HMGA1 has been recently described as RAGE ligand in TNBC mediating migration and invasion [189], there are no information about the role of HMGA1-RAGE in other cancers.

5.2.4. S100 FAMILY

Calcium is important for different biological processes into the cell, and variations in calcium levels are linked with cancer. The S100s proteins, which are exclusively from vertebrates, are a family of over 20 small proteins with different expression and functions. They are characterized by binding calcium via EF-hand motifs, although, few of them can also bind to zinc and cooper [133,134]. S100 proteins form homodimers or heterodimers, like S100A8/S100A9, which display different roles inside the cell as calcium sensors such as cell proliferation, invasion and metastasis in breast cancer and colon cancer [200,201]. Several S100 proteins are secreted during inflammatory conditions in different cells types [134,143] acting as DAMPs. The extracellular S100 proteins can bind to toll-like receptors (TLRs) and RAGE, activating different signaling pathways [128,133,134,143]. S100 proteins are upregulated in different cancer types, and being multifunctional proteins, they have been associated to both tumor promoters

[200] and tumor suppressor phenotypes [133]. Besides cancer, S100 proteins play a role in different inflammatory diseases such as rheumatoid arthritis, chronic inflammatory bowel disease and systemic immune disease [133].

5.3. RAGE SIGNALING

RAGE activates multiple intracellular signaling pathways due to the variety of RAGE-ligands, the different cell types that express RAGE, and the three extracellular domains capable of ligand binding. The cytoplasmic domain of RAGE (ctRAGE) is essential for the interaction with downstream effectors including diaphanous-1 (DIAPH1), ERK1/2, TIRAP and DOCK7 [128,143,148,202]. Little is known about how these interactors bind to the ctRAGE. DIAPH1 is the most studied intracellular RAGE interactor, which binds to the Arg-5 and Gln-6 residues of the ctRAGE by its formin homology domain (FH1). The ctRAGE-DIAPH1 interaction regulates different signaling pathways like actin and microtubule polymerization, and it is involved in processes such as cell migration and proliferation [203,204]. Although DIAPH1 is the most studied intracellular interactor, ERK1/2 and TIRAP are also reported to bind to the ctRAGE [202,205]. Other signaling pathways activated upon RAGE ligand binding include mitogen-activated protein (MAP) kinase family (ERK1/2, p38, JNK), the phosphatidylinositide 3-kinase (PI3K)/protein kinase B (Akt), nuclear factor kappa B (NF-kB), the Janus kinase (JAK)-signal transducer and the activator of transcription (STAT) and the Rho family GTPases (Rac1 and Cdc42) (Fig. 11) [128,143,165,206]. The transduction of RAGE signaling through the above mentioned pathways leads to cell motility, proliferation, apoptosis and inflammatory response in different cell types [143,203,204,207,208]. In cancer, RAGE activation is involved in tumor growth, migration and metastases [140,150,151].

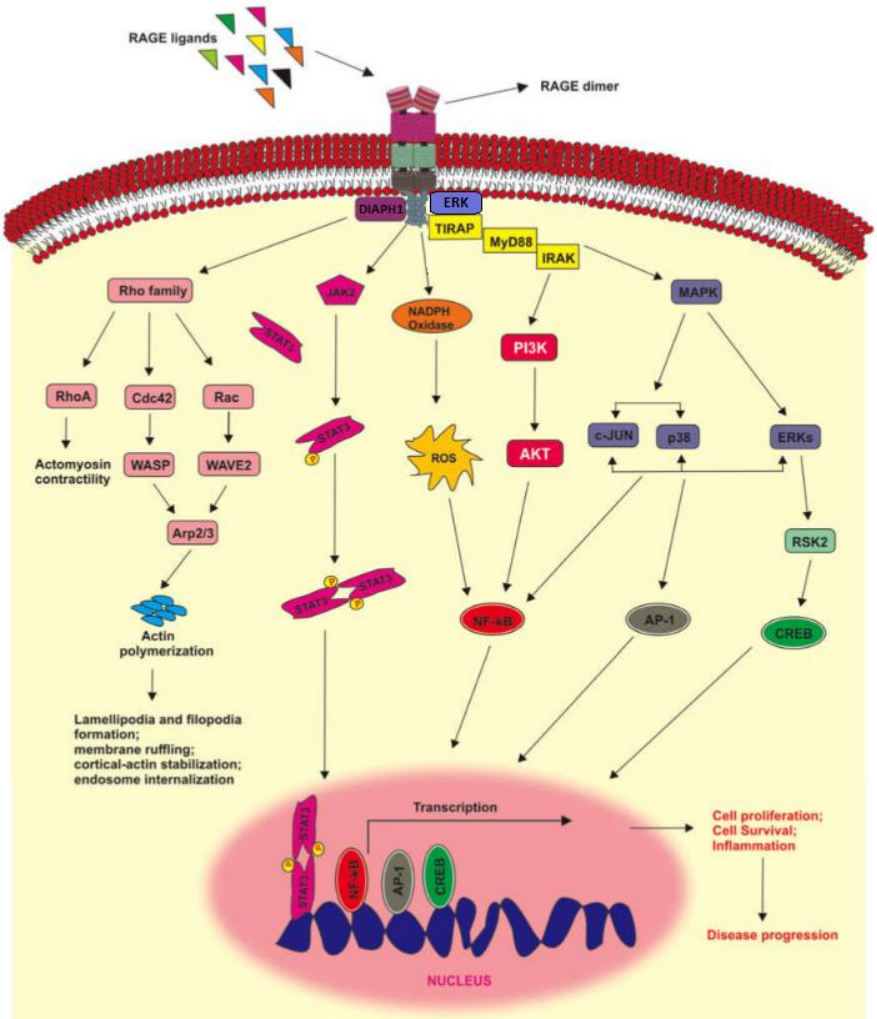

Figure 11. RAGE signaling pathways. Different ligands bind to RAGE activating multiple signaling pathways. Then, cellular interactors including DIAPH, ERK1/2 and TIRAP bind to the cytoplasmic domain of RAGE activating different signaling cascades involving Rho family proteins, JAK-STAT3, PI3K-AKT, MAP Kinases and NF-kB. Finally, the signaling mediated by RAGE activates transcription factors that induce transcriptional programs associated to different cellular processes (proliferation, migration, inflammation and cell survival) promoting cancer progression. Figure adapted from *Olaoba O.T. et al. 2020.*

5.4. RAGE AND INFLAMMATION

RAGE is expressed in most immune cells linked to the inflammatory response (Fig. 12) [124–126,209]. In neutrophils, RAGE mediates adhesion and migration across epithelial monolayers, while in monocytes/macrophages contribute to exaggerated vascular

inflammation and stress. Activation of RAGE in lymphocytes is essential for migration, mature differentiation and proliferation [210]. Furthermore, in endothelial cells, RAGE acts as an adhesion receptor for leucocytes, promoting leucocyte recruitment [207,210].

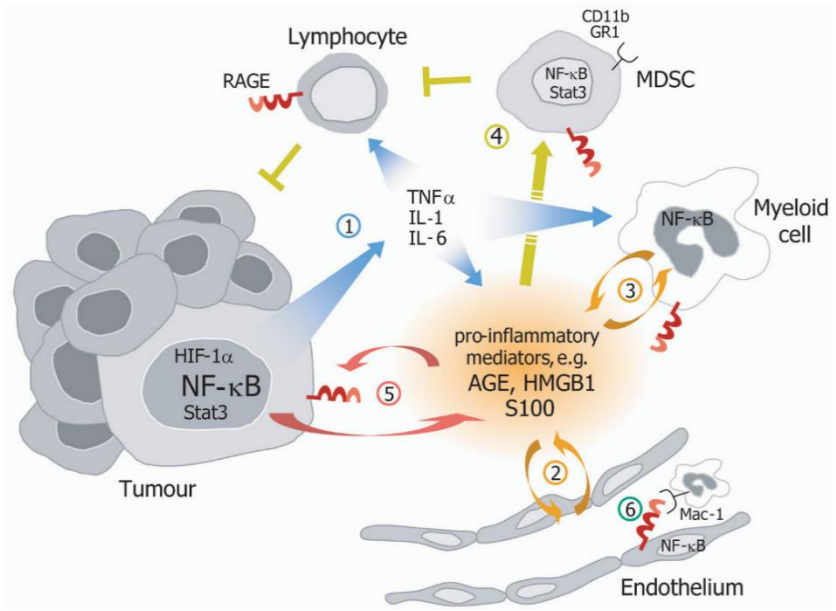

Figure 12. RAGE in tumor and inflammatory cells. RAGE is expressed in tumor cells and also in different inflammatory cells including lymphocytes, monocytes, endothelial cells, myeloid and myeloid-derived suppressor cells (MDSC). In a pro-tumorigenic environment, RAGE-ligands are accumulated (1), which activate endothelial and myeloid cells for the recruitment of lymphocytes and MDSC (2 and 3). The MDSC inhibit lymphocytes blocking their anti-tumoral activity (4). RAGE is also activated in tumor cells also contributing to cancer progression (5). Figure extracted from *Riehl A. et al. 2009.*

Despite the broad array of ligands and pathways regulated, most of the cellular effects induced by RAGE are linked to inflammation [133,143]. RAGE is involved in the resolution of acute inflammation in diverse settings, including wound healing, immune adaptative responses and nerve regeneration [138]. However, sustained activation of RAGE is directly linked to chronic inflammation, and mediates deleterious effects in common aging-associated diseases such as diabetes, neurodegenerative diseases, arthritis and cancer (Fig. 13) [143,210].

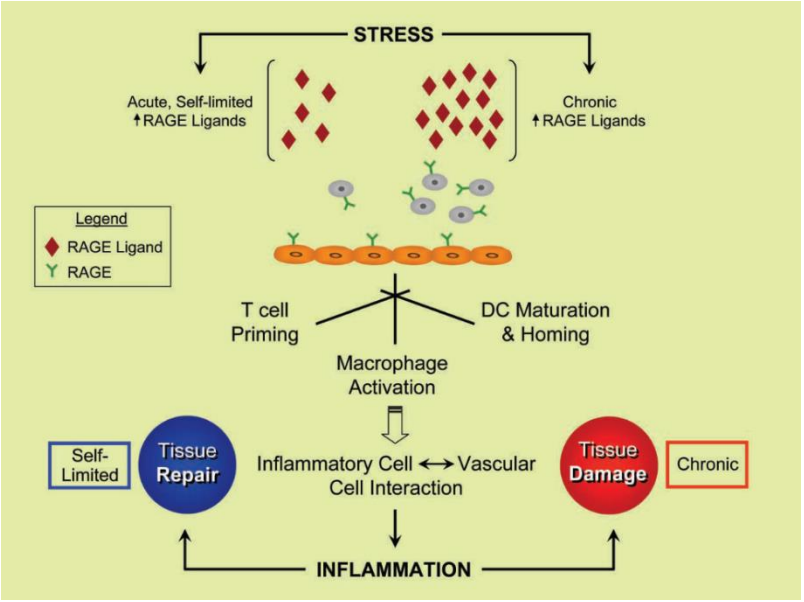

Figure 13. Role of RAGE in acute and chronic stress. Under acute stress RAGE ligands are expressed inducing an inflammatory response required for tissue repair. However, under chronic stress, RAGE ligands are over-expressed promoting a chronic inflammation and tissue damage. Figure extracted from *Yan, S.F. et al. 2009.*

5.5. RAGE IN CANCER

RAGE is expressed in different cancer types such as breast, pancreas, melanoma, prostate, gastric, colorectal, bladder among others [143,211]. Both *in vitro* and *in vivo* studies have shown that RAGE activation in cancer induces tumor progression and metastasis. For example, in colorectal and thyroid cancer cells the S100A4 induces cell mobility [212,213]. In breast cancer, various RAGE ligands (HMGA1, AGE, S100A7, S100A8/A9) have been described as inducers of cell proliferation, migration, invasion and metastasis [158,189,200,214]. In other cancer types such as gastric, pancreatic and cervical, RAGE ligands (HMGB1, S100A7, S100s) have a role in cancer progression [194,215,216]. RAGE activates different signaling pathways associated with malignant processes like migration, proliferation, invasion and resistance to apoptosis [143], which have a role in tumor progression. Therefore, RAGE is an attractive therapeutic target. Blocking RAGE signaling should reduce tumor growth and metastasis. Different strategies to inhibit RAGE signaling had been studied in pre-clinical models.

In vivo, Taguchi A, *et al*. demonstrated a decrease in tumor growth and metastasis in glioma using different strategies to block the RAGE-amphoterin signaling: 1) using sRAGE as a dominant negative to reduces RAGE activity; 2) using antibodies against RAGE or amphoterin to inhibit RAGE-ligand binding; and 3) generating a mutant of RAGE in the cytoplasmic domain to avoid RAGE signaling [151]. Other strategies have been studied recently, including the use of a dominant-negative of RAGE, RAGE inhibitors or the use of an antagonistic peptide for RAGE ligands [128,143,150,217].

HYPOTHESIS AND OBJECTIVES

Previous cancer research studies demonstrated that the tumor microenvironment tends to be hypoxic as a consequence of the higher proliferative rate of tumor cells and a resulting poor blood perfusion. Tumor cells under hypoxia up-regulate glycolysis to obtain energy. Indeed, even when hypoxia is reversed, tumor cells keep relying on glycolysis, a phenomenon known as the Warburg effect. The increased rate of glycolysis leads to an acidic extracellular microenvironment. These tumor microenvironmental stress conditions have been associated to tumor aggressiveness.

Cellular stress activates specific signaling pathways evolutionary designed to restore homeostasis. However, under chronic stress, these pathways mediate the onset of different chronic diseases. One of these pathways is driven by RAGE, a multiligand receptor known to mediate different inflammatory diseases, diabetes, Alzheimer's, and also cancer. Here, we hypothesize that tumor microenvironmental stress could activate RAGE signaling and impact on breast cancer tumorigenesis. To demonstrate this hypothesis, we proposed the following objectives:

1. Characterizing the role of microenvironmental stress in the unconventional secretion linked to breast cancer invasion.

2. Studying the role of RAGE signaling in TNBC cells

3. Characterizing the role of RAGE linked to migration and invasion during microenvironmental stress.

4. Targeting RAGE in a TNBC *in vivo* model.

MATERIALS AND METHODS

1. CELL BIOLOGY

1.1. Cell lines

Breast cancer cell lines were purchased from the American Type Culture Collection (ATCC) and the National Institute of Health (NIH). MDA-MB-231, MCF-7, MCF10A, Hs578T and NMuMG cell lines were maintained in DMEM-F12 (#21331046, Gibco Invitrogen), while BT549 cells were maintained in RPMI (#52400041, Gibco Invitrogen) supplemented with 10% FBS (#10270106, Gibco Invitrogen) and 2 mmol/L L-Glutamine (#25030024, Gibco Invitrogen). NMuMG were also supplemented with 10 µg/mL insulin (#I9278, Sigma-Aldrich). MCF10A were supplemented with 20 ng/mL human EGF (#AF-100-15, Peprotech), 10 µg/mL insulin and 500ng/mL hydrocortisone (#H0888, Sigma-Aldrich). All cell lines were maintained at 37ºC with 5% CO_2 and 95% humidified atmosphere air. Cell lines were authenticated by short tandem repeat profiling (IdentiCell, Aarthus University Hospital).

1.2. Mycoplasma Test

All cell lines were regularly tested by PCR, to ensure they were Mycoplasma negative before being used for experiments.

Oligonucleotide	Sequence
Myco-F	5'- GGCGAATGGGTGAGTAACACG -3'
Myco-R	5'- CGGATAACGCTTGCGACCTATG -3'

Table 1. Oligonicleotides used for mycoplasma detection in cell lines.

1.3. Reagents for cell culture

Reagents: Azeliragon (#HY-50682, MedChemExpress) and FPS-ZM1 (#553030, Millipore) were used at 2 µM and 30 µM respectively, except for NMuMG cells that Azeliragon was used at 1.5 µM. Human TGF-β1 (#100-21-2UG, Petrotech) was used

at 1 ng/mL, inhibitor of the TGF-βRII (LY2109761, MedChemExpress) was used at 2 µM and MEK inhibitor was used at 10 µM (AZD6244; Selleckchem).

RAGE ligands: cells were treated with different recombinant human protein: S100A4, S100A7 and S100P used at 1 µg/mL from Leitat. Recombinant human protein HMGA1 used at 3 µg/mL also from Leitat. Recombinant human protein HMGN1 (#8187-HM-050, R&D System) and recombinant human protein HMGB1 (#1690-HMB-050, R&D System) were used at 2,5 µg/mL. Methylglyoxal (MGO) (#M0252, Sigma) was used at 100µM.

1.4. Microenvironmental stresses and chronic subpopulation generation

Acidosis

To induce acidosis DMEM-F12 media was mixed with 25mM HEPES (#H3375, Sigma) and 25 mM PIPES (#P6757, Sigma) buffer solutions to improve pH stability. The pH was adjusted at pH 6.5 using HCl (#H1758, Sigma) and NaOH (#S8045, Sigma). Before treating the cells, the media was sterilized using a sterile syringe filter with a 0.22 µm pore size hydrophilic Polyethersulfone (PES) membrane (#SLGP033RS, Millipore). For acute stress treatment, MDA-MB-231 cells were treated at pH 6.5 for the indicated time. However, for chronic treatment the pH was reduced every two weeks, from 7.4 to 7.1, then to 6.8, and finally to 6.5. Then cells were maintained at pH 6.5 to perform the experiments.

Hypoxia

To induce hypoxia, plates were inserted for 24h into hypoxic chamber incubator at 0.5% O_2, 5% CO_2 and 94.5% N_2 at 37ºC. Normoxic cells were maintained in an incubator environment of 20% O_2 and 5% CO_2.

Nutrient and glucose starvation

For chronic treatment with nutrient starvation the FBS was reduced every two weeks, from 10% to 5%, then to 3% and finally to 1% where it was maintained to perform the experiments.

Treatment with glucose starvation was done using a specific glucose deprived media (#11966025, Gibco Invitrogen), supplemented with 5%FBS.

1.5. Cell counting

Cells were detached from the plate with Trypsin-EDTA 0.05% (#25300054, Gibco) for 5 minutes. Then fresh media supplemented with FBS was used to inactivate Trypsin and cells were centrifuged 5 minutes at 200 g. Pellet was resuspended with 1 mL of the appropriate media and diluted 1:1 with Trypan Blue (#93595, Sigma). Cells were counted using a Neubauer Chamber and quantified using the following equation:

$$Nº\ cells/ml = (nº\ cells\ in\ Neubauer\ chamber/4) \cdot dilution\ factor \cdot 10^4$$

1.6. Secretome sample preparation and treatments

To generate the secretomes, 4 x 10^6 cells were seeded in 150 cc tissue culture plates and allowed to grow for 48 hours. After that, media were aspirated, and cells were washed 5 times, 2 times with PBS and 3 times with serum-free media. For secretomes in acidosis, the last wash was done with serum free-media adjusted at pH 6.5 or pH 7.4 and then, the appropriate serum-free media at pH 6.5 or 7.4 was added for 24h. Hypoxia was induced for 24h after the washes (see section 1.4). Glucose starvation serum-free media was added after the five washes for 8h. After each condition, secretome was collected. The secretomes were spun down at 200 g for 5 minutes, and the supernatants were collected and filtered through a sterile syringe filter with a 0.22 µm pore size (Millipore). Then, secretomes were concentrated using a 10 kDa NMWCO Millipore Amicon Ultra (#UFC901096 and #UFC501096, Millipore) until a final volume of 40-50 µL. Protein concentration was determined with a Pierce BCA protein assay kit (#23227, Thermo Fisher Scientific)

and quantified at 562 nm using the luminometer Spark™ 10M (Tecan). Triplicates were done for all conditions.

1.7. Invasion assay

Cell culture inserts (#353097, Corning Life Sciences) with 8 µm pore size polystyrene for 24-well plates were coated with Matrigel (#356234, Corning) using the following dilution: 12 µL in 1 mL of cold sterile water. 3,000 cells for MDA-MB-231, or 10,000 cells for MCF-7 and MCF10A cells were seeded onto the upper compartment of each chamber in 300 µL of DMEM-F12 without serum, and placed into wells containing 750 µL of DMEM-F12 complete medium in the lower chamber. After the appropriate time, transwells were washed twice with PBS 1X followed by 2 minutes fixation with methanol (#M/4058/17, Fisher). Then, cells were stained for 10 minutes with crystal violet 0.5% (#C6158, Sigma), and finally washed with PBS 1X. The number of invading cells was quantified using Image J software (NIH, Bethesda, MD, USA). Three independent experiments were done in triplicate. For acidic conditions media from the upper compartment was adjusted at pH 6.5, whereas the media from the bottom compartment was adjusted at pH 7.4 and left 16h in the incubator. For hypoxic conditions once cells were seeded in the upper chamber, hypoxia was induced to the plate for 24h. For glucose deprivation, cells were seeded for 24h in the upper compartment in media without glucose, while the lower compartment contained media without glucose supplemented with 5% FBS. RAGE antagonists were only added in the upper compartment together with the cells. The described conditioned were performed in three biological triplicates.

1.8. Gelatin degradation assay

Coverslips (#631-1577, VWR) were inserted in a 24 well plate with 500 µL 0.5% glutaraldehyde (Sigma) for 15min on ice. After three washes with cold PBS 1X, the plate was removed from ice and fluorescent gelatin (#G13186, Invitrogen), which was previously warmed at 60ºC for 2 minutes, was added at 50 µg/mL for 10 minutes. The coverslips were maintained in the dark. The excess of gelatin was

removed and the plate was leaved for 10 min at RT. After three washes with PBS, 500 µl of freshly made sodium borohydride 5mg/ml ($NaBH_4$) (#200050250, Acros Organic) were added for 15 min at RT to reduce and inactivate residual glutaraldehyde. Finally, coverslips were washed three times with PBS and sterilized in ethanol 70% (#ALCHALLMBT007, VWR) before be transferred to a new and sterile 24 well plate. 4,000 MDA-MB-231 cells were seeded in each well with batimastat 10 µM (a reversible MMP-2 and MMP-9 inhibitor) (#196440, Calbiochem). Cells were incubated overnight at 37ºC, 5% CO_2. The following day, batimastat was removed for 2h to allow invadopodias activity. Then, cells were washed twice with PBS 1X and fixed 15 minutes in 4%. Paraformaldehyde (PFA) After washing PFA twice with PBS, cells were incubated for 1 hour in 3% bovine serum albumin (BSA) (#A2058, Sigma-Aldrich) to block unspecific binding sites. Then, cells were stained with Red phalloidin–Tetramethylrhodamine B isothiocyanate (1:10000) (#P1951, Sigma-Aldrich) and Hoechst (bisBenzimide H 33342 trihydrochloride) 5 mg/mL (#B2261, Sigma-Aldrich) for 1h at RT. Finally, coverslips were mounted in mounting media (#P36965, Invitrogen). The samples were visualized in the Olympus FluoView FV1000 Confocal Microscope.

1.9. 3D culture

To generate tumoroids MDA-MB-231 cells were cultured in Matrigel. Firstly, cells were detached and counted (see section 1.5). 5,000 cells were resuspended in a solution 60% BD-Matrigel matrix (Corning) and 40% growth medium – organoid medium consisting of DMEM/F12, B27 supplemented (#17504-044, Thermo Fisher Scientific), and insulin (250ng/mL; Sigma-Aldrich) – and plated as 50 µl droplets on top of a coverslip. After 15 minutes in the incubator, 500 µL of specific media for 3D culture was added carefully. RAGE antagonists' treatment was started when tumoroids reached the right size and generated protrusions. Azeliragon was used at 2 µM and FPS-ZM1 at 30 µM. For tumoroids staining see section 3.5.

1.10. Protein extraction from cell culture

Cells were seeded in complete growth medium and allowed to grow at the specified times and conditions. When they reached 80-90% confluence they were lysed. Before protein extraction the cells were washed twice with cold PBS keeping the plate on ice. Then, the cells were scrapped and after centrifugation the cell pellet was collected. The protein extraction was done on ice using lysis buffer: 1% NP-40 (#1175499001, Roche), 10% glycerol (#G7893, Sigma), 2 mM EDTA (#324503, Merck Millipore) pH 8, 20 mM Tris pH 7.4, 137 mM NaCl and distillated water, mixed with 1% protease inhibitor cocktail (#P8340, Sigma-Aldrich), 1 µM PMSF (#7626, Sigma-Aldrich), 1 µM sodium orthovanadate (S6508, Sigma-Aldrich), the phosphatase inhibitors 1 µM NaF (#7920, Sigma-Aldrich), and 10 µM β-glycerolphosphate disodium salt hydrate (#G9422, Sigma-Aldrich). Cell pellets were resuspended in the described solution, incubated 30 minutes on ice, and the lysate solution was collected after 30 minutes centrifugation at 20,000 g at 4ºC.

1.11. Quantification of protein extraction

Protein quantitation was determined using Pierce™ BCA protein kit (#23227, Thermo Fisher Scientific). BSA was used to generate a standard curve ranging from 0 to 2 mg/ml. Samples were diluted 1:10 in MiliQ water. Twenty-five microliters of the different concentrations of BSA and samples were added in triplicated in a 96 well plate, mixed with 200 µl of Pierce™ BCA protein kit prepared at 50:1 (from reagent A:B). The plate was incubated at 37ºC for 30 minutes. Finally, the absorbance was measured at 562nm wavelength by spectrophotometry (Spark™ 10M instrument, Tecan). The protein concentration was extrapolated from the BSA standard curve.

1.12. Cell adhesion

A 24-well plate was coated with 30 µg/mL collagen (#A10483-01, Gibco) or 10 µg/mL fibronectin (#sc-29011, SantaCruz) and incubated for 1h at 37ºC. During this time,

cells were detached with 0.5 mM EDTA (Merck), resuspended in medium and centrifuged 5 minutes at 200 g. The supernatant was removed and the pellet was resuspended in 1mL of media. After counting the cells (see section 1.5), 200,000 cells were seeded in each well. Cells were incubated for 90 minutes keeping the appropriate treatment and cell adhesion was analyzed by crystal violet staining. Specifically, vehicle and drug treated cells were washed twice with cold PBS and fixed for 10 minutes with ice-cold 100% methanol. The methanol was aspired and cells incubated with 0.5% crystal violet solution in 25% methanol for 20 minutes. The cells were washed several times and let them dry overnight. Crystal violet staining was quantified dissolving the dye in 10% acid acetic and measuring the absorbance at 595 nm using the luminometer Spark™ 10M (Tecan). To study the effect of RAGE antagonists in cell adhesion, MDA-MB-231 cells were previously treated with DMSO, 30 µM FPS-ZM1 or 2 µM Azeliragon, for 72h until cells reach the MET phenotype. The described conditioned were performed in three biological triplicates.

1.13. Cell proliferation

1.13.1. Cell counting

After cell counting, 40,000 cells for each condition were seeded in triplicates and cell proliferation was measured at 24h, 48h, 72h and 96h by cell-counting. Specifically, cells were detached and counted as explained in section 1.5. Cell pellets were resuspended adding from 50 µl to 150 µl of media and counted using the Neubauer chamber.

1.13.2. CellTiter assay

MDA-MB-231 cells previously treated for 72h with DMSO, 30 µM FPS-ZM1 or 2 µM Azeliragon were collected and counted as explained in section 1.5. 10,000 cells were seeded in triplicated in a 96 well plate. After 72h, the media was removed and 100 µL of fresh media was added in each well with 20 µl CellTiter (#G8080, Promega) and

incubated 90 min in the incubator at 37ºC. Finally, fluorescence was measured at 530nm excitation and 590nm emission in the luminometer Spark™ 10M (Tecan).

2. MOLECULAR BIOLOGY

2.1. RNA analysis

2.1.1. RNA extraction and quantification

Cells were plated in a 100 mm plate and treated with the appropriate condition. When cells reach 90% confluence the RNA extraction was performed. Total RNA was isolated using TRIzol (Life Technologies) protocol. Specifically, 1 mL of TRIzol reagent (#15596-018, Thermo Fisher Scientific) was used to collect the samples. The cells with TRIzol were pipetted several times to be lysated and then incubated for 5 minutes at room temperature. 200 μL Chlorophorm (#C4232, Sigma- Aldrich) was added and the tubes were shacked vigorously by hand for 15 seconds and incubated 3 minutes at RT. Then, tubes were centrifuged 15 minutes at 12000 g at 4ºC to separate the samples in different phases. The colorless upper phase, which contains the RNA, was collected in a new tube and mixed with 500 μl of isopropanol (#I9516, Merck) to precipitate the RNA. After 10 minutes RT incubation, the samples were centrifuged at 4ºC for 10 minutes at 12000 g. The supernatant was removed and the pellet that contains the RNA was washed with 1 mL of 75% ethanol and centrifuged at 7500 g for 5 minutes at 4ºC. The supernatant was removed and samples were warmed for 5 minutes at 55ºC to evaporate the excess of ethanol. Finally, the RNA pellet was resuspended in Rnase-free water (#AM9937, Invitrogen) and incubated 10 minutes at 60ºC to improve RNA resuspension. The RNAs were quantified using the Nanodrop 2000 spectrophotometer (Thermo Scientific).

2.1.2. cDNA synthesis

For the reverse transcription, a High Capacity RNA-to-cDNA kit (#4387406, Appliedbiosystems) was used following the manufacturer's instructions. Specifically, cDNA was synthesized from 1 μg of RNA using the High-capacity RNA to cDNA

synthesis kit (Applied Biosystems) and the Veriti Thermal Cycler (Applied Biosystems).

2.1.3. Real-Time quantitative PCR (RT-qPCR)

In order to detect and compare RNA extraction, RT-qPCR was performed. 20 ng of cDNA were added in triplicates in a 384-well plate for each gene under consideration. The cDNA was mixed with 10 μM of forward and revers primers (Table 2), together with 5 μL of the PerfeCTa SYBR Green Fast Mix (#95073-012, Quantabio). dH_2O without RNA sample was used as negative control to avoid false negative results. The PCR step was performed using QuantStudio 6 Flex (Applied Biosystems), with each sample run in triplicate and following the standardized protocol (Table 3).

Oligonucleotide	Sequence	Manufacturer
AGER-forward	5'-ATTCAGTTCTGCACGCTCCT-3'	Sigma-Aldrich
AGER-reverse	5'-GCTGTCAGCATCAGCATCAT-3'	Sigma-Aldrich
Snai1-forward	5'-ACCACTATGCCGCGCTCTT-3'	Sigma-Aldrich
Snai1-reverse	5'-GGTCGTAGGGCTGCTGGAA-3'	Sigma-Aldrich
GAPDH-forward	5'-GGACTCATGACCACAGTCCATGC-3'	Sigma-Aldrich
GAPDH-reverse	5'-TCAGGGATGACCTTGCCCACAG-3'	Sigma-Aldrich

Table 2. Sequences of primers (forward and reverse) used to detect RNA expression by RT-PCR of a specific gene.

Temperature	Time	
50ºC	2 minutes	
95ºC	10 minutes	
95ºC	15 seconds	(40 cycles)
60ºC	1 minute	(40 cycles)
95ºC	15 seconds	
60ºC	1 minute	
95ºC	15 seconds	

Table 3. Detailed RT-qPCR cycling conditions.

Thanks to the software QuantStudio™ Real-Time PCR v1.3 that quantifies the Cycle threshold (Ct) proportional to the amount of target sample, results were analyzed using the comparative ΔΔCt method using the formulas:

$\Delta Ct = Ct_{(target)} - Ct_{(GAPDH)}$

$\Delta\Delta Ct = \Delta Ct - \text{mean } \Delta Ct_{(control\ treatment)}$

Data were expressed as the fold difference in gene expression (normalized to the housekeeping gene GAPDH) relative to a reference sample.

2.2. Knockdown of RAGE expression using shRNA

2.2.1. Bacteria transformation

Transformation of short-hairpins RNA (shRNA) (Fig. 14) lentiviral vector into One Shot™ Stabl3™ *E. coli* competent cells (#C7373-03, Invitrogen). For this purpose, 50 ng of DNA were added to the competent cells and incubated on ice for 30 minutes. Then, cells were heated-shock for 45 seconds at 42ºC and incubated on ice for 2 minutes. After adding 250 µL of Lysogeny Broth (LB) (1551.00, Condalab) medium, the vials were leaved at 37ºC for 1h at 225rpm in a shaking incubator. Finally, 50 µL and 100 µL of each transformation were spread in two plates of LB agar with 100 µg/mL ampicillin (#A9518, Sigma) selection. Plates were incubated overnight at 37ºC. The following day a colony was selected to be amplified (see section 2.2.2).

A

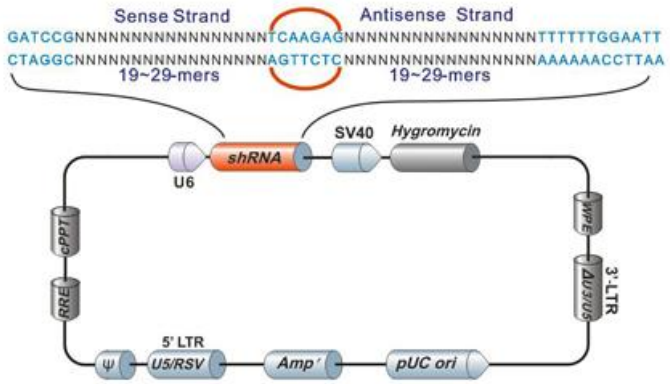

Figure 14. Lentiviral RAGE shRNA plasmid.

2.2.2. Plasmid amplification and DNA purification

Bacteria, grown overnight at 37 ºC, were amplified in an Erlenmeyer adding 500 µL of the pre-culture in 100 mL LB with ampicillin selection, and incubated O/N in a shaking incubator at 37ºC. Next day, bacteria were collected with 10min centrifugation at 6000 g. The kit Xtra Midi-Plus NucleoBond (#740412.50, Macherey-Nagel) was used to lysate the bacteria and precipitate the DNA following the manufacturer's instructions. Specifically, the bacteria pellet was resuspended with 8 mL of RES buffer and lysated using 8 mL LYS buffer. After that, 8 mL of NEU buffer was added inverting the tubs 3-4 times until obtaining a colorless solution. This solution was then filtered in the column previously hydrated with 12 mL of EQU buffer. Then the column was washed with 5 mL of EQU buffer followed by 8mL of WASH buffer to clean the filter where the DNA precipitated. The DNA was eluted in a new falcon using 5 mL of ELU buffer. Finally, the purified DNA was precipitated with 3.5 mL isopropanol (#I9516, Merck) and filtered with a specific filter of silica (NucleoBond Finalizers) were it bind. The DNA of the filter was washed with 2 ml of 70% ethanol, dried pressing air 5-6 times through the filter, and finally eluted with 200-800 µl buffer TRIS. The concentration of each plasmid was measured using the

Nanodrop 2000 spectrophotometer (Thermo Scientific). For lentiviral vectors that were previously transformed in *E. coli* bacteria, a stock in 25% glycerol was done.

2.2.3. Lentiviral production and infection of breast cancer cells

The HEK293T cells were used in order to produce lentivirus vectors with the specific shRNA. 700,000 HEK293T cells were seeded in a 100 cc plate the day before the transfection. To produce the virus, a mix was prepared: 36 µL Fugene HD transfection (#E2311, Promega), 4.5 µg of the plasmid, 1.5 µg of pCMV-VSV-G plasmid and 6 µg of pHR'8.2deltaR plasmid in 1 mL of DMEM-F12 media without serum. The mix was homogenized, leaved 30min at RT, and added drop by drop into the HEK293T cells. The media of HEK293T, which contains the virus vectors, was collected at 24h, 48h and 72h after transfection. A pool of the supernatants was obtained, centrifuged at 200 g to remove cell debris, and filtered through a sterile syringe filter with a 0.45 µm pore size hydrophilic PVDF membrane (#SLHVM33RS, Millipore).

MDA-MB-231 cell-line was infected with shRAGE lentivirus vectors (#HSH004399-4-LVRU6H, GeneCopoeia) (Fig. 14) with an overnight incubation. To infect the cells, the media that contains the virus was added to the cells adding 8 µg/mL polybrene (Hexadimethrine bromide #H9268-10G, Sigma). After 48h of infection 500µg/mL of hygromycin B (#10687010, Thermo Fisher Scientific) was added to select the cells positive to the transfection.

For shHMGA1 cells we used a previous lentivirus vector infection done in our lab (pIRES-HMGA1, Addgene), selected with 1 µg/mL puromycin [189].

2.3. Knockdown of RAGE expression using siRNA

The day before transfection cells were detached and counted as explained in section 1.5. Respectively, 300,000 and 200,000 cells were seeded in a 12-well plate for 24h and 48h transfection. The next day, 4 µL lipofectamine RNAiMAX transfection reagent (#12323563, Invitrogen), which increases the efficacy of the siRNA delivery, were mixed with 96 µL of the reduced serum medium Opti-MEM (#31985062, Gibco)

(Tube 1). In a separate tube (Tube 2), the small interfering RNA (siRNA) was diluted in Opti-MEM medium to a final concentration of 25 nM. Both tubes were gently mixed and incubated 5 minutes at RT. Then the content of Tube 1 was added on Tube 2. The mix was mixed carefully and incubated 20 minutes at RT. Finally, the solution of the siRNA transfection was added to the cells for 24-48h incubation before protein extraction (section 1.10) to perform Western blot analysis (section 3.1).

A SMARTpool of four RAGE siRNAs (#SO-2774565G, Dharmacon) was used to transfect the cells. As negative control, a non-targeting pool (#77D-001810-10-05, Dharmacon) was used.

2.4. Plasmid transfection of the extracellular region of RAGE

Bacteria that contain the plasmid pcDNA3-RAGEdeltaCyto (FL-RAGE) (#71436, Addgene) and the pcDNA3-RAGE (DN-RAGE) (#71435, Addgene) (Fig. 15) were grown O/N at 37ºC in an LB agar plate with 100 µg/mL ampicillin (Sigma). The next day, a selected colony was amplified in a pre-culture of 5ml LB and incubated over day at 37ºC in a shacking incubator. The following steps are explained in section 2.2.2. After DNA purification and quantification, 100,000 MDA-MB-231 cells plated the day before in a 6-well plate were transfected with 1 µg and 2 µg of the plasmids. To do that, 3 µL Fugene HD transfection (Promega) were mixed with DMEM-F12 without serum, homogenized by inversion and incubated 5 min at RT. Then the plasmids (1 µg and 2 µg) were added to this solution and incubated 30 minutes at RT. Finally, the plasmids were added drop by drop to the cells in new fresh media, and leaved 48h at 37ºC and 5% CO_2. After this incubation, 2000 µg/mL of geneticin (#11811031, Thermo Fisher Scientific) was added to select the positive transfected cells.

MDA-MB-231 cells were previously transfected in our lab using X-Treme- Gene (Roche) with the plasmid pGL4 expressing the firefly luciferase 2 (Photinus pyralis) gene (kindly provided by Dr. Abasolo, CIBBIM-Nanomedicine, VHIR) [189]. Positive transfected cells were selected with 1000 µg/mL geneticin.

A

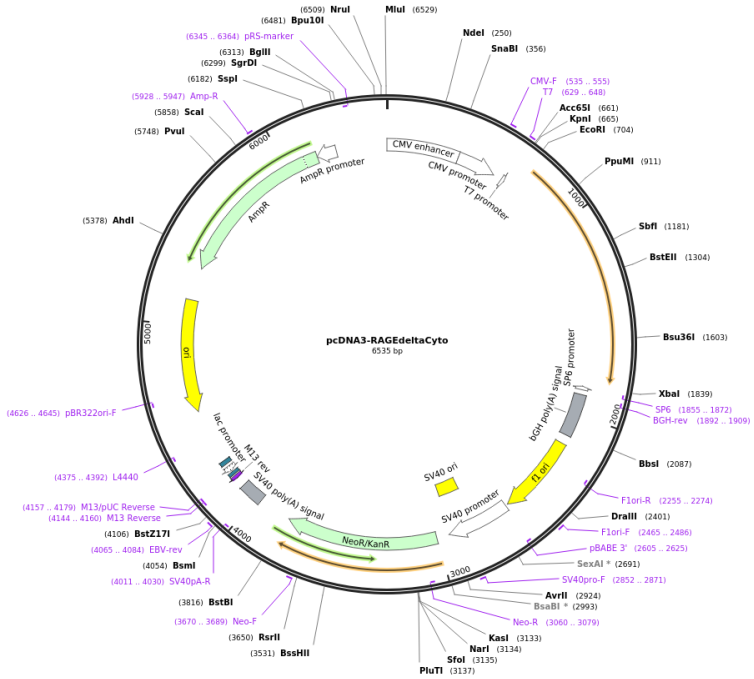

B

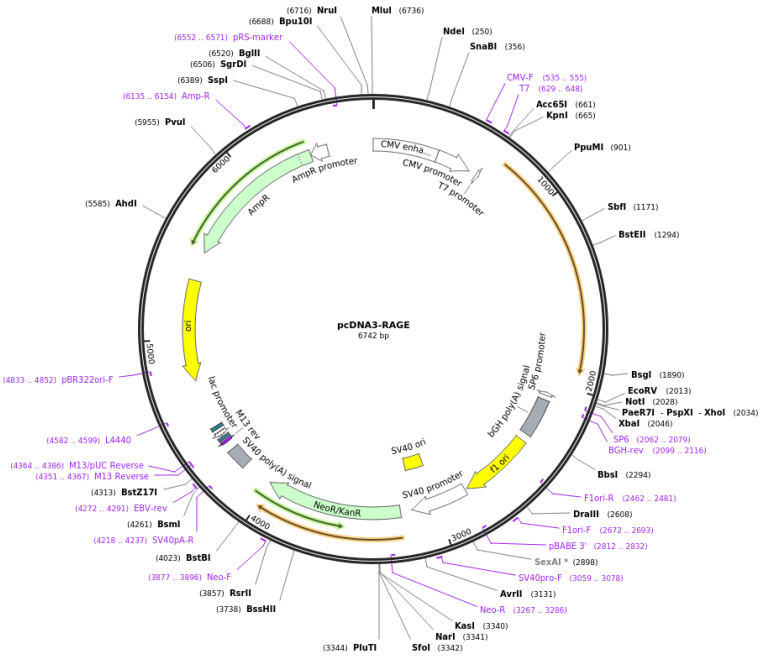

Figure 15. Full sequence map of the plasmid pcDNA3-RAGEdeltaCyto (A) and pcDNA3-RAGE (B).

3. IMMUNOASSAYS

3.1. Protein analysis by Western blot

Electrophoresis was performed to separate the proteins depending on their mass. Specifically, we used gels at 12% poly-acrylamide (#1610158, Bio-Rad) or 8% to detect RAGE oligomers. The gel contains two parts, the stacking which compacts the proteins to enter at the same time to the other part of the gel, and the resolving, that separate the proteins depending on their molecular weight. To avoid that the structure of the proteins and their charge effect on the electrophoresis, the detergent SDS (#A0675, PanReac Applichem) and the reductor agent DTT (#17-1318-02, GE Healthcare) were mixed with proteins. To analyze RAGE oligomers, DTT was not added to avoid disruption of disulfide bonds. The resolving gel was prepared with 1.5M Tris pH 8.8, poly-acrylamide, SDS, APS (#A3678, Sigma) and TEMED (#T22500, Sigma) mixed with dH_2O. The stacking gel contained 1M Tris pH 6.8, poly-acrylamide, SDS, APS and TEMED mixed with dH_2O.

30μg of protein lysate (section 1.10) were mixed with the loading buffer 5X with or without DTT (225mM Tris pH6.8, 50% glycerol (#G7893, Sigma), 5% SDS, 0.075% bromophenol blue (#17-1329-01, GE Healthcare) and 0.26M DTT, heated for 5 minutes at 96ºC, followed by 5 minutes on ice incubation, and loaded into the gel. A molecular weight marker (#1610374, BioRad) was used as control of the different proteins' molecular weights. After electrophoresis, proteins were transferred to polyvinylidene difluoride (PVDF) membrane (#IPVH00010, Millipore) for 2h at 100V. The membrane was blocked with 5% dry milk in 0.1% PBS-Tween (#P7949, Sigma) for 1h at RT and incubated overnight at 4ºC with the appropriate primary antibodies (Table 4).

The following day, the membrane was washed twice with 0.1% PBS-tween (Sigma) for 10 minutes and incubated for 1h with a horseradish peroxidase–conjugated anti-rabbit or anti-mouse antibody (Table 5) at RT. Immunodetection was performed using SuperSignal West Pico Plus Chemiluminiscent substrate (#34580, Thermo

Fisher Scientific) and visualized with the Imager600 instrument and analyzed using Image J software.

Protein	Antibody	Manufacturer	Specie	Dilution	Dilution buffer
Phospho-ERK1/2 (Tyr202/204)	9101	Cell signaling	rabbit	1:4000	BSA 5%
ERK1/2	9102	Cell signaling	rabbit	1:1000	milk 2%
Phospho-NF-kB (Ser536)	3031	Cell signaling	rabbit	1:1000	BSA 5%
NF-kB	Ab32536	Abcam	rabbit	1:1000	milk 2%
Phospho-SMAD2 (Ser465/467)	3108	Cell signaling	rabbit	1:1000	BSA 5%
SNAIL1	3879	Cell signaling	rabbit	1:1000	BSA 5%
SNAIL2	9585	Cell signaling	rabbit	1:1000	milk 2%
ZEB1	GTX105278	GeneTex	rabbit	1:1000	milk 2%
Phospho-cortactin (Tyr421)	44-854G	invitrogen	rabbit	1:1000	BSA 5%
RAGEe	sc-80652	Santa Cruz	mouse	1:1000	milk 2%
RAGEi	Ab3611	Abcam	mouse	1:1000	milk 2%
Claudin-1	GTX134842	GeneTex	rabbit	1:1000	milk 2%
ZO-1	GTX08592	GeneTex	rabbit	1:1000	milk 2%
Vinculin	V9131	Sigma	mouse	1:1000	milk 2%
β-Actin	A2228	Sigma	mouse	1:10000	milk 2%
α-Tubulin	T9026	Sigma	mouse	1:10000	milk 2%

Table 4. List of primary antibodies used for protein detection by western blot.

Antibody	Reference	Manufacturer	Dilution	Dilution buffer
Anti-mouse	NA931	GE Healthcare	1:1000	milk 2%

Anti-rabbit	NA934	GE Healthcare	1:1000	milk 2%

Table 5. List of secondary antibodies used in western blot.

3.2. Immunofluorescence of 2D culture

Cells were seeded on previously collagen-coated glass coverslips. Specifically, coverslips were coated with collagen (Gibco) (1:100 in PBS) for 1h in the incubator at 37ºC. To analyze the effect of the recombinant human proteins in the cortactin, 24h before fixation, cell media was replaced with serum-free media and cells were treated with the indicated concentration for 24h (see section 1.3). For acidic conditions, cells were exposed to 24h acidosis to analyze RAGE, cortactin, SNAIL1, β-catenin and DIAPH1 expression. To analyze the effect of RAGE antagonists, MDA-MB-231 and BT549 cells were treated with DMSO, 30 µM FPS-ZM1 or 2 µM Azeliragon for 72h before analyzing cortactin, SNAIL1 and β-catenin expression. To analyze the effect of RAGE antagonists and TGF-β1 on β-catenin and E-cadherin expression, NMuMG cells were treated for 72h with DMSO, 30 µM FPS-ZM1 or 1 µM Azeliragon 72h followed by 24h TGF-β1 treatment keeping the antagonists' treatment. Cortactin, β-catenin and ZO-1 expression were analyzed in RAGE knockdown cells.

After treatments, cells were washed twice with PBS and fixed with 4% PFA (#sc-281692, Santa Cruz) 30 minutes incubation. For protein detection, cells were permeabilized with 0.1% triton X-100 (#T9284, Sigma- Aldrich) 15 min incubation, except for the extracellular RAGE analysis in which cells were not permeabilized. Then cells were washed twice in PBS and coated with 3% BSA (#A2058, Sigma-Aldrich) for 1h to block the unspecific antibody binding sites. Primary antibodies (Table 6) were prepared in 3% BSA, and incubated O/N at 4ºC.

Antibody	Reference	Manufacturer	Specie	Dilution
Cortactin	Sc-55579	SantaCruz	Mouse	1:150
β-catenin	610154	BD	Mouse	1:100

SNAIL1	3895	Cell signaling	Mouse	1:100
RAGE	AF1145	R&D system	goat	1:15
DIAPH1	610848	BD	mouse	1:100
ZO-1	33-9100	Invitrogen	Mouse	1:100
E-cadherin	3195	Cell signaling	Rabbit	1:200

Table 6. List of primary antibodies used for protein detection by immunofluorescence.

The following day, primary antibody was removed and coverslips were washed twice with PBS for 10 minutes and incubated 1h at RT with the appropriate secondary antibody (1:250) (Table 7). Then, after two washes with PBS, coverslips were mounted on the slide using a specific mounting-media with DAPI (#P36966 Invitrogen).

To stain both the extracellular domain of RAGE and the intracellular cortactin, cells were incubated 1h with BSA 3% to block the unspecific antibody binding sites followed by anti-RAGE antibody incubation O/N at 4ºC (Table 6). The following day, the antibody was washed twice with PBS for 10 min and incubated 1h with the secondary antibody at RT (Table 7). After two washings, cells were fixed with 10 min 4% PFA incubation. Then, cells were permeabilized with 15 min 0.05% triton X-100 (Sigma) incubation and blocked with 3% BSA. Primary antibody for cortactin was incubated O/N at 4ºC (Table 6). The following day, after incubation with the specific secondary antibody (Table 7), coverslips were mounted as previously described.

Antibody	**Wave-length**	**Reference**	**Manufacturer**	**Specie**
Anti-Rabbit	Alexa Fluor 488	A11008	Invitrogen	Goat
Anti-Mouse	Alexa Fluor 488	A21200	Invitrogen	Goat
Anti-Mouse	Alexa Fluor 594	A11032	Invitrogen	Goat
Anti-Goat	Alexa Fluor 488	A21467	Invitrogen	Chicken

Table 7. List of secondary antibodies used for immunofluorescence detection.

3.3. Immunofluorescence of 3D culture

Tumoroids grown in Matrigel were washed carefully twice with cold PBS and fixed at RT for 1h with 4% PFA. Then, organoids were incubated with Corning cell recovery solution (#45354253, Cultek) for 20 minutes on ice to recover cells from Matrigel matrix. After two washes, cells were permeabilized 3h with 1% triton X-100 (Sigma) in PBS. Then, triton X-100 was removed following by two washings with PBS, and blocked in PBS + 3% BSA + 0.1% Tween (Sigma) for 1h to reduce unspecific antibody binding sites. Finally, phalloidin (1:1000) and Hoechst (1:10000) (Sigma-Aldrich) staining was done with 15 minutes incubation at RT and after two washings with PBS, coverslips were mounted with mounting media Prolong (Invitrogen).

3.4. Microscopy and fluorescence analysis

An Olympus FluoView FV1000 Confocal Microscope was used to visualize fluorescence staining and gelatin degradation and acquire images from more than eight representative fields of each sample. Pictures were acquired at magnification 60x with an oil immersion objective lens. Protein staining was quantified using Image J software.

4. TUMORIGENESIS AND METASTATIC ASSAYS

8-weeks old female-immunodeficient NOD-SCID mice (Charles River Laboratories) were maintained in pathogen-free conditions. $5x10^6$ of MDA-MB-231 cells previously transfected for luciferase were mixed in 100 µL of a solution 1:1 of PBS and Matrigel (#356234, Corning) and injected into the mammary fat pad. Two experimental arms were performed randomly: vehicle (10% DMSO, 40% PEG300, 5% Tween-80 and 45% PBS), and 5 mg/kg Azeliragon arm. Treatments were administered with IP injection 6 days a week. Mice weight was monitored every week. Tumor growth was monitored twice a week by caliper and tumor volume was measured using the formula $D \cdot d^2/2$, where *D* is the major diameter and *d* the minor diameter of the tumor. When the volumes reached 300-400 mm^3, the primary tumors were excised

and fixed in 4% formaldehyde (#VWRC9713.5000, VWR) overnight and embedded in paraffin for hematoxylin and eosin staining. Metastasis were controlled every week using IVIS Spectrum imager. When animals reached the endpoint, organs were examined for the presence of metastatic foci by *ex-vivo* bioluminescence imaging. Positive organs for bioluminescence were washed with PBS, fixed in formaldehyde (VWR) and embedded in paraffin for hematoxylin and eosin staining. Animal care was handled in accordance with the Guide for the Care and Use of Laboratory Animals of the Vall d'Hebron University Hospital Animal Facility, and the Animal Experimentation Ethical Committee at the institution-approved experimental procedures.

5. STATISTICAL ANALYSIS

Graphs and statistical analysis were performed using GraphPad Prism 8 software. Data from replicate experiments are shown as mean values ± standard deviation. Comparisons between groups were analyzed by a two-tailed Student *t* test, one-way ANOVA or two-way ANOVA, as appropriate. A *p*-value < 0.05 was considered statistically significant (*p<0.05; **p<0.01; ***p<0.001 and ****p<0.0001 as it is represented in the figures).

6. PROTEOMICS

Digestion (section 6.1.) and liquid chromatography (LC-MS/MS) (section 6.2) of the collected secretome (see section 1.6) was performed by the Proteomic facility at VHIO.

6.1. In-solution Digests

Samples were in-solution digested previous to HPLC-MS analysis. Fifteen micrograms of each secretome preparation were first dissolved in 50% 2,2,2-Trifluoroethanol and reduced with tris(2-carboxyethyl)phosphine hydrochloride to a final concentration of 5mM for 1h at 60°C, and alkylated in 10mM of Iodoacetic acid at 25°C for 20min. Before trypsin digestion, samples were diluted with 50mM of

ammonium bicarbonate to a final concentration of 10% 2,2,2-Trifluoroethanol. Then proteins were digested in a ratio of 1:20 (w/w) with trypsin for 5h at 37°C. The reaction was stopped with formic acid (FA). After digestion samples were cleared at 10,000 rpm for 10min, dried, and re-dissolved in 30% acetonitrile, 0.1% FA to a final concentration of 1µg/µl before liquid chromatography (LC)-MS analysis

6.2. Liquid chromatography-Mass spectrometry analysis (LC-MS/MS)

Tryptic digests were analyzed using a linear ion trap Velos-Orbitrap mass spectrometer (Thermo Fisher Scientific, Bremen, Germany). Instrument control was performed using Xcalibur software package, version 2.2.0 (Thermo Fisher Scientific, Bremen, Germany). Peptide mixtures were fractionated by on-line nanoflow liquid chromatography using an EASY-nLC 1000 system (Proxeon Biosystems, Thermo Fisher Scientific) with a two-linear-column system. Samples were first loaded onto a trapping guard column (Acclaim PepMap 100 nanoviper, 2 cm long, ID 75 µm and packed with C18, 3 µm particle size from Thermo Fisher Scientific) at 4uL/min. Then, samples were separated on the analytical column (Dr Maisch, 25 cm long, ID 75 µm, packed with Reprosil Pur C18-AQ, 3 µm particle size). Elution was performed using 0.1% formic acid in water (mobile phase A) and acetonitrile with 0.1% formic acid (mobile phase B), with a linear gradient from 0 to 35% of mobile phase B for 120 min at a flow rate of 300 nL/min. Ions were generated applying a voltage of 1.9 kV to a stainless-steel nano-bore emitter (Proxeon, Thermo Fisher Scientific), coupled to end of the analytical column, on a Proxeon nano-spray flex ion source.

The LTQ Orbitrap Velos mass spectrometer was operated in data-dependent mode. A scan cycle was initiated with a full-scan MS spectrum (from m/z 300 to 1600) acquired in the Orbitrap with a resolution of 30,000. The 20 most abundant ions were selected for collision-induced dissociation fragmentation in the linear ion trap when their intensity exceeded a minimum threshold of 1000 counts, excluding singly charged ions. Accumulation of ions for both MS and MS/MS scans was performed in the linear ion trap, and the AGC target values were set to 1×10^6 ions for survey MS

and 5000 ions for MS/MS experiments. The maximum ion accumulation time was 500 and 200 ms in the MS and MS/MS modes, respectively. The normalized collision energy was set to 35%, and one microscan was acquired per spectrum. Ions subjected to MS/MS with a relative mass window of 10 ppm were excluded from further sequencing for 20 s. For all precursor masses a window of 20 ppm and isolation width of 2 Da was defined. Orbitrap measurements were performed enabling the lock mass option (*m*/*z* 445.120024) for survey scans to improve mass accuracy.

6.3. Protein identification and quantitative differential analysis.

LC-MS/MS data were analyzed using the Proteome Discoverer v. 2.1 software (Thermo Fisher Scientific). Proteins were identified using Mascot v. 2.5 (Matrix Science, London UK) to search the SwissProt database (2018_11, taxonomy restricted to human proteins, 20,413 sequences). MS/MS spectra were searched with a precursor mass tolerance of 10 ppm, fragment tolerance of 0.7 Da, trypsin specificity with a maximum of 2 missed cleavages, cysteine carbamidomethylation set as fixed modification and methionine oxidation as variable modification.

Files generated from Mascot (.DAT files) were loaded into Scaffold (version 3.00.07; Proteome software, Inc., Portland, OR), resulting in a no redundant list of identified proteins per sample. Peptide identification was given as valid as long as a PeptideProphet probability greater than 95% was determined. Those proteins whose identification could be established with a probability higher than 95% and contained at least two identified spectra were accepted. Using these filters, a false protein discovery rate (FDR) below 1.0%, as estimated by a database search, was achieved. The generated "scaffold" files containing all the "spectral counts" (SpC) for each sample and their replicates were exported to the POMAcounts 1.1.0 software for normalization and statistical analysis (see section 6.4).

6.4. Secretomes statistical analysis

All statistical normalizations and calculations of proteomic data were performed using the software POMAcounts 1.1.0. Exploratory data analysis was performed using principal component analysis (PCA) and hierarchical clustering of the samples in the SpC matrix to find possible outliers and patterns in the data. For statistical modeling, a GLM model based on the Poisson distribution was used as a statistical test. Adjusted *p*-value < 0.05, fold change > 0.8 and number spectral counts (SpC) > 2 thresholds were applied during the analysis.

RESULTS

1. MODELING TUMOR MICROENVIRONMENTAL STRESS IN THE CONTEXT OF TUMOR INVASION

Previous cancer research studies, demonstrated that the tumor microenvironment tends to be hypoxic as a consequence of the higher rate proliferation of tumor cells and poor blood perfusion. Tumor cells under hypoxia up-regulate glycolysis to produce energy, even when hypoxia is reversed. This phenomenon is known as the Warburg effect. The increased rate of glycolysis leads to microenvironmental acidosis, which has been associated to tumor aggressiveness [21]. Here, we decided to study the effect of microenvironmental stresses on breast cancer secretomes to identify new candidate drug targets.

1.1. Studying migration and invasion in breast cancer (BC) cell lines during chronic and acute stress

In order to study the effect of microenvironmental stresses on tumor cell invasion and migration, we generated subpopulation of BC cells subjected to chronic microenvironmental stresses. Specifically, we used two different breast cancer cell lines: MDA-MB-231, MCF-7, which represent different BC subtypes. The MDA-MB-231 cell line belong to the triple negative breast cancer (TNBC) subtype, meaning that they do not express hormone receptors (ER, PR) and HER2. These cells have a mesenchymal phenotype and are very aggressive *in vitro* and *in vivo*. MCF-7 cells belong to the ER+ subtype. This cell line expresses both estrogen (ER) and progesterone (PR) receptors, and have an epithelial phenotype.

The microenvironmental stresses induced in this project were acidosis and nutrient starvation. To generate the corresponding subpopulations, the pH of the media was reduced from 7.4 until 6.5 for chronic acidosis, and the FBS was reduced from 10% until 1% for nutrient deprivation during 6 and 8 weeks respectively, until reaching the final conditions (pH 6.5 and FBS 1%). Then, we analyzed the invasive capacity of the subpopulations (growing either at pH 6.5 or at 1% FBS) using the transwell assay. As observed in figure 16A, these cells were less invasive than cells grown in normal conditions. These results could be explained by the fact that cells under chronic

stress have a hard time to survive. Evidence of it was an increase of vacuoles in the cytoplasm (Fig. 16B). Besides the lack of invasion capacity, cells under a chronic stress showed a decreased proliferation rate near 20-30%, especially MDA-MB-231 cells. The results suggest that cells under chronic treatment try to survive rather than being more aggressive.

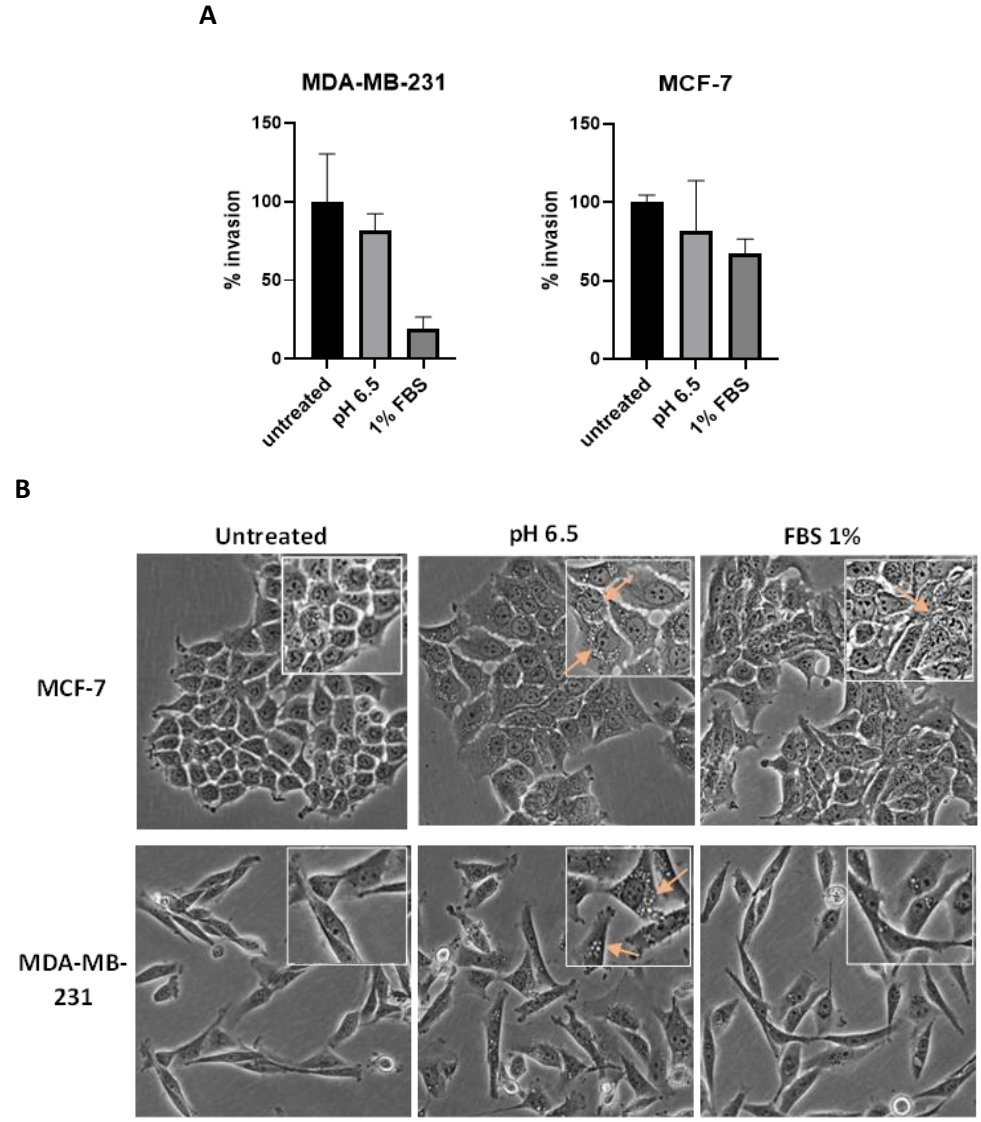

Figure 16. Subpopulation generated with chronic acidosis and nutrient starvation. (A) Graphs showing the percentage of invasion at 24h measured with a transwell assay of MDA-MB-231 and MCF-7 subpopulation. **(B)** Cell pictures showing the specific morphology of MCF-7 and MDA-MB-231 cells after induced chronic acidosis (pH 6.5) and nutrient starvation (1% FBS). The vacuoles generated under chronic acidosis are highlighted with the arrows

Then, we hypothesize that cells responsible for tumor invasion and metastasis *in vivo* should be the ones located at the edge of the tumor. In this region, cells probably experience acute stresses rather than chronic environmental stress, which is more characteristic of the inner part of the tumor. To test this hypothesis, we decided to study the effect of acute stress on three different microenvironmental conditions: acidosis, hypoxia and glucose starvation. In this specific study, we also added a third cell line, the MCF10A cells, which are derived from a fibroadenoma and they are non-tumorigenic.

For induced acidosis experiments, cells were maintained at either pH 7.4 or pH 6.5 for 16h in MDA-MB-231 cells and for 24h in MCF-7 and MCF10A cells. We observed that acidosis induced an increase in the invasive capacity of the three cell lines (Fig. 17A). Similar results were obtained after inducing 24h of hypoxia (0.5% O_2). Under hypoxia, MDA-MB-231 and MCF-7 cells were more invasive than in normoxic conditions. However, the effect of hypoxia on MCF10A cells was not statistically significant as it was in the other two cell lines (Fig. 17B). Glucose starvation was induced using a specific media without glucose for 24h supplemented with 5% FBS. Absence of glucose increased the invasion capacity of MDA-MB-231 and MCF-7 cells through the Matrigel matrix. However, the differences for MCF-7 cells were not statistically significant.

A

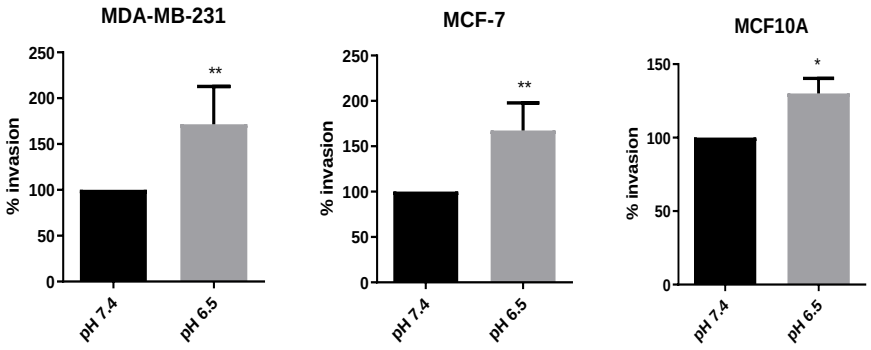

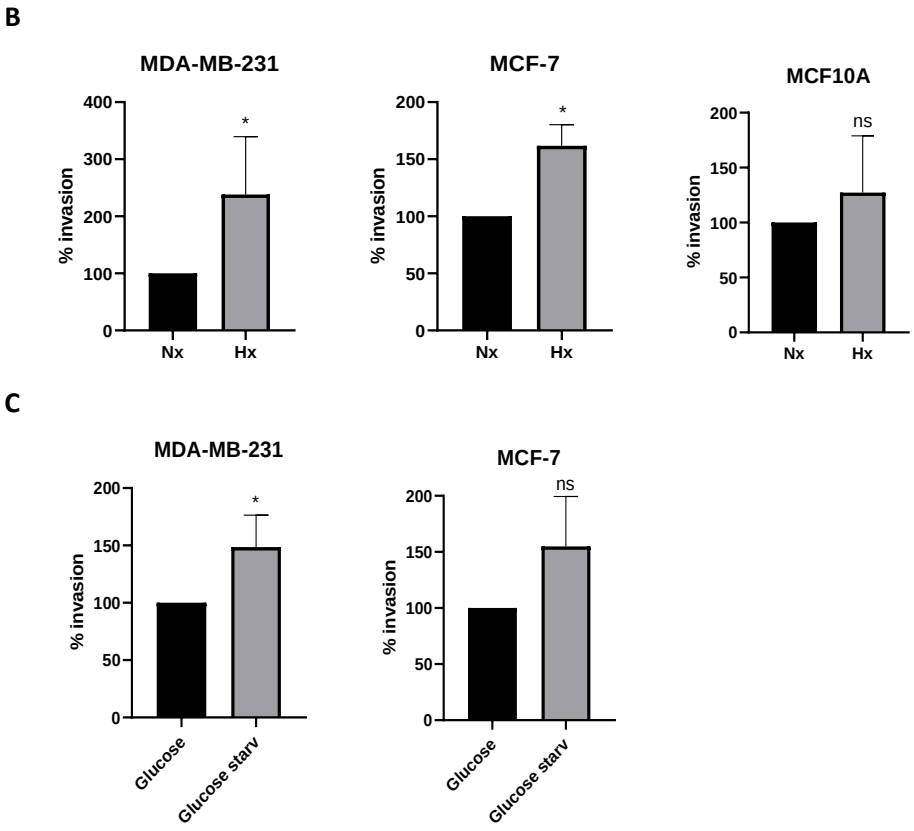

Figure 17. Acute stress increases cells invasion. Graphs showing the percentage of invasion of MDA-MB-231, MCF-7 and MCF10A cells treated with different acute stresses: acidosis **(A)**, hypoxia **(B)** and glucose starvation **(C).** Statistical analyses were done using unpaired t-test. *p<0.05; **p<0.01, ns=not significant. Normoxia (Nx), Hypoxia (Hx), glucose starvation (Glucose starv.).

Since acidosis was the stress condition that induced the highest increase in cell invasion, we decided to analyze how it affects cell migration. We used cortactin subcellular localization as a read-out of cell migration. Cortactin is an actin-binding protein associated to cell migration and invasion, which accumulates in the lamellipodia, invadopodia and membrane ruffles formed at the leading edge of the cells during migration [218–220]. In our case, we observed that after 24h of acidosis, cortactin was relocated to the plasma membrane (Fig. 18).

These data confirm that acute stress induces an increase in cell invasion and migration.

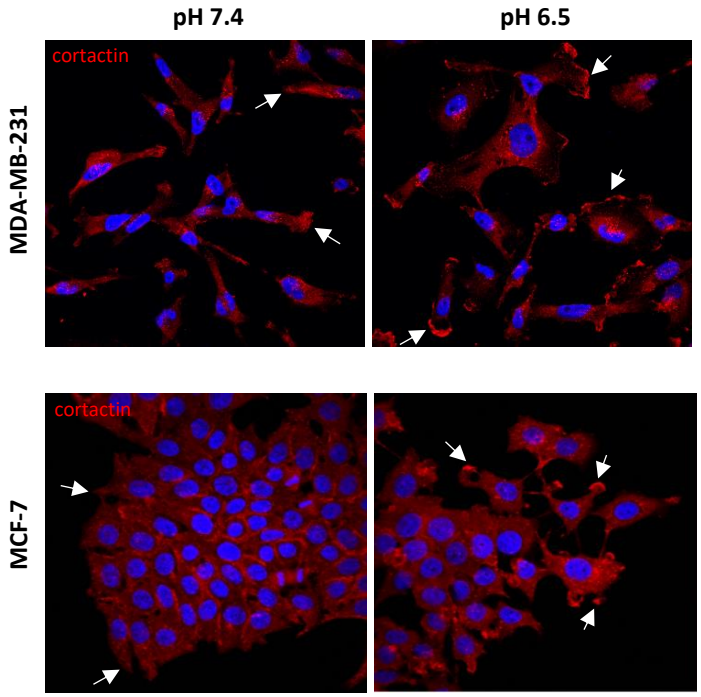

Figure 18. Cell migration is promoted by acute acidosis. Immunostaining of cortactin protein localized at the leading edge of the lamellipodia in MDA-MB-231 and MCF-7 cells treated for 24h with acidosis. The cortactin localization in the different acidosis conditions (pH 7.4 and pH 6.5) is highlighted with arrows.

1.2. Profiling the secretomes of acute stress-tolerant BC subpopulation

Once we demonstrated that microenvironmental stresses increase the invasive phenotype of tumor cells, next step was to identify proteins unconventionally secreted that could be linked to this increase in invasiveness. To do that, we generated secretomes from the considered three cell lines under the acute stresses described above. The secretome is a sub-proteome made of proteins present in the extracellular space. The cancer secretome contains conventional and unconventional secreted proteins that tumor cells use to communicate with each other and their tumor microenvironment during tumorigenesis. Recent reports [187,221] have evidenced that there are intracellular proteins with alternative extracellular functions, suggesting that new protein functions associated with alternative subcellular localizations might be implicated in tumorigenesis.

We generated 24h-secretomes from the three cell lines with or without acidosis or hypoxia. For glucose starvation, secretomes were obtained at 7h treatment, since cells did not survive for a longer time without glucose and FBS. Since secretomes collected at 7h are more difficult to analyze due to the lower number of proteins present, we decided to focus on the secretomes from acidosis and hypoxia conditions.

After collecting and concentrating the secretomes, we analyzed them by label-free LC-MS/MS on an LTQ-Orbitrap Velos mass spectrometer at the VHIO Proteomics Core Facility. After protein identification using the Mascot algorithm, the secretome data was uploaded into the Scaffold 3.0 software (Proteomic Software) for the validation of the protein identification and quantification. Next, the secretome profiles were uploaded into the statistical environment R for differential secretion statistical analysis using two workflows developed in the laboratory [222]. The first workflow, called Exploratory Data Analysis (EDA), does an exploratory analysis using unsupervised tools including hierarchical clustering and principal component analysis (PCA). EDA also performs a batch effects correction to account for the effect of environmental factors on the mass spec analysis, providing that an appropriate experimental design was used. These analyses, through the use of visualization tools such as PCA, allow us to check the quality of the data. The principal components (PC1 and PC2) in the PCA quantify the amount of variance explained by the dataset. The PC1 is always the axis that explain more variance in the dataset, and in our case, separates samples by biological condition (stress) (Fig. 19 and 20). Given these premises, the EDA analysis showed that the triplicates of our secretomes were similar among them.

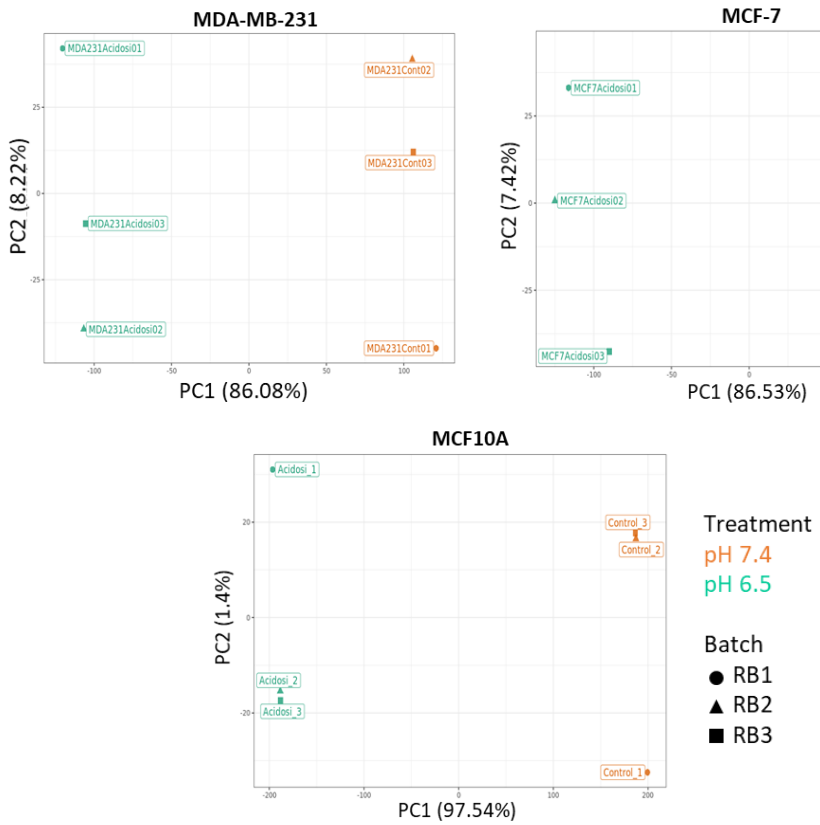

Figure 19. PCA analysis of secretomes collected after treatment with or without acidosis. PCA analysis after a batch effect normalization of the secretomes profiles from the three breast cancer cells lines (MDA-MB-231, MCF-7 and MCF10A) treated with or without 24h acidosis. Green represents the triplicates of cells treated at pH 7.4 and orange the triplicates of cells treated at pH 6.5. Each triplicate is represented with a circle, triangle and square.

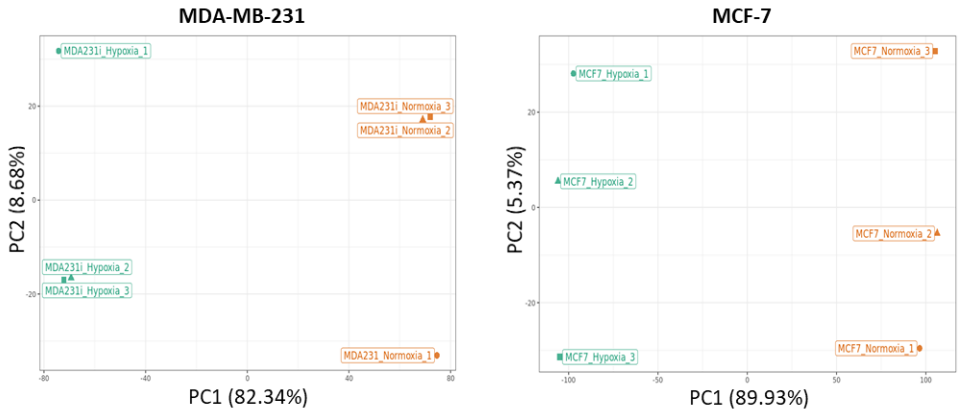

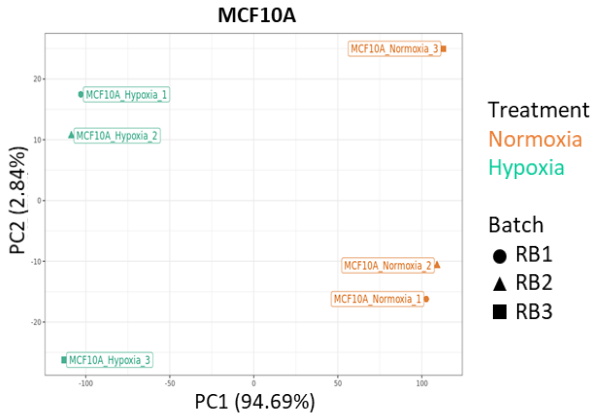

Figure 20. PCA analysis of secretomes collected after treatment with or without hypoxia. PCA analysis after a batch effect normalization of the secretomes profiles from the three breast cancer cells lines (MDA-MB-231, MCF-7 and MCF10A) treated with or without 24h hypoxia. Green represents hypoxic triplicates and orange the normoxic triplicates. Each triplicate is represented with a circle, triangle and square.

In the second workflow, we performed inferential statistics by modeling the spectral counts data using Poisson statistics. The goal was to find differentially secreted proteins between the control and the test condition for each of the different microenvironmental stresses assayed in our project. By setting three different thresholds (minimum signal ≥ 2 spc; log2 fold change ≥ 0.8; and p-value ≤ 0.05), we obtained lists of proteins that were over-secreted in our experiments [222]. Figure 21 shows the heatmaps of the differentially secreted proteins during 24h of acidosis (Fig. 21A) or hypoxia (Fig. 21B) for the three cell lines tested after setting the thresholds mentioned above.

The total number of proteins secreted was higher in breast cancer cell lines (near 1200 proteins for both stresses), than in the non-tumorigenic cell line (843 in acidosis and 588 in hypoxia). The number of proteins was consequently reduced after setting up the thresholds. Under acidosis the number of proteins significantly over-secreted were 164, 70 and 98 respectively for MDA-MB-231, MCF-7 and MCF10A. However, under hypoxic conditions the number of proteins significantly differentially secreted were 21, 28 and 83 respectively for the same cell lines mentioned before. Therefore, acidosis induces more differences in protein secretion than hypoxia.

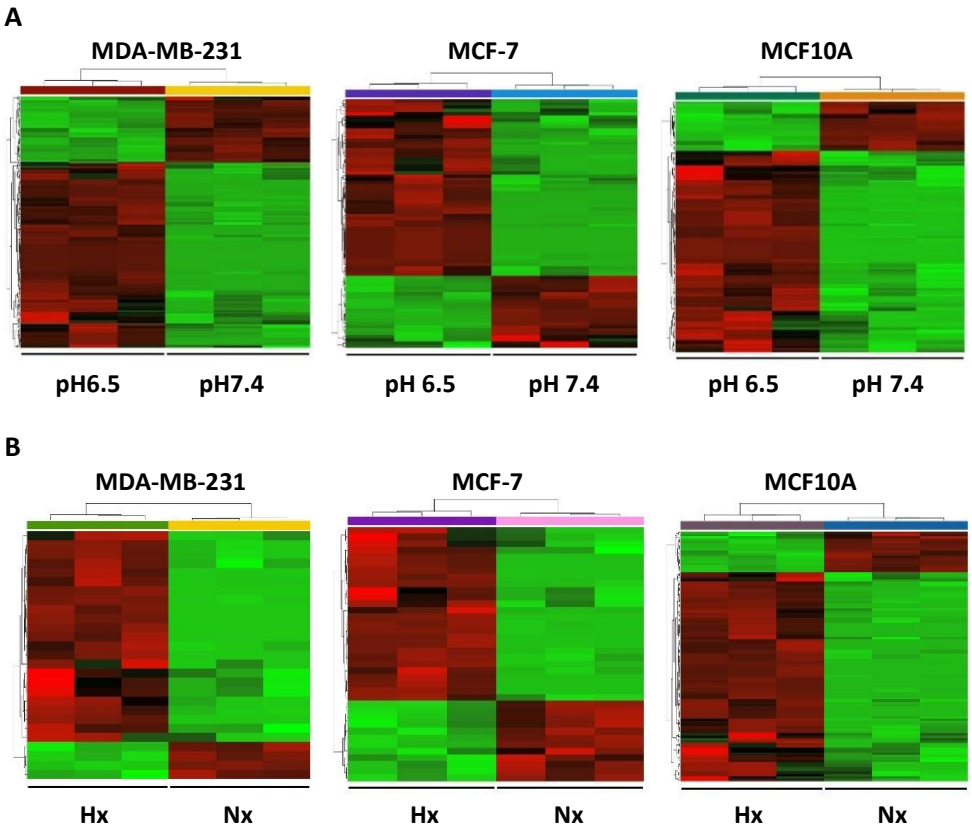

Figure 21. Proteins significantly secreted in acute stress conditions. Heatmaps show the proteins differentially secreted after setting the thresholds (minimum signal ≥ 2 spc; log2 fold change ≥ 0.8; and p-value ≤ 0.05) in MDA-MB-231, MCF-7 and MCF10A cells. **(A)** Cells treated 24h with or without acidosis (pH 7.4 and pH 6.5). **(B)** Cells treated 24h under normoxia (Nx) or hypoxia (Hx). In red are the proteins over-secreted and in green the proteins under-secreted.

When we analyzed the list of significant proteins over-secreted during acidosis, we observed differences in groups of proteins unconventionally secreted, like the high mobility group (HMG) family proteins. Although some of the HMG proteins were not significantly over-secreted, there was a clear tendency in the over-secretion of the HMG family of proteins during acute acidosis (Table 8). We also detected a slight increase in some of the S100 proteins under acidosis, although none of them was significantly different (Table 8).

A

MDA-MB-231				
GeneName	MeanAcidosi	MeanControl	log2FC	p.value
HMGA1	25,46	16,62	0,64	0,014809685
HMGB1	16,36	8,85	0,92	0,007209651
HMGB2	14,06	8,8	0,7	0,050156199
HMGN3	7,39	5,52	0,38	0,418663642
HMGB3	2,98	0,02	33,59	0,000859414
HMGN1	2,75	0,31	3	0,012678745
HMGN5	2,33	0	33,4	0,001822955
S100A6	18,78	19,27	-0,05	0,860811242
S100A16	6,35	6,2	0	0,994481022
S100A4	5,29	6,89	-0,39	0,414248994
S100A11	4,68	5,23	-0,1	0,857410321
S100A13	3,59	1,74	1	0,190955503

B

MCF-7				
GeneName	MeanAcidosi	MeanControl	log2FC	p.value
HMGB1	27,39	15,45	0,84	0,001315766
HMGB2	16,34	11,02	0,57	0,075113312
HMGN1	14,98	12,35	0,28	0,372738122
HMGB3	10,04	3,92	1,32	0,004681886
HMGA1	9,04	1,68	2,44	4,47392E-05
HMGN3	7,66	4,69	0,83	0,092484378
S100A11	12,01	10,67	0,17	0,622880549
S100A16	8,35	8,05	0,06	0,882001296
S100A13	5,99	4,68	0,36	0,476137438
S100A14	3,36	5,71	-0,76	0,176768115

C

MCF10A				
GeneName	MeanAcidosis	MeanControl	log2FC	p.value
HMGB1	17,9	8,21	1,14	0,000823692
HMGA1	14,36	5,8	1,34	0,000645267
HMGB2	8,49	0,96	3,7	7.831426E-07
HMGN1	6,35	0,29	4,25	8,69036E-06
HMGA2	5,6	2,46	1	0,099354265
S100A2	13,92	10,81	0,36	0,29216916
S100A11	9,35	8,59	0,11	0,786356054
S100A10	6,23	5,26	0,34	0,492790659
S100A6	5,58	5,89	-0,08	0,865034374
S100A13	4,54	3,01	0,53	0,392856987
S100A16	4,46	2,2	1,22	0,069753608

Table 8. List of HMGs and S100 proteins secreted in acute acidosis. Tables show the gene name of the different HMGs and S100 proteins secreted during 24h acidosis in **(A)** MDA-MB-231, **(B)** MCF-7 and **(C)** MCF10A cells. Spectral counts in the control (third column) and acidosis (second column) conditions are shown. Besides, log2 fold change and p-value are also presented after normalization of the batch effect.

Volcano plots helped us to visualize the statistical differences of proteins secreted under microenvironmental acidosis (Fig 22) and hypoxia (Fig. 23).

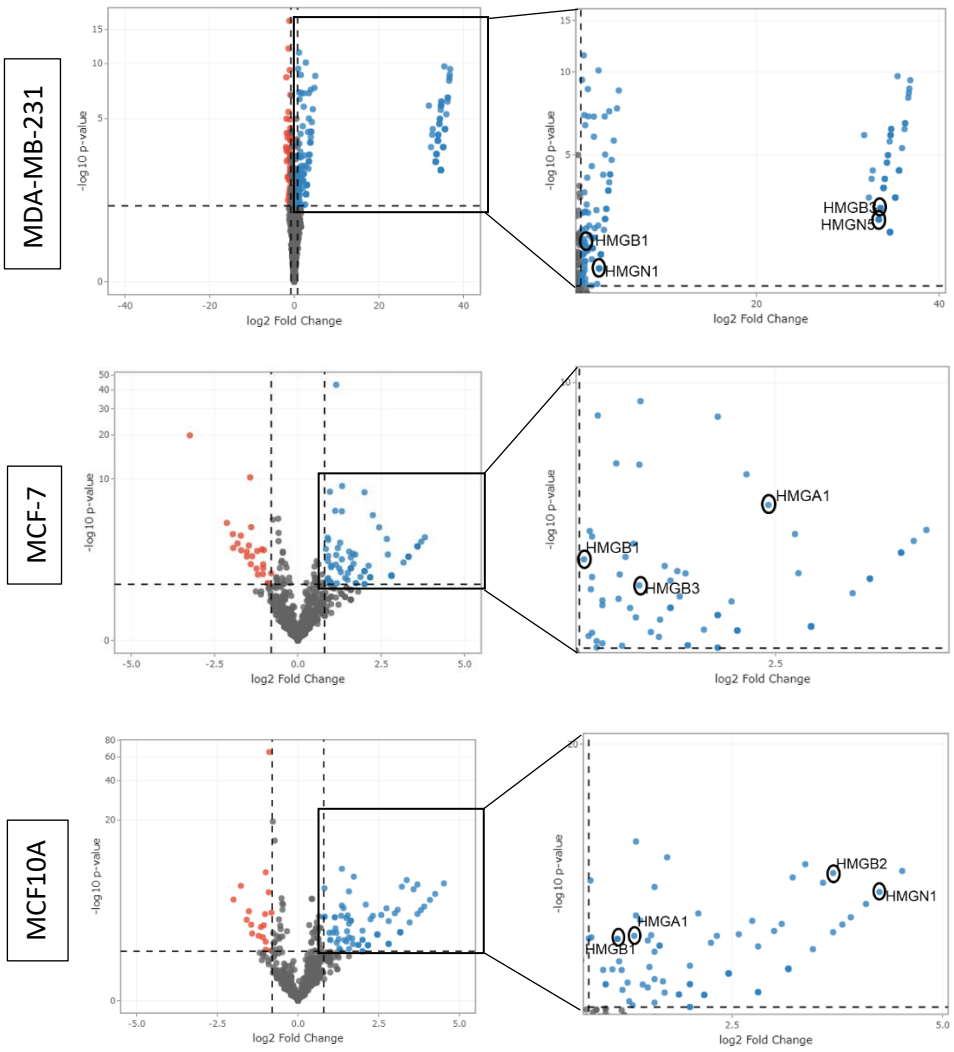

Figure 22. Proteins over- and under-secreted in acute acidosis. Volcano plots representing the significant proteins up-regulated and down-regulated after 24h acidic conditions in MDA-MB-231, MCF-7 and MCF10A secretomes. On the right, zoom of proteins over-secreted labeling the HMGs proteins. Red shows the proteins down-regulated; blue shows the proteins up-regulated, and grey shows the proteins not-significantly different based on the selected thresholds.

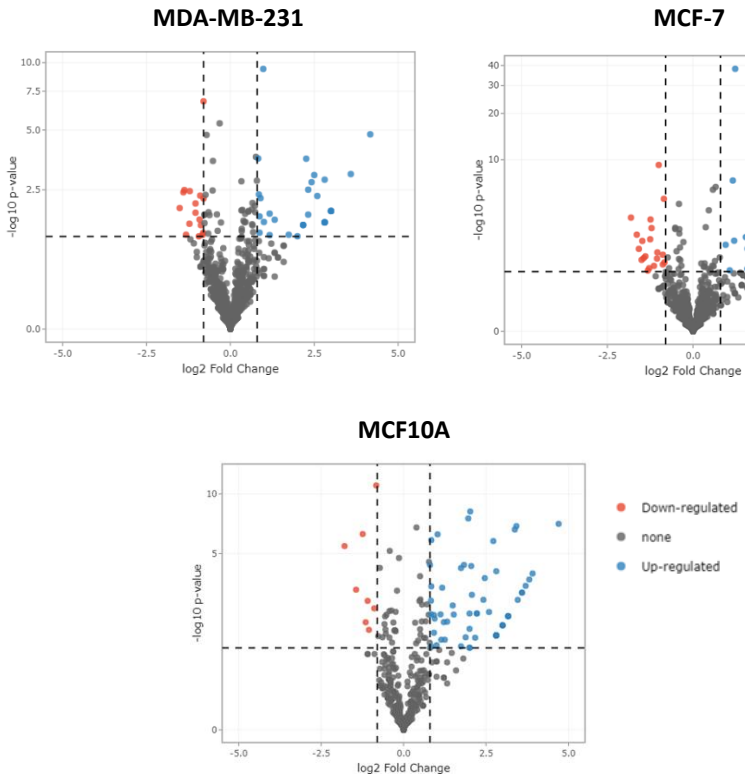

Figure 23. Proteins over and under-secreted in acute hypoxia. Volcano plots representing the proteins significantly up-regulated and down-regulated in the secretomes of MDA-MB-231, MCF-7 and MCF10A cells treated 24h in hypoxia. of hypoxic conditions. Red shows the proteins down-regulated; blue shows the proteins up-regulated, and grey the proteins not-significantly different based on the selected thresholds.

Taking into account that several of the unconventional proteins over-secreted in acidosis are RAGE-ligands (HMGs and S100 proteins), and considering previous studies in our lab indicating that extracellular HMGA1 promotes tumor invasion and metastasis through RAGE in TNBC [189], we decided to study the role of RAGE in breast cancer.

Altogether, the results obtained in breast cancer cells lines validate that acute microenvironmental stresses induce aggressiveness and increase the release of proteins unconventionally secreted. Besides, some of the proteins unconventionally over-secreted under acute acidosis in our experimental models are RAGE-ligands.

2. STUDYING THE ROLE OF RAGE ASSOCIATED TO MIGRATION AND INVASION IN TNBC CELLS

RAGE is a multi-ligand receptor activated during inflammation, which mediates different chronic diseases such as diabetes, Alzheimer's and cancer. The binding of ligands to RAGE activates different signaling pathways depending on the ligand and the cell type. In order to study the role of RAGE in tumor progression and metastases, we knocked-down the expression of RAGE in BC cell lines. We also treated BC cells with RAGE-ligands to study the transduction signaling pathways mediated by RAGE in our experimental models.

2.1. The down-regulation of RAGE decreases cell migration and invasion

In order to study the role of RAGE in breast cancer, we performed a knockdown of RAGE expression in MDA-MB-231 cells. Despite multiple initial attempts, we had several problems to generate a good knockdown using the stable expression of short-hairpins RNA (shRNA) against RAGE (Fig. 24A). Therefore, we also tried to down-regulate the expression of RAGE using other techniques including different siRNA sequences. However, the siRNA transfections done for 24h and 48h did not yield a decrease on RAGE expression (Fig. 24B). Then, we combined both siRNA and shRNA together by transfecting the shRAGE cells with siRNA for 24h. However, neither of these strategies was initially effective to down-regulate the expression of RAGE (Fig. 24C).

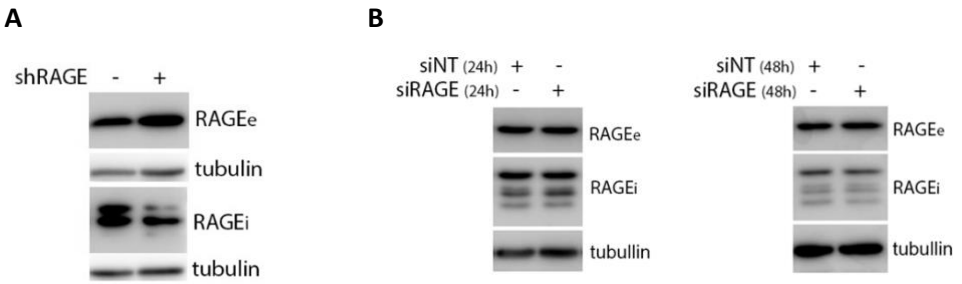

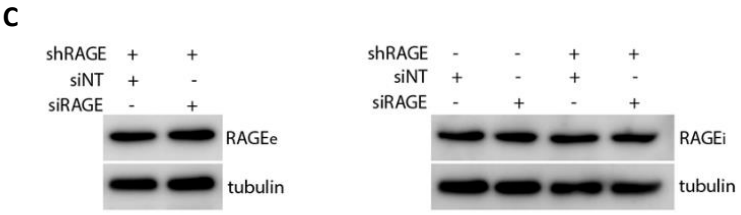

Figure 24. RAGE expression is not affected in shRAGE and RAGE siRNA cells. Western blots of the intracellular (RAGEi) and extracellular RAGE (RAGEe) expression in MDA-MB-231 cell lysates. **(A)** RAGE levels in RAGE knockdown cells generated after 2 lentiviral infections of 4h. **(B)** RAGE expression after 24h and 48h of RAGE siRNA transfection. **(C)** 24h of siRNA transfection in shRAGE cells. Tubulin was used as loading control.

Then, we tried a different strategy to down-regulate RAGE signaling by expressing a dominant negative of RAGE (DN-RAGE), which only contains the extracellular and transmembrane domains of RAGE protein, but lacks the intracellular region of the receptor. Therefore, this protein cannot activate RAGE downstream pathways [223]. As a control we used a plasmid that expresses the full length of the protein (FL-RAGE) which can activate the downstream effectors. Two concentrations of each plasmid (1 and 2 µg) were transfected and, as seen in figure 25A, cells transfected with 1 µg, showed a higher expression of the constructs. Those cells transfected with FL-RAGE and DN-RAGE, expressed high amounts of extracellular RAGE (RAGEe) compared to the endogenous RAGE levels (Fig. 25A). However, in our experiments there was no effect on the intracellular RAGE (RAGEi) expression. After observing that the transfection with 1µg of the plasmid worked, we expected a reduction in the signaling pathway of RAGE in cells transfected with the DN-RAGE compared to FL-RAGE. Strangely, there were no differences on the basal levels of ERK1/2 and NF-kB phosphorylation between DN-RAGE and FL-RAGE cells (Fig. 25B). The activation of the downstream signaling pathways did not change either when cells were treated with a RAGE-ligand such as rhS100A4 (Fig. 25C). Therefore, DN-RAGE cells did not behave as expected and we stopped this experimental strategy.

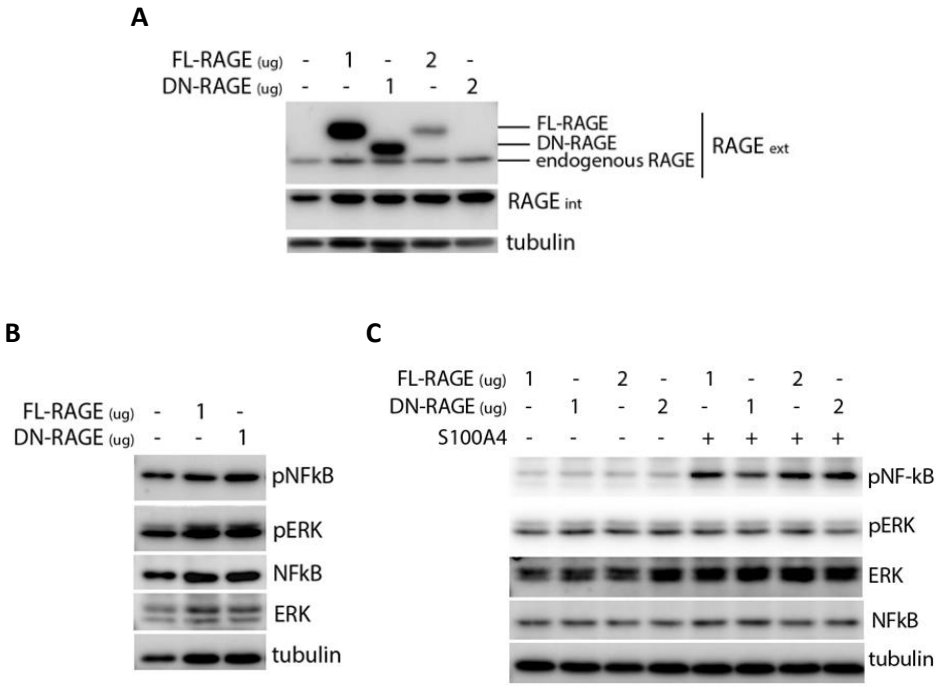

Figure 25. Dominant-negative of RAGE in MDA-MB-231 cells. (A) Western blot of intracellular and extracellular RAGE in DN-RAGE and FLRAGE cells. **(B)** RAGE signaling of DN-RAGE and FL-RAGE cells. **(C)** Activation of RAGE pathway of DN and FL-RAGE cells treated 1h with rhS100A4. Tubulin was used as loading control.

Finally, an overnight lentiviral infection of the shRAGE in MDA-MB-231 cells partially reduced the levels of RAGE protein expression (Fig. 26A). Fortunately, the shRAGE cells also showed significantly decreased levels of *AGER* mRNA. (Fig. 26B). Therefore, we used these cells to study the role of RAGE in cell invasion. Transwell assays showed that shRAGE cells had an impaired invasive ability compared to shControl MDA-MB-231 cells (Fig. 26C).

We also studied the effect of RAGE knockdown in 3D culture settings making tumoroids [224]. 3D culture is used for a broad range of applications such as basal lamina formation, extracellular matrix influence, cell differentiation, invasion and proliferation, protein expression as well as cells interactions with the extracellular matrix [225]. Specifically, in our study, 3D culture of MDA-MB-231 allows mammary cells to generate a more physiological-like structures similar as the branching

morphogenesis that happens in the mammary gland during puberty [226]. These extensions created by the migratory cells to form the branching are protuberances that we called protrusions. We observed that RAGE knockdown cells reduced the capacity of these cells to create protrusions in a Matrigel matrix (Fig. 26D).

Furthermore, when we looked at cortactin by immunofluorescence, we saw that in the shRAGE cells cortactin was relocated to the cytoplasm instead of being located in the plasma membrane (Fig. 26E). All these results collected using more physiologically conditions, confirm that RAGE is involved in tumor cell invasion and migration, since the down-regulation of RAGE generate cells with less invadopodia, lamellipodia and protrusion formation reducing their invasive capacity.

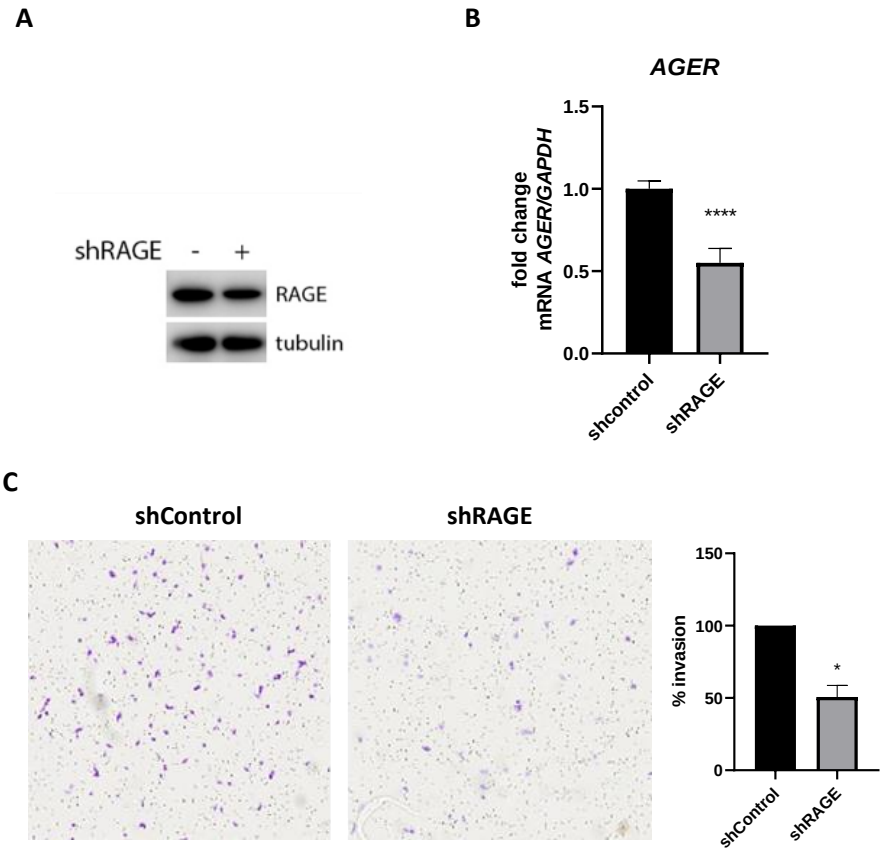

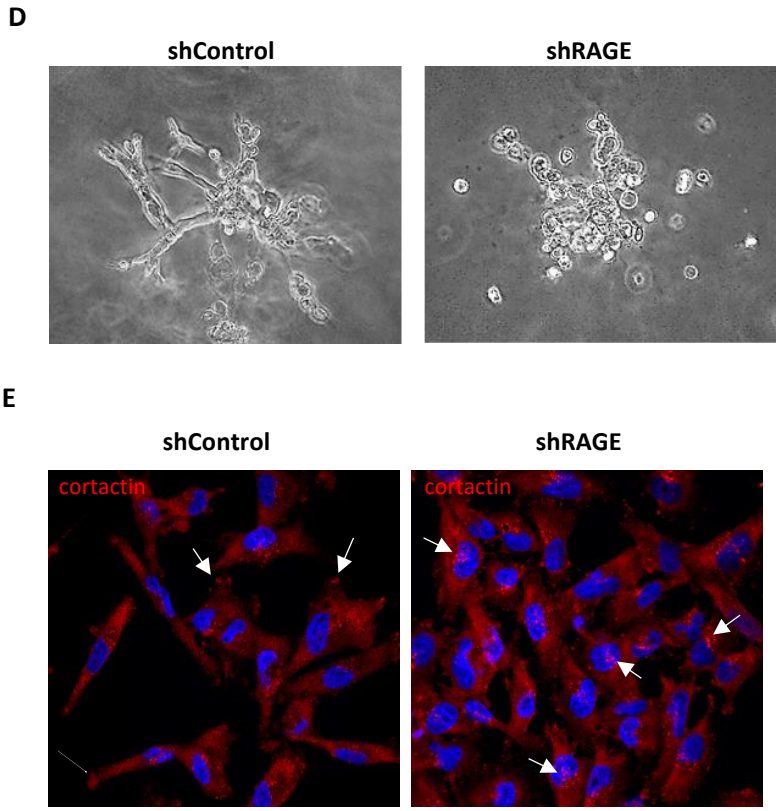

Figure 26. Knockdown of RAGE expression by shRNA reduces cell invasion and migration. Knockdown RAGE in MDA-MB-231 cells generated with a short-hairpin infection O/N. **(A)** Protein expression of RAGE by western in shRAGE and shControl cells. Tubulin was used as loading control. **(B)** *RAGE* mRNA expression after knockdown infection O/N of RAGE. **(C)** Analysis of the effect in invasiveness of shRAGE cells using transwell assay**. (D)** Tumoroids from knockdown RAGE cells growing in Matrigel 3D-culture. **(E)** Differences in cortactin (red) localization between shControl and shRAGE cells. Statistical analyses were done using unpaired t-test. *p<0.05; ****p<0.0001

2.2. The activation of RAGE induces migration in MDA-MB-231 cells

We studied the effect of different RAGE-ligands in cell migration by treating MDA-MB-231 cells with recombinant human (rh) proteins of S100P, S100A4, S100A7, HMGB1 and HMGA1. We used the sub-cellular localization of cortactin by immunofluorescence (IF) as a read-out of the ligand induction of cell migration. We observed that in cells treated with recombinant RAGE ligands, cortactin was accumulated at the leading edge of the cell membrane, indicating that cells become more migratory (Fig. 27A). In addition to protein ligands, we also tested

methylglyoxal (MGO), a byproduct of glycolysis and a precursor of AGEs, which is implicated in diabetes and other chronic inflammatory diseases [166]. MGO treatment also induced cortactin relocation to the lamellipodia of the cells (Fig. 27A). In the case of rhHMGA1, we used the MDA-MB-231 shHMGA1 cells already generated in our lab [189], since they do not express HMGA1 and the observed effects can be assigned to the interaction of the extracellular rhHMGA1 protein with RAGE (Fig. 27B). Interestingly, we observed that rhHMGA1 treatment also gave rise to cortactin relocation in the invasive front of shHMGA1 cells (Fig. 27B).

A

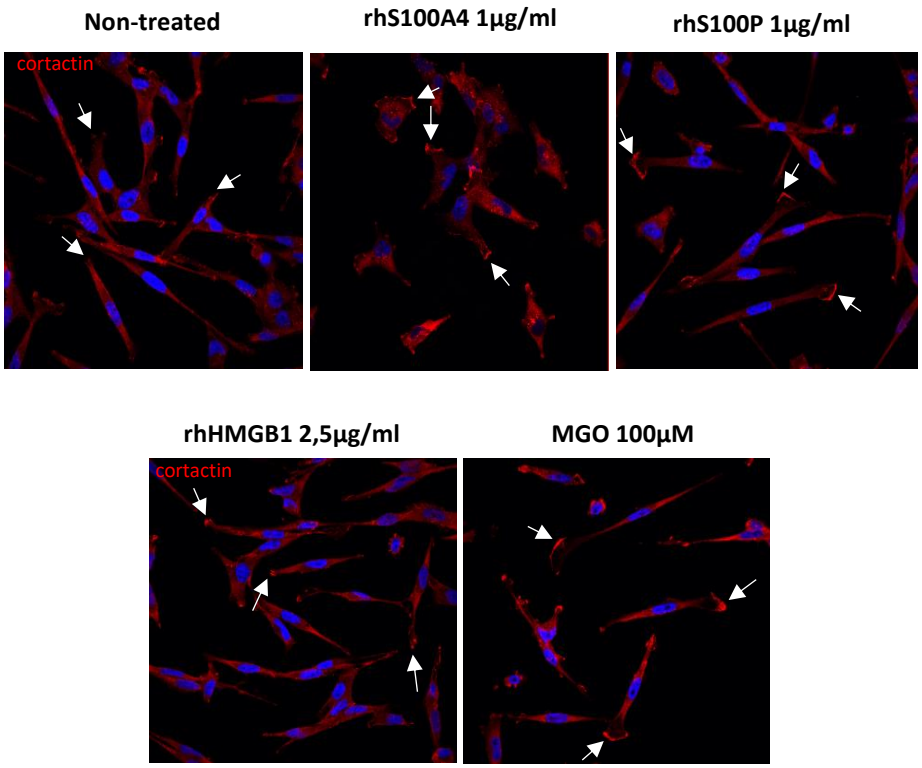

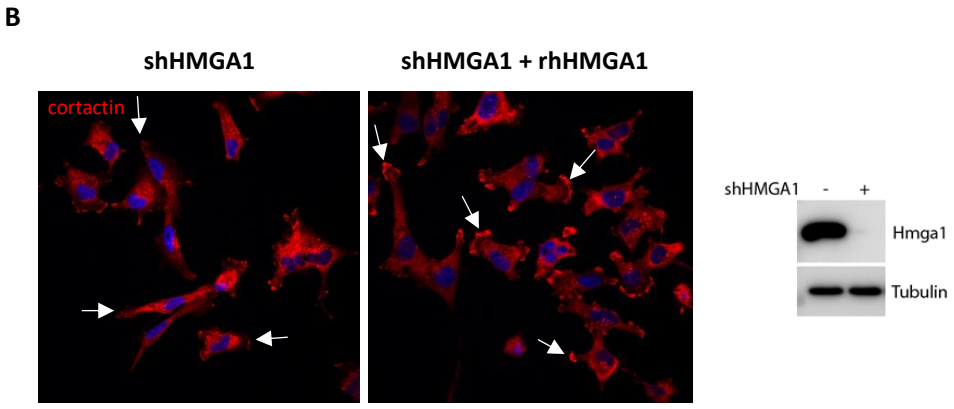

Figure 27. RAGE ligands induce migration in MDA-MB-231 cells. (A) Cortactin IF-staining (red) of MDA-MB-231 cells treated 24h with different recombinant human proteins: 1µg/mL S100A4, 1µg/mL S100P, 2,5µg/mL HMGB1 and 100µM MGO. **(B)** Western blot of HMGA1 expression in shHMGA1 cells, and cortactin staining (red) in shHMGA1 cells treated 24h with the recombinant human protein 3µg/mL HMGA1. Tubulin was used as loading control.

After confirming cortactin relocation in cells treated with RAGE-ligands, we studied the RAGE signaling pathways involved in cell invasion. We tested the two main pathways well known in literature for the transduction of RAGE activation, NF-kB and MAP Kinase (ERK1/2) pathways. We observed that NF-kB was clearly activated by different S100 proteins, although the activation by rhS100A7 was smaller than S100A4 and S100P. We also observed that none of the rhS100 proteins activated ERK1/2 pathway (Fig. 28A). By contrast, MGO did the opposite, it induced ERK1/2 activation but not NF-kB (Fig. 28C). The rhHMGA1 protein activated both pathways ERK1/2 and NF-kB. However, rhHMGN1 did not activate any of them (Fig. 28A and 28B).

To confirm if the activation of these pathways was RAGE-specific, we used the MDA-MB-231 shRAGE cells stimulated with some of the RAGE ligands. We observed that in the shRAGE cells, the activation of phospho-ERK1/2 and phospho-NF-kB was lower than in the knockdown control cells, proving that the activation of ERK1/2 and NF-kB by the recombinant ligands is RAGE-specific (Fig. 28D).

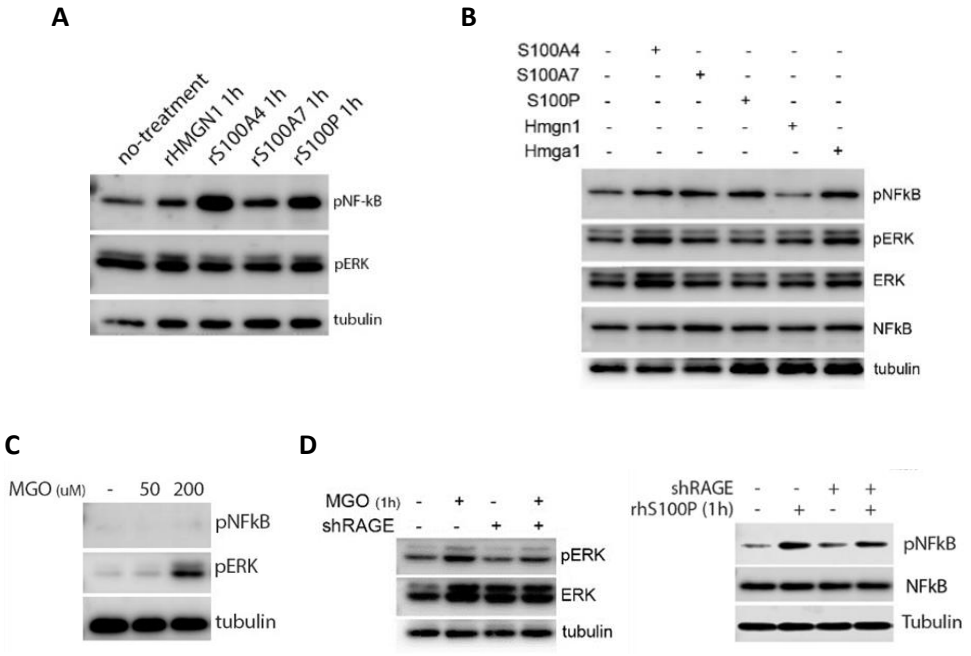

Figure 28. RAGE-ligands induce NF-kB and ERK1/2 activation in MDA-MB-231 cells. (A and B) Western blots of RAGE signaling induced for 1h with different RAGE-ligands: recombinant human proteins of 1µg/mL S100A4, 1µg/mL S100P, 1µg/mL S100A7, 2,5µg/mL HMGN1 and 3µg/mL HMGA1. **(C)** Activation of RAGE signaling pathway with MGO. **(D)** Effect of RAGE-ligands in the RAGE signaling pathway of shRAGE cells. 100uM MGO and 1ug/ml rhS100P. Tubulin was used as loading control.

2.3. RAGE antagonists decrease cell invasion through MAPK pathway

Finally, to confirm the role of RAGE in breast cancer invasion, we decided to use RAGE inhibitors, specifically we used two RAGE antagonists, FPS-ZM1 and Azeliragon. We used two invasion assays, the transwell assay and the gelatin degradation assay. Boyden chambers were coated with Matrigel and cells treated with or without RAGE antagonists were allowed to invade for 24h through a membrane with 8µm pore size. The results showed that cells treated with RAGE antagonists are less invasive (Fig. 29A). Similar results were obtained with the gelatin degradation assay, in which cover-slips were coated with a fluorescent gelatin matrix. After cell attachment in the presence of a reversible matrix metalloproteinases inhibitor (batimastat), cells were washed and allowed to degrade the gelatin for 2h with or without FPS-ZM1. The gelatin degradation caused by the

cells was analyzed by confocal microscopy. The analysis of images containing approximately 100 cells confirm that a RAGE antagonist reduced the ability of the cells to degrade the gelatin matrix (Fig. 29B). Therefore, RAGE antagonists reduced the cell migration and invasion capacity in MDA-MB-231 compared to the non-treated cells (DMSO).

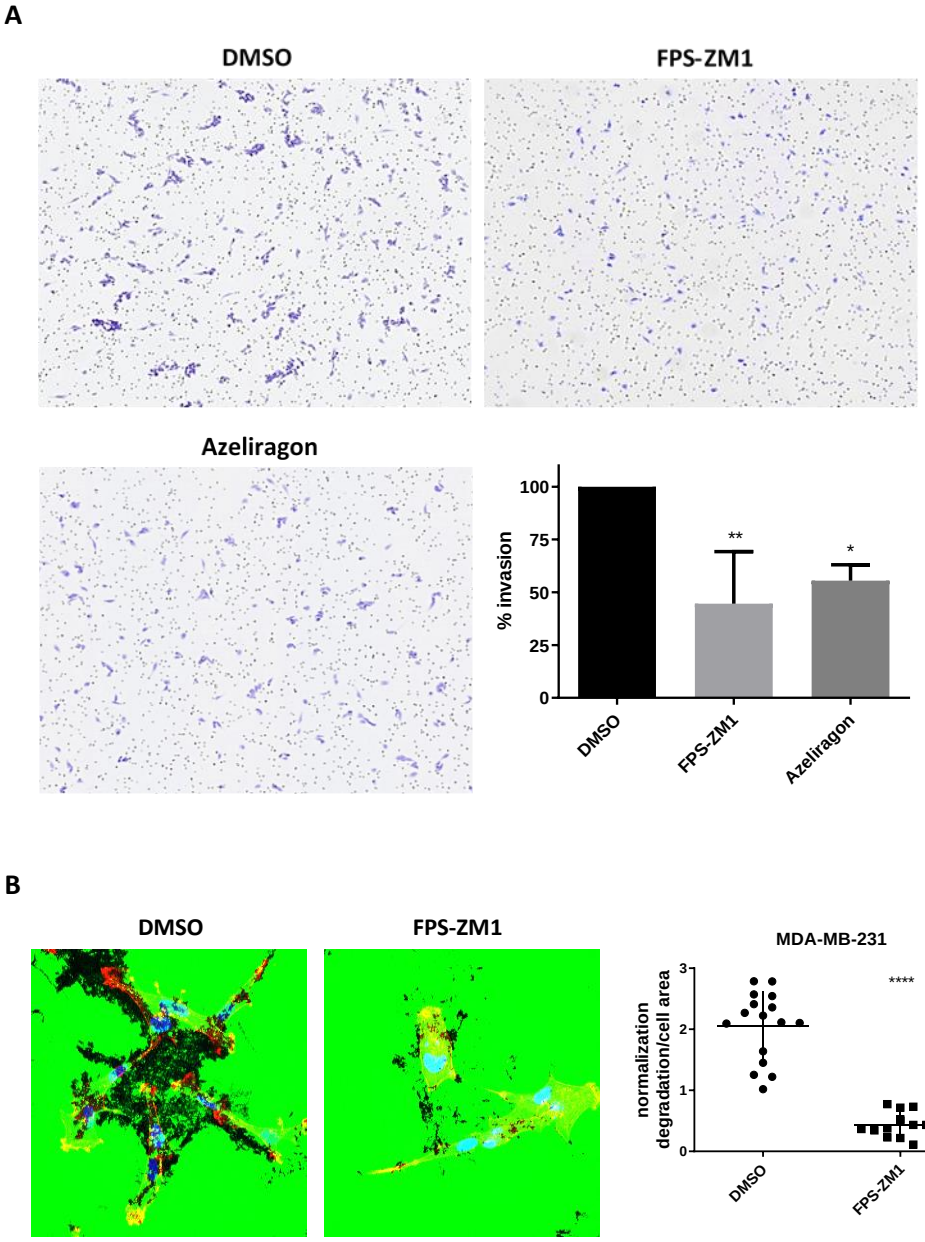

Figure 29. RAGE antagonists reduce cell invasion in breast cancer. (A) Images from transwell assay of RAGE antagonists (30µM FPS-ZM1 and 2µM Azeliragon) on cell invasion in a transwell assay compared to control cells treated with DMSO. **(B)** Analysis of the effect of 30µM FPS-ZM1 on cell invasion in a gelatin degradation assay from 15 fields (approx. 100 cells). Actin was stained in red to visualize cell surface. Statistical analyses were done using one-way ANOVA and unpaired t-test. *p<0.05; **p<0.01, ****p<0.0001.

The effect of the antagonists on cell migration was similar as the results previously obtained with the RAGE knockdown cells. In two different TNBC cell lines, MDA-MB-231 and BT549, we observed that RAGE antagonists induce cortactin relocation to the cytoplasm, whereas in non-treated cells cortactin was located in the lamellipodia and invadopodia promoting cell motility (Fig. 30).

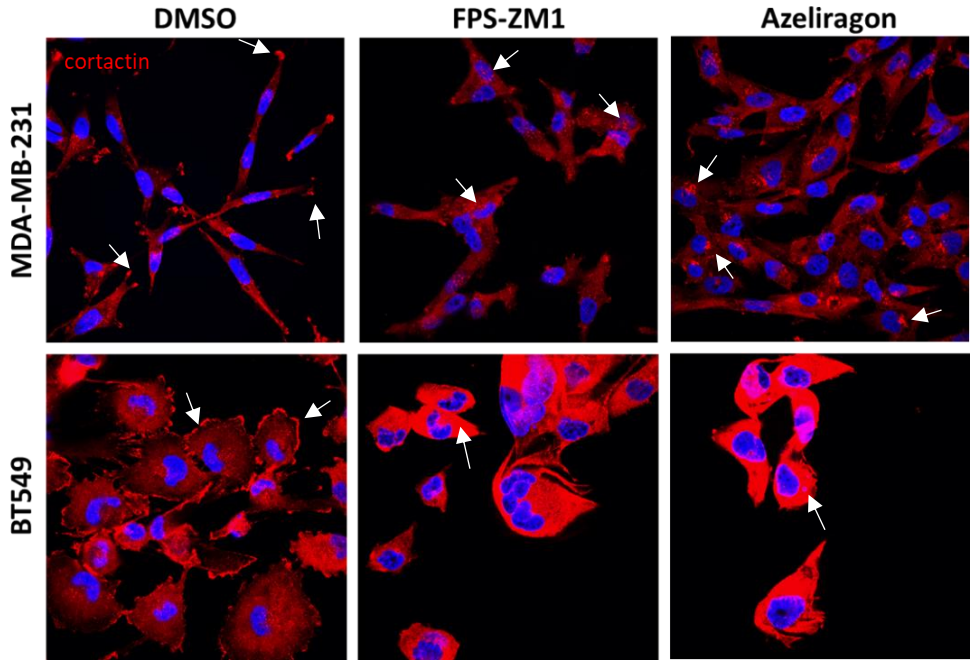

Figure 30. Cell migration was reduced by RAGE antagonists. Differences in cortactin localization (red) in MDA-MB-231 and BT549 cells treated 72h with 30µM FPS-ZM1 and 2µM Azeliragon. The regions of cortactin accumulation were highlighted with the arrows.

After observing a decrease in cell migration and invasion in cells treated with RAGE antagonists, we decided to investigate which transduction signaling pathway linked to RAGE was specifically affected. Therefore, we starved cells from FBS overnight to

avoid the unspecific activation of the pathway induced by the growth factors of the FBS. Then, we did a short time treatment with the antagonists. The results showed that two antagonists reduced ERK1/2 activation in MDA-MB-231 cells (Fig. 31). However, no differences were detected in NF-kB pathway.

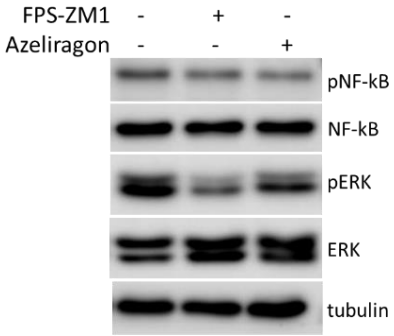

Figure 31. RAGE antagonists inhibit RAGE signaling pathway. Treatment of MDA-MB-231 cells with 30µM FPS-ZM1 for 20 minutes and 2µM Azeliragon for 1h blocks RAGE downstream signaling pathways. Tubulin was used as loading control. Statistical analyses were done using one-way ANOVA **p<0.01, ***p<0.001.

Since in 3D culture (tumoroids) cells are embedded in a matrix that mimics the extracellular matrix of the tissue, tumoroids are useful for drug sensitivity studies [224,227,228]. In our case we studied the effect of RAGE antagonists. In our experiment, MDA-MB-231 cells were embedded in Matrigel. RAGE antagonists' treatment was not started until the protrusions from tumoroids were visible. After 4 days of treatment with RAGE antagonists we observed that the tumoroids of MDA-MB-231 cells started reducing the number of protrusions, although the effect was even higher after 12 days of treatment (Fig. 32A). After 12 days of treatment tumoroids were completely collapsed. The actin staining of tumoroids, confirmed that RAGE antagonists reduced the ability of tumoroids to generated protrusions (Fig. 32B).

Overall, the results with RAGE antagonists and shRAGE cells suggest a role of RAGE in breast cancer migration and invasion. These results led us to hypothesize that RAGE could be a new drug target for TNBC therapy.

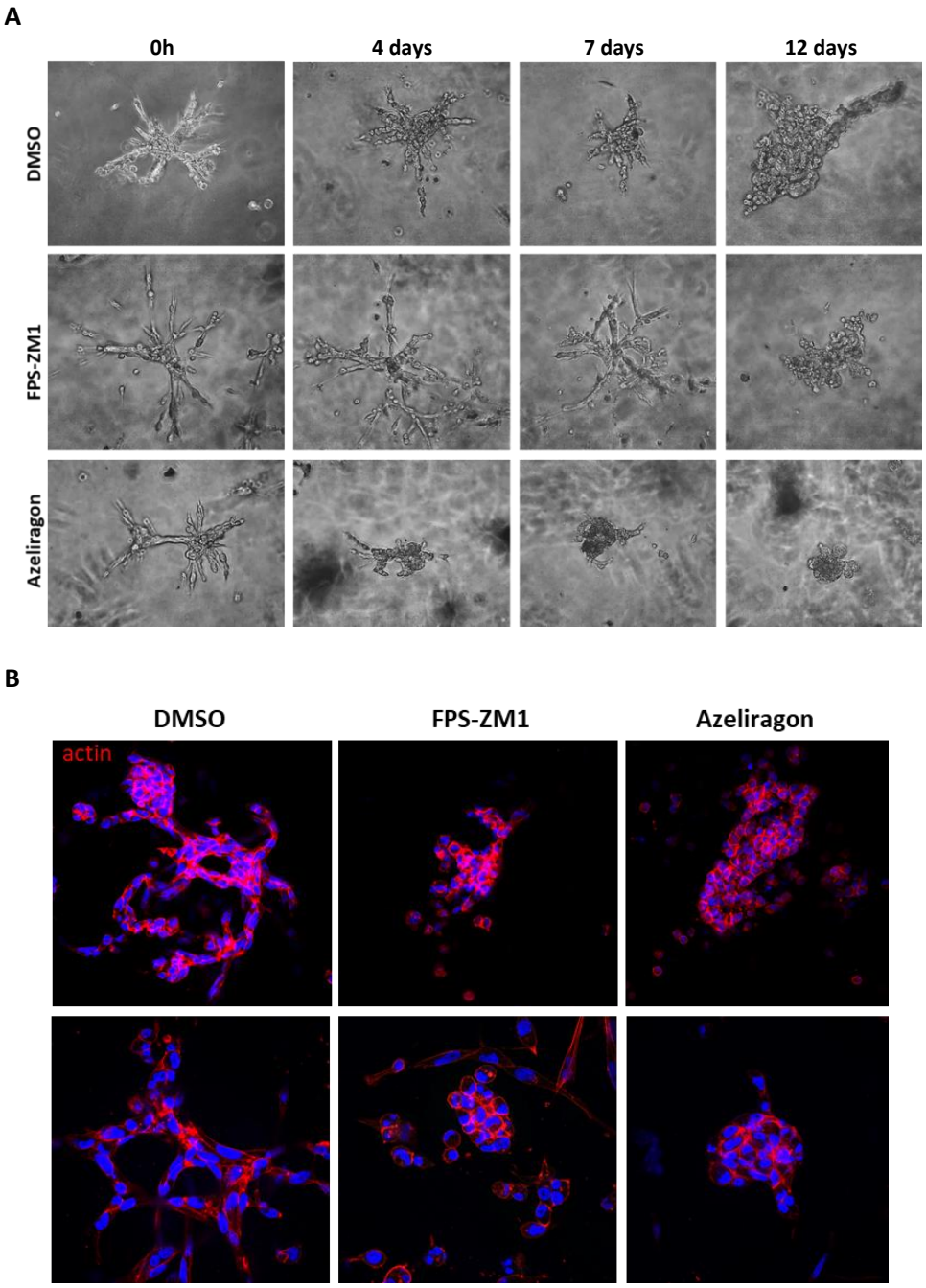

Figure 32. RAGE antagonists reduce tumoroids protrusions of MDA-MB-231 in 3D-culture. (A) Effect on tumoroids growth and protrusion formation in MDA-MB-231 cells after 12 days treatment with 30µM FPS-ZM1 or 2µM Azeliragon. **(B)** Actin staining (red) of MDA-MB-231 tumoroids treated 4 days with 30µM FPS-ZM1 and 2µM Azeliragon.

3. CHARACTERIZING THE ROLE OF RAGE LINKED TO EPITHELIAL-MESENCHYMAL PLASTICITY (EMP) IN BREAST CANCER

Previous evidence linked RAGE to tumor cell plasticity, particularly during fibrosis [229–231], but also with migration and invasion of tumor cells [200,232]. Since, we observed changes in cell morphology when RAGE was inhibited, we decided to study the morphological effects caused by RAGE inhibition in breast cancer cells.

3.1. RAGE down-regulation/inhibition decreases SNAIL1 expression inducing a Mesenchymal-Epithelial Transition (MET) in MDA-MB-231 cells

MDA-MB-231 cells are triple negative breast cancer cells with a clear mesenchymal phenotype and few cell-cell adhesions. However, with the knockdown of RAGE, cells became flatter and they were closer to each other as if they were forming colonies (Fig. 33A). A similar phenotype was detected in cells treated for 72h with RAGE antagonists (Fig. 33B). These changes in cell morphology led us to hypothesized that RAGE has an effect in tumor cell plasticity. Therefore, we studied if there was an effect in any transcriptional factor (TF) that could be involved in epithelial-mesenchymal plasticity (EMP).

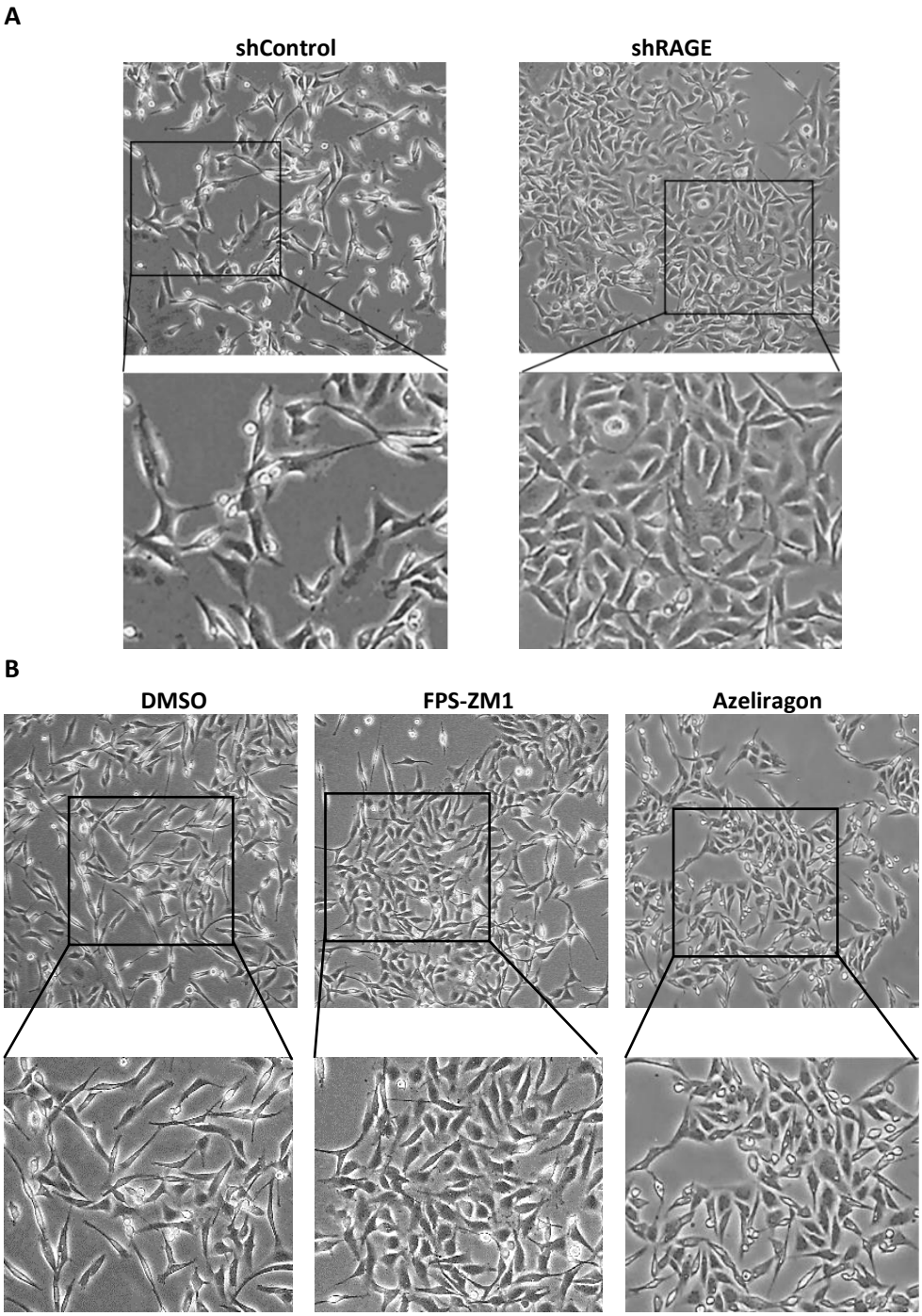

Figure 33. RAGE inhibition induces plasticity change in MDA-MB-231 cells. (A) Cell pictures showing phenotypical differences on shRAGE cells compared to shControl cells. **(B)** Cell pictures showing morphological differences in MDA-MB-231 cells treated with 30µM FPS-ZM1 and 2µM Azeliragon for 72h.

First, we analyzed the expression of EMP transcriptional factors in MDA-MB-231 cells treated for 72h with FPS-ZM1 and Azeliragon. Western blot (Fig. 34A) and IF (Fig. 34C) analyses showed a decrease in SNAIL1 expression in cells treated with RAGE antagonist, although other TFs such as SNAIL2 and ZEB1 were not affected. SNAIL1 expression was also down-regulated in shRAGE-cells compared to the shControl cells (Fig. 34B). Moreover, RT-PCR analysis confirmed the down-regulation of *SNAI1* mRNA after RAGE antagonists' treatment (Fig. 34D) and in shRAGE cells (Fig. 34E), although the levels of mRNA of other EMT-TFs were not affected (Fig. 34D).

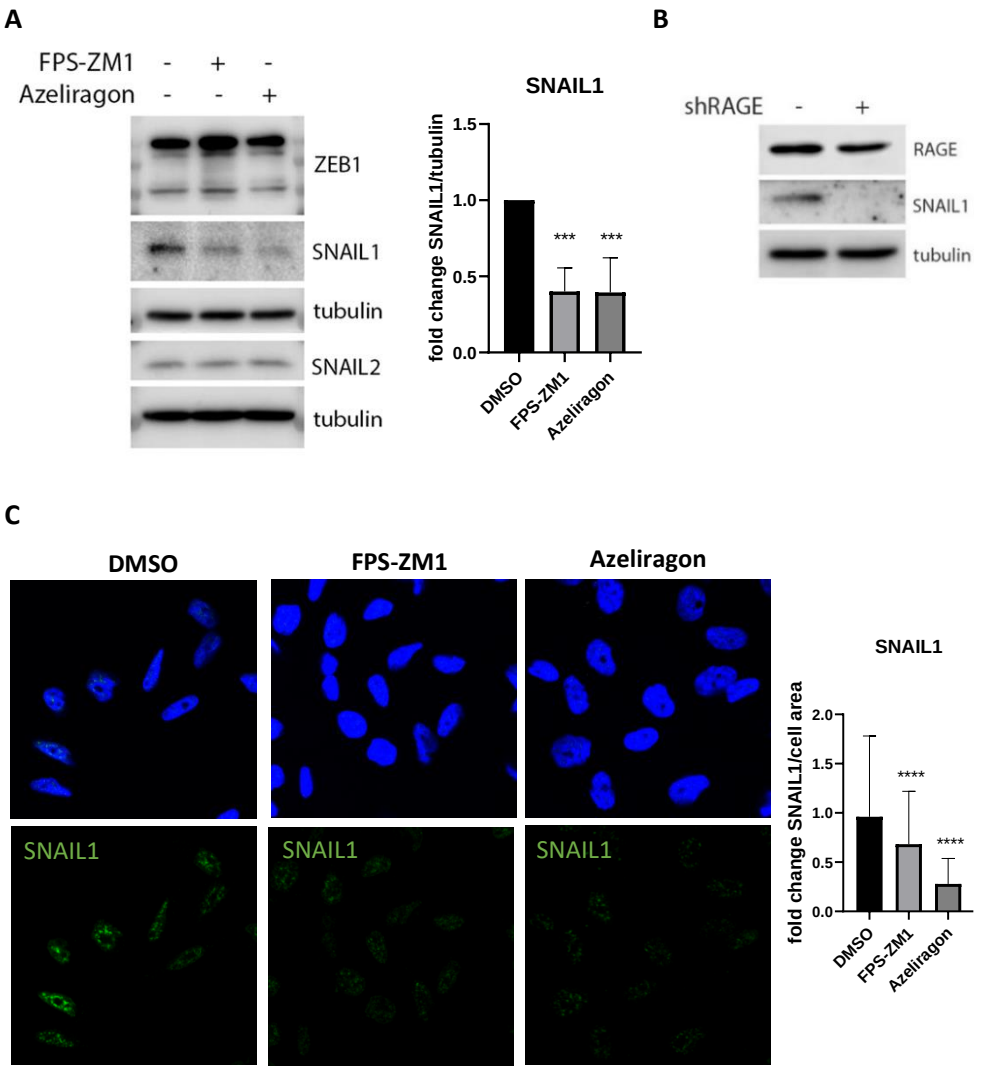

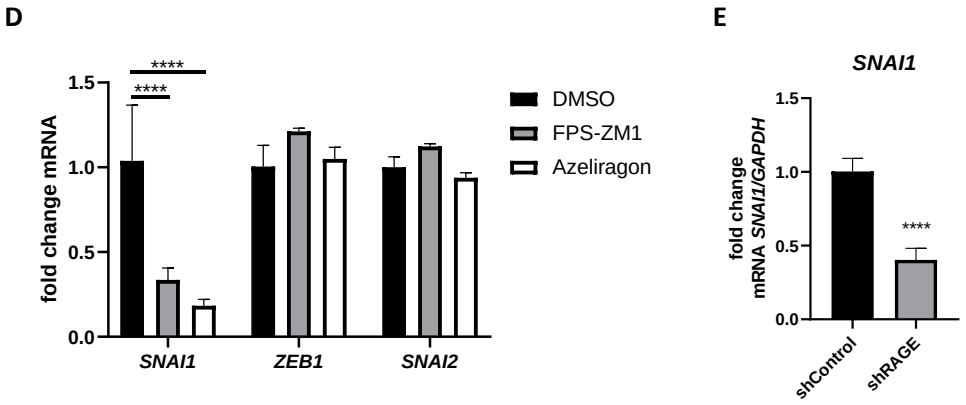

Figure 34. Blocking/Down-regulating RAGE reduces SNAIL1 expression in MDA-MB-231 cells. (A) Western blot showing expression of different transcription factors in MDA-MB-231 cells treated with 30vM FPS-ZM1 or 2µM Azeliragon for 72h. SNAIL1 quantification considering at least 3 independent experiments. **(B)** SNAIL1 expression in shRAGE cells. **(C)** Immunostaining of SNAIL1 in MDA-MB-231 cells treated 72h with RAGE antagonists and quantification of more than 300 cells for treatment. **(D)** mRNA expression of *SNAI1*, *SNAI2*, and *ZEB1* in cells treated 96h with RAGE antagonists. **(E)** mRNA expression of *SNAI1* in RAGE knockdown cells. Statistical analyses were done using one-way ANOVA (A and C), two-way ANOVA (D) and unpaired t-test (E). ***p<0.001, ****p<0.0001. Tubulin was used as loading control.

To validate our data, we analyzed other triple negative breast cancer cell lines such as BT549 and Hs578T, and we also detected a decrease in SNAIL1 expression in cells treated with RAGE antagonists. FPS-ZM1 also reduced SNAIL2 in BT549 cells. However, no differences were detected on ZEB1 in any cell line after the treatment with RAGE antagonists (Fig. 35).

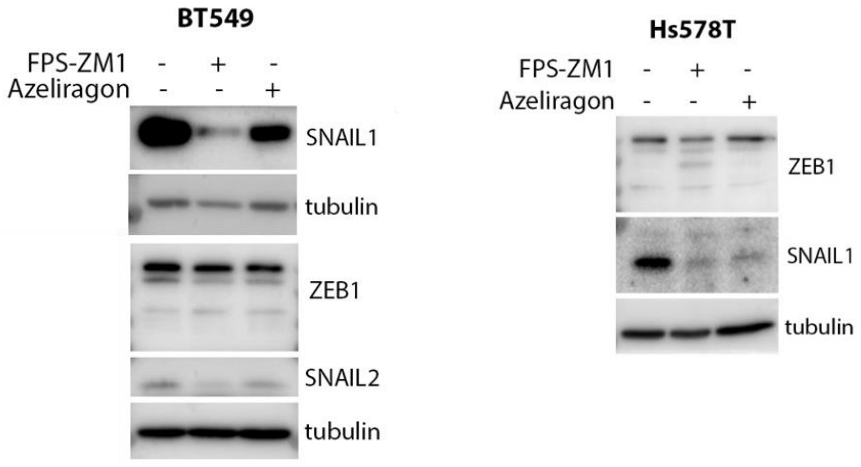

Figure 35. RAGE antagonists reduce SNAIL1 expression in breast cancer cells. Western blots showing SNAIL1, SNAIL2 and ZEB1 expression in BT549 and Hs578T cells treated for 72h with 30μM FPS-ZM1 or 2μM Azeliragon. Tubulin was used as loading control.

SNAIL1 down-regulation is likely to reverse EMT inducing a mesenchymal-epithelial transition (MET) associated with loss of cell motility, expression of cell-cell adhesions and increasing cell polarization. Therefore, we analyzed the expression of epithelial markers involved in cell adhesions.

E-cadherin is a well-known epithelial marker that mediates cell-cell adhesion important to maintain the homeostasis of epithelial tissue. Considering that SNAIL1 is a repressor of E-cadherin, we expected an increase in E-cadherin expression when SNAIL is down-regulated. However, although in our cells the down-regulation of SNAIL1 was significant when RAGE was either blocked or down-regulated, we were not able to detect significant differences in E-cadherin *(CDH1)* expression (Fig. 36A). These results are counterintuitive, but the results could be explained due to the partial EMT (pEMT) concept. Between the mesenchymal and epithelial states, it has been proposed that there are intermediary states that undergo a partial EMT program expressing different levels of mesenchymal and epithelial characteristics. These intermediate cell states are known as E/M hybrid phenotype [53]. Perhaps, in MDA-MB-231 cells, which are highly invasive and have a really mesenchymal phenotype, the treatment with RAGE inhibitors reverse EMT to a hybrid state. On top of the lack of E-cadherin expression, differences in N-cadherin *(CDH2)* were only detected with shRAGE, but not with RAGE antagonists (Fig. 36B), reinforcing our hypothesis that RAGE inhibition induces a partial MET.

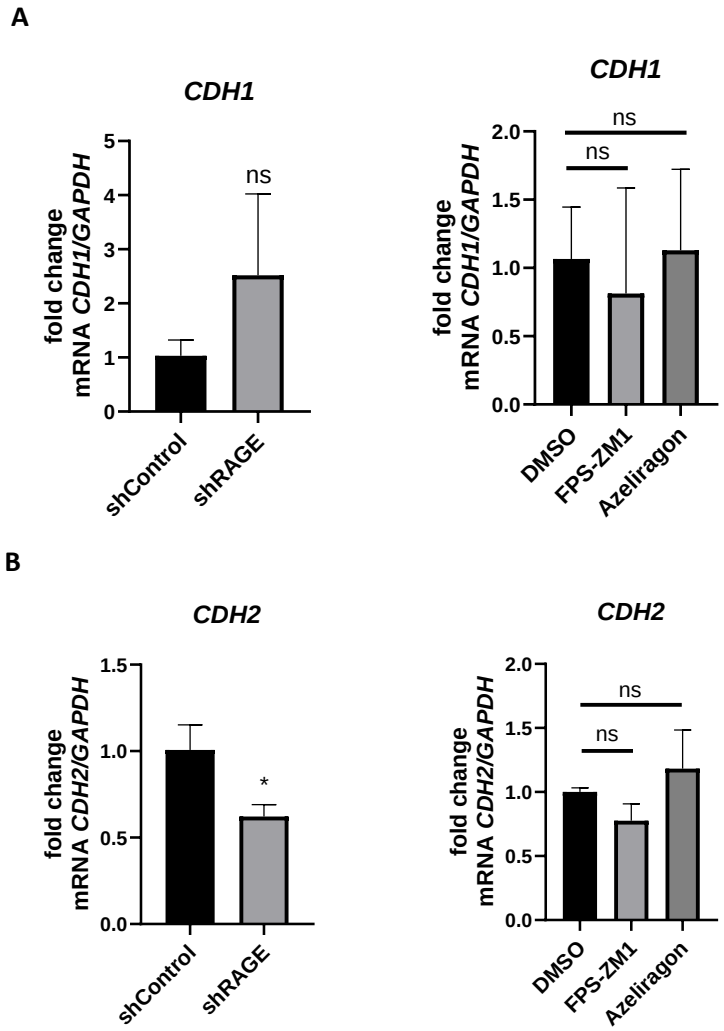

Figure 36. RAGE inhibition does not affect cadherins expression in MDA-MB-231 cells. (A) E-cadherin *(CDH1)* mRNA expression in shRAGE cells and cells treated for 96h with RAGE antagonists (30µM FPS-ZM1 or 2µM Azeliragon). **(B)** Effect on N-cadherin *(CDH2)* expression in shRAGE cells and cells treated with RAGE antagonists for 96h. Statistical analyses were done using unpaired t-test for knockdown experiments and One-way ANOVA for RAGE antagonists' experiments. *p<0.05, ns=not significant. The error bars reflect the SD.

Despite we could not detect a regulation in E-cadherin, we observed β-catenin relocation to the plasma membrane during RAGE inhibition (Fig. 37). β-catenin is a dual function protein. In the nucleus is involved in gene transcription, but in the plasma membrane it has a role in epithelial cell-cell adhesion [233,234]. Therefore, β-

catenin expression in the plasma membrane confirms the MET induced by RAGE inhibition.

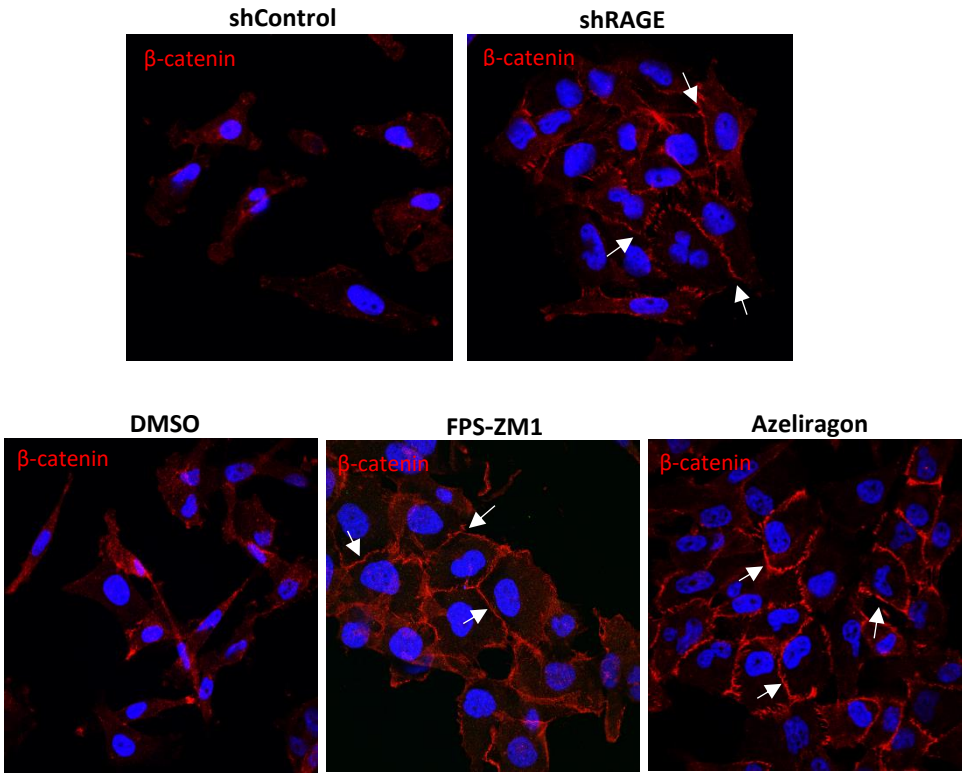

Figure 37. Blocking RAGE induces β-catenin relocation to the plasma membrane in MDA-MB-231 cells. Effect on β-catenin localization in shRAGE cells (upper panel) and cells treated 72h with 30μM FPS-ZM1 or 2μM Azeliragon (lower panel).

Finally, to further validate these results, we also analyzed the expression of proteins such as ZO-1 and Claudin 1, involved in tight junctions. These proteins are responsible to maintain the polarity of epithelial cells, while in mesenchymal cells these are down-regulated. Interestingly, we detected an increase in the levels of Claudin 1 and ZO-1 expression in shRAGE cells (Fig. 38A). Specifically, ZO-1 was detected in the plasma membrane (Fig. 38B) playing a role in tight junctions.

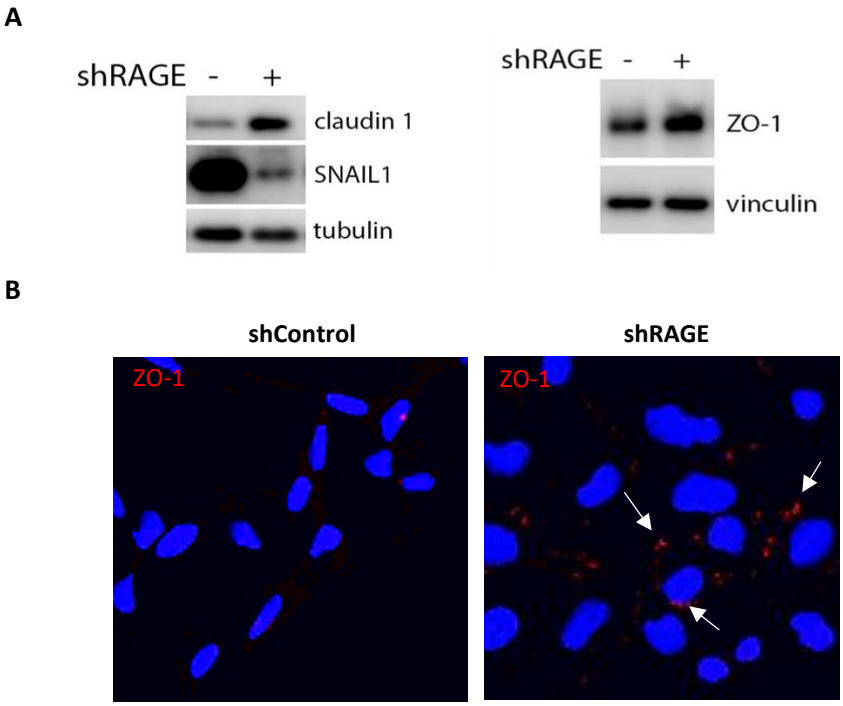

Figure 38. Knockdown RAGE induces tight junction expression in MDA-MB-231 cells. (A) Western blot of two tight junction proteins Claudin 1 (left) and ZO-1 (right) expressed in shRAGE cells. Tubulin and vinculin were used as loading control. **(B)** IF-staining of ZO-1 protein (red) in shRAGE cells.

After demonstrating that RAGE inhibition induced a pMET in MDA-MB-231 cells, and that these cells increase the expression of cell-cell adhesions and tight junctions, we decided to study the effect on cells' adhesion to the extracellular matrix. We tested two different matrices, collagen I and fibronectin, and the results showed an increase in the cell adhesion to both matrices in shRAGE cells (Fig. 39A). Cell adhesion was also increased in cells treated with Azeliragon, but not with FPS-ZM1 treatment (Fig. 39B), although the molecular and morphological effects were similar as Azeliragon. This increase in cell adhesion validates our previous results and reinforces our hypothesis that RAGE plays a role in EMP in TNBC.

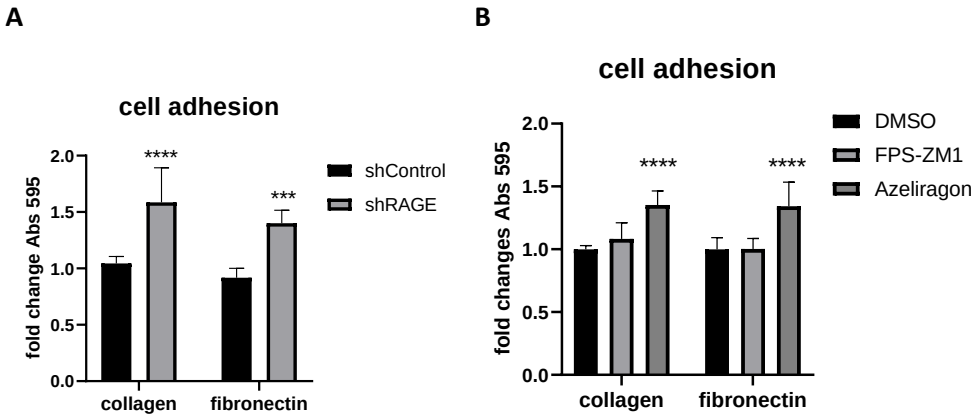

Figure 39. RAGE inhibition increases MDA-MB-231 adhesion in extracellular matrix. Left panel shows adhesion of shRAGE cells in collagen and fibronectin matrices. Right panel shows adhesion of cells treated for 96h with 30µM FPS-ZM1 or 2µM Azeliragon in collagen and fibronectin matrices. Statistical analyses were done using two-way ANOVA. ***p<0.001, ****p<0.0001

Epithelial cells tend to have a higher proliferative rate than mesenchymal cells. Therefore, taking into account that the inhibition of RAGE reverses the EMT process inducing an epithelial phenotype, we hypothesized an increase in cell proliferation when RAGE activity was inhibited by antagonists or RAGE ablation. However, the results only confirm partially the hypothesis. While the RAGE knockdown cells have a higher proliferative rate than shControl cells (Fig. 40A), cells treated with FPS-ZM1 reduced their proliferation, although no differences were detected in cells treated with Azeliragon (Fig. 40B). The difference between the two antagonists could be explained by the fact that they bind to different regions of the V-domain [128].

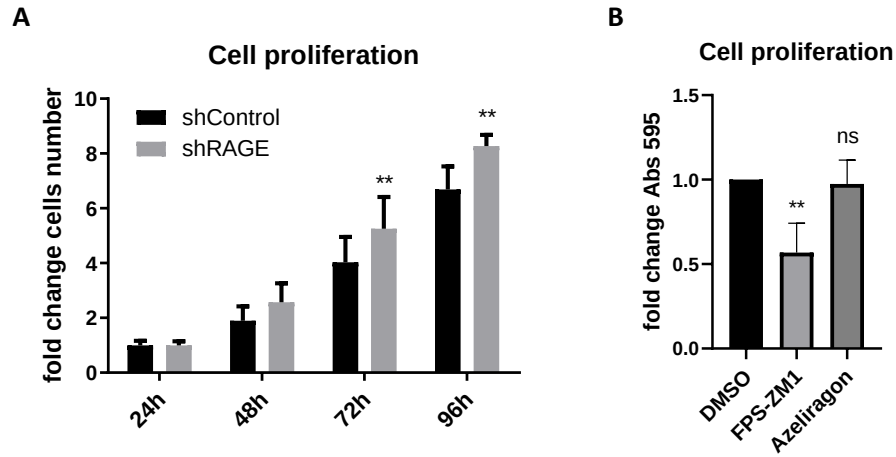

Figure 40. RAGE effect on cell proliferation. **(A)** Cell proliferation analysis of shRAGE and shControl cells from 24h to 96h tested with cell counting **(B)** Cell proliferation analysis tested with CellTiter after 72h treatment with 30µM FPS-ZM1 or 2µM Azeliragon. Statistical analyses were done using two-way ANOVA. **p<0.01

Overall, these results confirm the involvement of RAGE in tumor cell plasticity and cell motility. Moreover, the inhibition and down-regulation of RAGE reverses the EMT inducing a partial mesenchymal-epithelial transition (pMET) in TNBC cells.

3.2. RAGE antagonists impair EMT mediated by TGF-β1 in breast cancer cells

After showing that RAGE mediates EMT in MDA-MB-231 cells, and considering that transforming growth factor beta 1 (TGF-β1) is one of the best-known mediators of EMT, we decided to study whether there is a link between RAGE and the TGF-β pathway. To do so, we used the NMuMG cell line, which is a non-transformed mouse mammary gland epithelial cell line, and one of the best EMT cellular experimental models. NMuMG cells are epithelial but become fully mesenchymal after 48h treatment with TGF-β1. This EMT process is perfectly blocked by an inhibitor of TGF-β receptor II (iTGF-βRII) (LY2109761) (Fig. 41). Since RAGE antagonists induce a MET in MDA-MB-231 cells, we studied whether the antagonists could block the EMT induced by TGF-β1 in NMuMG cells. Cells were pretreated with RAGE antagonists for 72 hours before adding the TGF-β1 for 48 hours. The results showed that RAGE antagonists partially blocked the EMT induced by TGF-β1, since cells cannot become fully mesenchymal in the presence of the antagonists (Fig. 41).

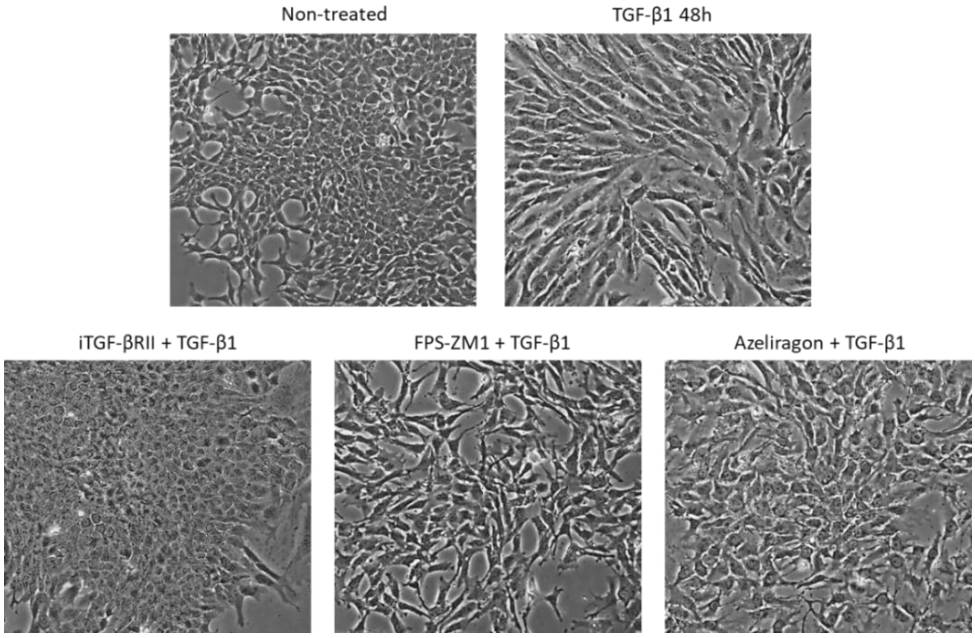

Figure 41. RAGE antagonists reduce EMT induced by TGF-β1 in NMuMG cells. Upper panels show pictures of non-treated NMuMG cells and cells treated with 1ng/mL TGF-β1 for 48h. Lower panels show pictures of cells treated with TGF-β1 for 48h and 2μM TGF-β1 inhibitor (iTGF-βRII) O/N (left); cells pre-treated for 72h with 30μM FPS-ZM1 and then 48h with TGF-β1 (middle); and cells pre-treated for 72h with 1.5μM Azeliragon and then TGF-β1 for 48h (right).

To confirm these results, we analyzed the expression and subcellular localization of E-cadherin and β-catenin, two main markers of the epithelial phenotype. We observed that NMuMG cells treated with TGF-β1 reduced the expression of both epithelial markers. This loss was almost totally blocked on cells treated with FPS-ZM1, and partially blocked on cells treated with Azeliragon (Fig. 42). Therefore, RAGE antagonists impaired EMT induced by TGF-β1.

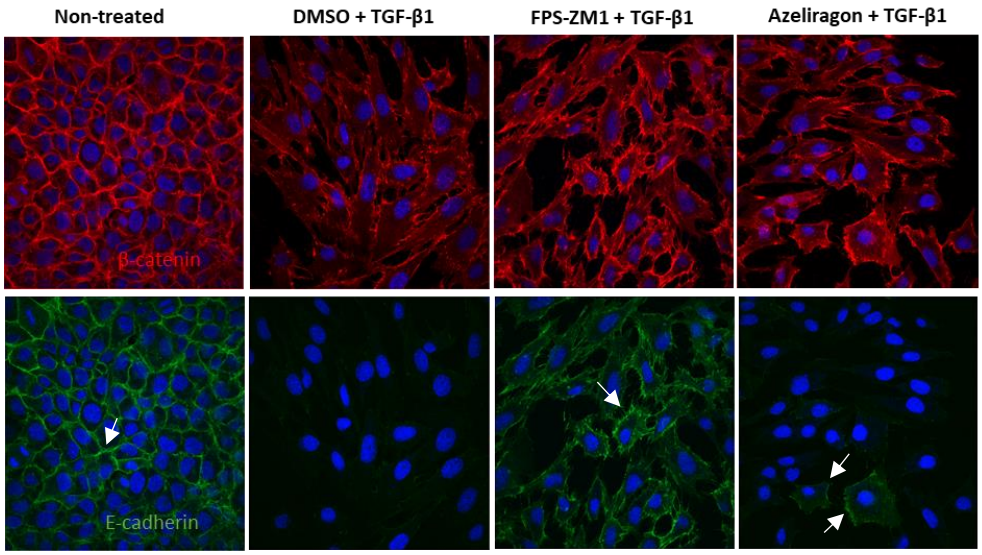

Figure 42. RAGE antagonists impaired the effect of TGF-β1 in NMuMG cells. IF show the effect on E-cadherin (green) and β-catenin (red) expression induced by 24h of TGF-β1 with or without 96h pre-treatment with 30μM FPS-ZM1 and 1.5μM Azeliragon.

Once we observed morphological differences in cells treated with TGF-β1 with or without RAGE antagonists, we decided to study the molecular mechanism that could link TGF-β and RAGE pathways.

Previous studies demonstrated that TGF-β1 and TGF-β-2 bind to the specific receptors TGF-βR I and II activating the SMAD signaling pathway, which it is known as its canonical pathway. Alternatively, TGF-β can also activate SMAD-independent pathways, such as ERK1/2, AKT and JAK-STAT, which are known as non-canonical pathways [235]. To study the link between RAGE and TGF-β, first, we analyzed the activation state of both TGF-β1-canonical and non-canonical pathways in NMuMG cells. The results show that TGF-β1 activates the canonical (SMAD2), and non-canonical (ERK1/2) pathways (Fig. 43A, line 2). Inhibition of the TGF-β pathway, using an inhibitor of TGF-βRII (LY2109761), reduces the activation of both SMAD2 and ERK1/2 induced by TGF-β1 (Fig. 43A, line 7). Furthermore, blocking RAGE activity with FPS-ZM1 also reduces the phosphorylation of both SMAD2 and ERK1/2 (Fig. 43A, line 3), suggesting a link between RAGE and TGF-β pathway. Although Azeliragon did not affect the SMAD pathway, it reduced the phosphorylation of

ERK1/2. Besides, the effect on SMAD2 and ERK1/2 inhibition was higher when both pathways were inhibited by Azeliragon and iTGF-βRII (Fig. 43B), suggesting a synergy between the RAGE and TGF-β pathways. In these experiments a MEK inhibitor (AZD6244) was used as a positive control of the inhibition of ERK1/2 activity (Fig. 43A, line 5).

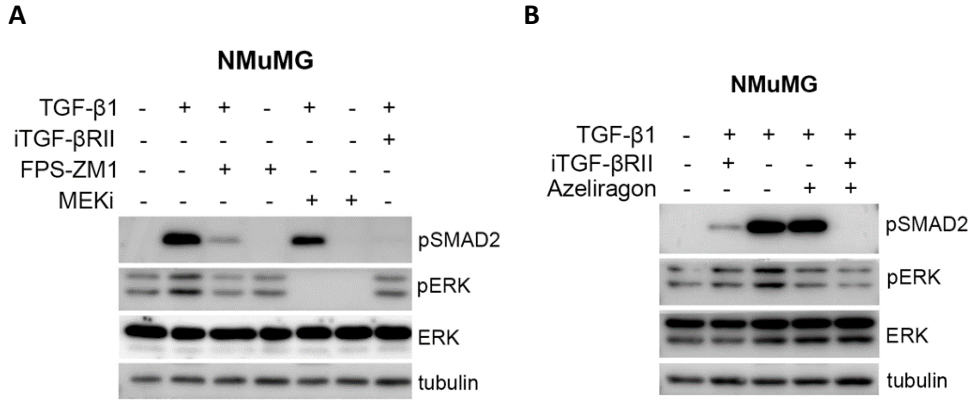

Figure 43. RAGE antagonists block the signaling pathways induced by TGF-β1 in NMuMG cells. (A) Effect of FPS-ZM1, iTGF-βRII and MEKi in the TGF-β1 signaling after 30min treatment with 1μg/mL TGF-β1. 30μM FPS-ZM1 and 10μM MEKi were added O/N. **(B)** Effect of Azeliragon and iTGF-βRII in the TGF-β1 signaling on cells treated with 1μg/mL TGF-β1 for 30min. 1.5μM Azeliragon and 2μM iTGF-βRII were added O/N.

Then, we analyzed the expression of SNAIL1, consistent with its important role in EMT induced by TGF-β, and also by RAGE as we previously described. Although we detected a decrease in SNAIL1 with both RAGE antagonists (Fig. 44A), the effect was even higher after the combination of both signaling inhibitors (against RAGE and TGF-β) (Fig. 44B, line 8), reinforcing the synergy previously detected in the ERK1/2 and SMAD2 activation. Overall, these results suggest a possible synergy between the TGF-β and RAGE pathways during cell plasticity.

Moreover, considering that Azeliragon did not affect SMAD pathway, but it reduced SNAIL1 expression, we suggest that RAGE antagonists can impair the EMT mediated by TGF-β1 through both the canonical and the non-canonical pathway ERK1/2.

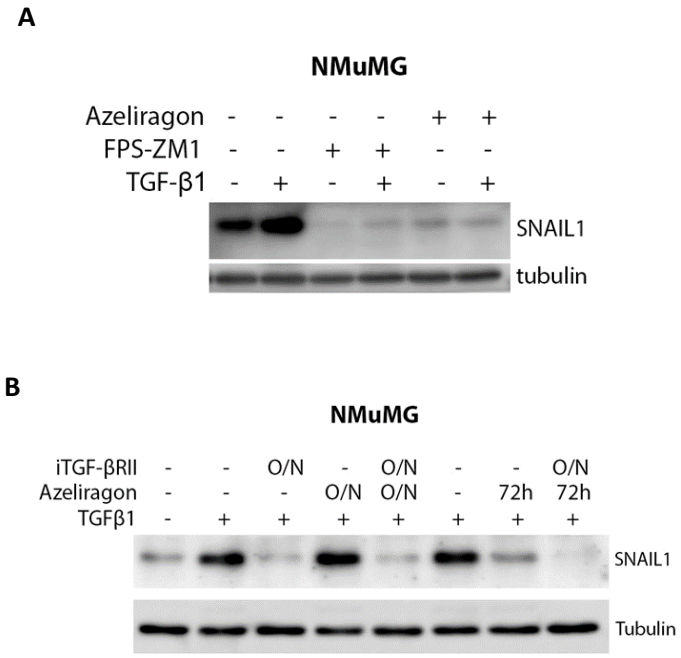

Figure 44. RAGE antagonists block SNAIL1 induced by TGF-β1 in NMuMG cells. (A) Analysis of SNAIL1 expression on cells pre-treated 72h with RAGE antagonists (30μM FPS-ZM1 and 1.5μM Azeliragon) following 30min 1μg/mL TGF-β1. **(B)** Effect of 1.5μM Azeliragon, 2uM iTGF-βRII and their combination on SNAIL1 expression in cells treated 30min with 1μg/mL TGF-β1. Tubulin was used as loading control.

We also analyzed the link between RAGE and TGF-β pathways in MDA-MB-231 cells. As observed in NMuMG cells, TGF-β1 activates the canonical (SMAD2) and non-canonical (ERK1/2) pathways of TGF-β in MDA-MB-231 cells (Fig. 45A, line 2). In these cells, the iTGF-βRII only inhibits SMAD2 activation (Fig. 45A, line 10). In contrast, FPS-ZM1 reduces ERK1/2 activation but not SMAD2 (Fig. 45A, line 3). Interestingly, as in NMuMG cells, blocking both pathways increase the effect on ERK1/2 suggesting a possible synergy between RAGE and TGF-β1 pathways (Fig. 45A, line 9). In these experiments, the MEK inhibitor was also used as a positive control of ERK1/2 inhibition (Fig. 45A, line 6).

Next, we analyzed SNAIL1 expression in MDA-MB-231 cells stimulated with TGF-β1. TGF-β1 treatment increases SNAIL1 expression (Fig. 45B, line 2), although MDA-MB-231 cells are already mesenchymal and express EMT-TF. SNAIL1 expression was

blocked by both RAGE antagonists (Fig 45B, line 4 and 6), as well as with the iTGF-βRII (Fig. 45C, line 3). Furthermore, as we previously observed in NMuMG cells, a possible synergy between the two pathways was detected, because the combination of inhibitors of both pathways increases the inhibitory effect on SNAIL1 expression (Fig. 45C, line 5 and 7).

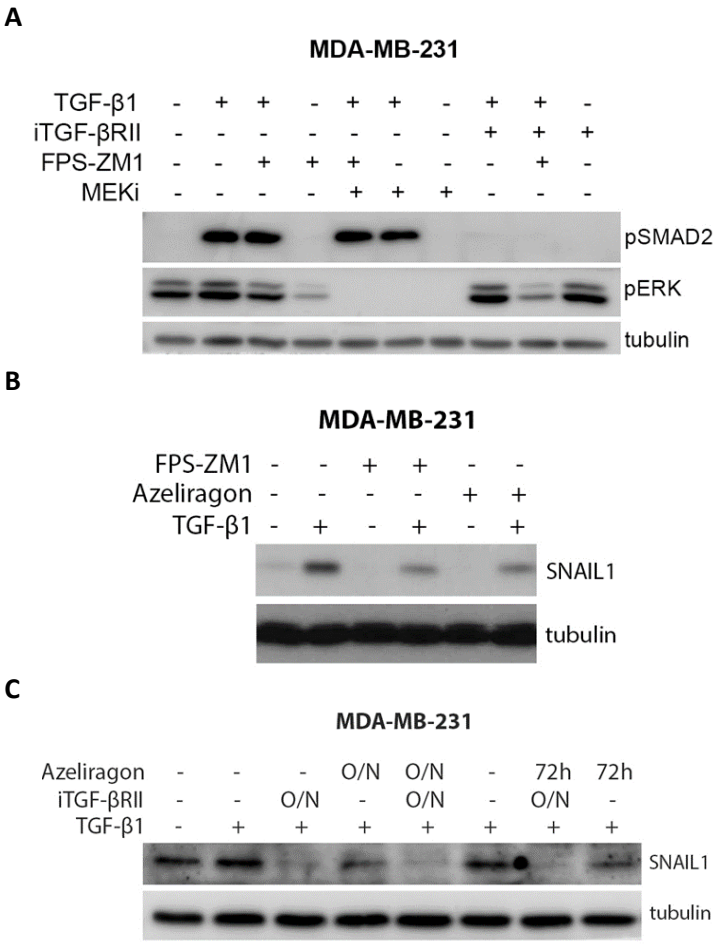

Figure 45. RAGE antagonists block ERK1/2 and SNAIL1 induced by TGF-β1 in MDA-MB-231 cells. (A) Analysis of TGF-β1 signaling after incubation O/N with 30μM FPS-ZM1, 2μM iTGF-βRII or 10μM MEKi followed by 30min of 1μg/mL TGF-β1. **(B)** Effect of RAGE antagonists (30μM FPS-ZM1 and 2μM Azeliragon) (72h) in SNAIL1 expression. **(C)** Analysis of the effect of 2μM Azeliragon, 2μM iTGF-βRII and their combination on SNAIL1 expression in cells treated 30min with 1μg/mL TGF-β1. Tubulin was used as loading control.

Therefore, TGF-β1 mediates EMT through SMAD2 and ERK1/2 signaling in breast cancer cells promoting the expression of SNAIL1. The combined inhibition of TGF-β and RAGE signaling increases the inhibitory effect on ERK1/2 and SNAIL1 expression in MDA-MB-231, and also blocks SMAD2 activation in NMuMG cells, suggesting a cross-talk between RAGE and TGF-β pathways during tumor cell plasticity.

4. STUDYING THE LINK BETWEEN RAGE AND TUMOR ACIDOSIS

Returning to the microenvironmental stresses, we have demonstrated that acute acidosis induces breast cancer invasion and migration, and it also increases the secretion of RAGE ligands. These ligands are responsible for enhancing the migratory potential of breast cancer cells, since the migration is reduced when RAGE is inhibited. Therefore, considering that there is a link between acidosis and RAGE, we decided to study how the molecular pathway of RAGE is affected by the acidic microenvironment and how this affects cell migration and invasion.

4.1. Acute acidosis induces RAGE oligomerization in the plasma membrane

To study the acidosis effect on RAGE expression, first MDA-MB-231 cells were exposed to acidosis for 24 h. Surprisingly, no differences were detected on either RAGE protein (Fig. 46A) or mRNA levels (*AGER*) (Fig. 46B). However, the IF analysis using an Ab against the extracellular domain of RAGE showed a relocation of RAGE to the plasma membrane (Fig. 46C) forming some sort of aggregates. Related to that, it has been proposed that during ligand binding, RAGE generate dimers or oligomers to activate different signaling pathways [147,165]. We also observed that cortactin was localized in regions near RAGE aggregates (Fig. 46C). Furthermore, a RAGE downstream effector, which binds to its intracellular domain, the DIAPH1 (mammalian diaphanous-1), was also relocated to the plasma membrane in cells exposed 24h to acidosis (Fig. 46D).

A

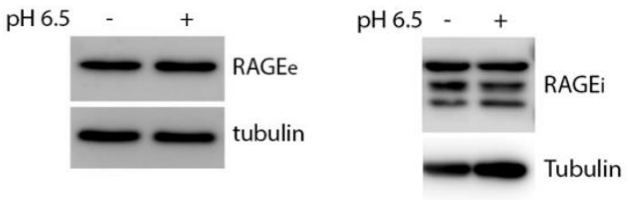
pH 6.5 - +
RAGEe
tubulin
pH 6.5 - +
RAGEi
Tubulin

B

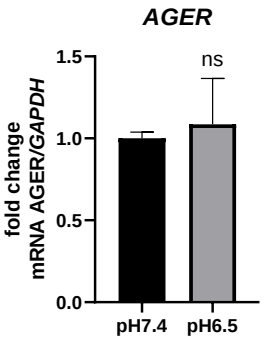
AGER
ns
fold change
mRNA AGER/GAPDH
1.5
1.0
0.5
0.0
pH7.4
pH6.5

C

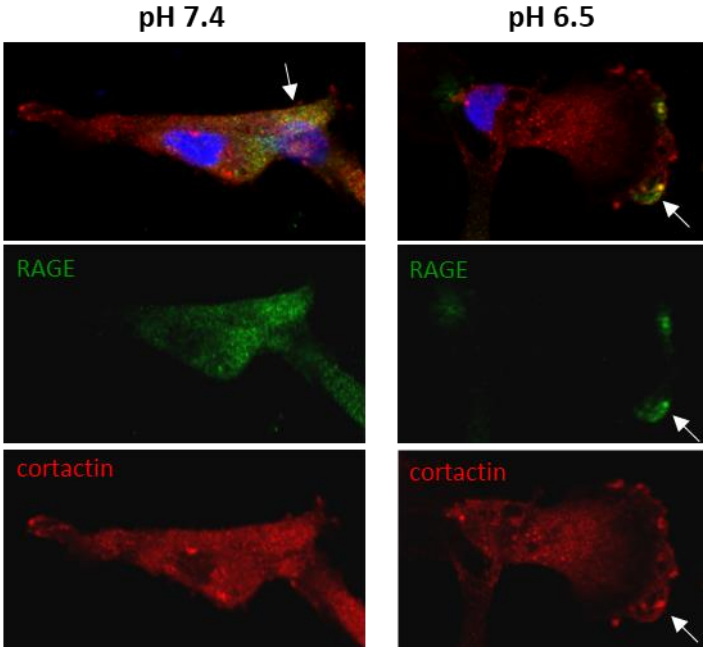
pH 7.4
pH 6.5
RAGE
RAGE
cortactin
cortactin

D

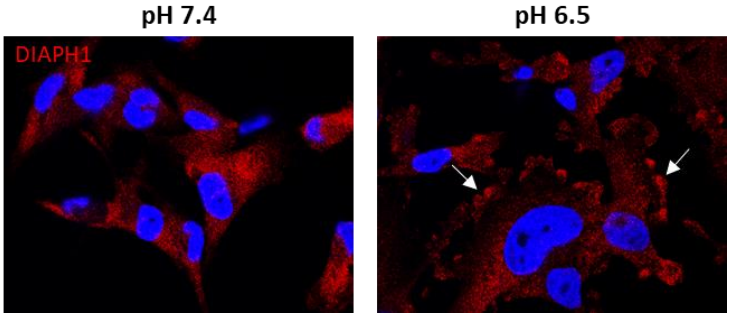
pH 7.4
pH 6.5
DIAPH1

Figure 46. Acidosis induces RAGE aggregates in the plasma membrane in MDA-MB-231 cells. (A) Effect of acidosis on the expression of RAGE protein. Two different RAGE antibodies were used, one against the intracellular regions (RAGEi) and another against the extracellular domain (RAGEe). Tubulin was used as loading control. **(B)** Analysis of the mRNA levels of *AGER* in cells subjected 24h to acidic conditions. **(C)** IF staining of cells exposed 24h at pH 6.5. Staining against the extracellular domain of RAGE was done without permeabilization. Then the same samples were permeabilized to stain the cortactin (red). **(D)** Staining of DIAPH1 protein (red) of MDA-MB-231 cells subjected to acidosis 24h. Hoechst stains the nucleus in blue.

The IF results prompted us to study in more detail RAGE oligomerization in cells subjected to acidic conditions. We performed western blot under non-reducing conditions (without adding DTT to the protein lysates), to avoid the disruption of disulfide bonds. Under these conditions, we observed an increase in the upper band (>250kDa) that corresponds to RAGE oligomers. Cells exposed 24h to acidic conditions increase RAGE oligomerization (Fig. 47A, line 2), which correlates with the increase in RAGE aggregates observed in the plasma membrane by IF (Fig. 46C). Interestingly, although 24h of Azeliragon treatment does not affect the RAGE oligomerization induced by acidosis (Fig. 47A, line 4), a decrease in RAGE oligomers formation was observed after 72h Azeliragon treatment (Fig. 47A, line 6). This could be related with the fact that pMET induced by Azeliragon starts at 72h, not before. However, FPS-ZM1 does not inhibit RAGE oligomerization induced by acidosis (Fig. 47B, line 2). This could be explained because the two antagonists bind to different regions of RAGE V-domain [128]. Additionally, less RAGE oligomers were generated in knockdown RAGE cells (Fig. 47C).

Therefore, the results suggest that acidosis induces RAGE oligomerization in the plasma membrane near cortactin, which is inhibited by Azeliragon but not FPS-ZM1.

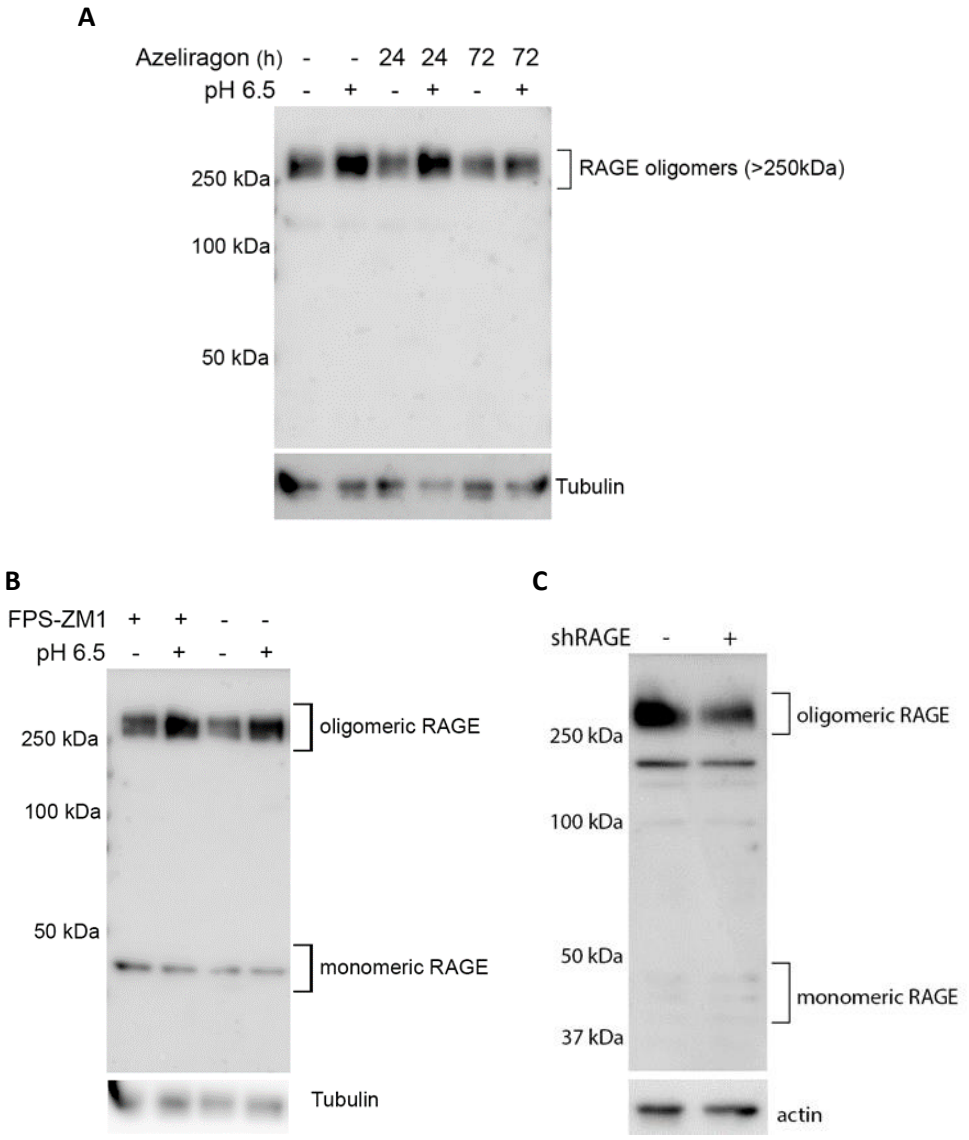

Figure 47. Acidosis induces RAGE oligomerization. Non-reducing conditions were used to detect RAGE aggregates in MDA-MB-231 cells exposed 24h to acidosis with or without RAGE antagonists. **(A)** Cells were pre-treated or not 48h with 2μM Azeliragon and then were subjected 24h to acidic conditions. **(B)** Detection of RAGE oligomers in MDA-MB-231 cells previously treated 48h with 30μM FPS-ZM1 or 2μM Azeliragon following 24h acidosis maintaining RAGE antagonists' treatment. **(C)** RAGE oligomerization in knockdown RAGE cells. Tubulin and actin were used as loading control.

4.2. The RAGE-ERK1/2-SNAIL1 pathway is required for the tumor cell invasion induced by acute acidosis

Previous results (in chapter 3) demonstrated that RAGE inhibition reduces SNAIL1 expression causing a MET in MDA-MB-231 cells, and reducing their migratory and invasive capacities. After establishing that acidosis induces RAGE relocation on the plasma membrane and increases cell invasion, we decided to test whether under acidic conditions SNAIL1 is involved in the increase of cell motility through RAGE. To do that, we measured the mRNA and protein levels of SNAIL1 in MDA-MB-231 cells exposed at pH 6.5 for short periods of time. As observed in figure 48, SNAIL1 was overexpressed at both protein and mRNA (*SNAI1*) levels in acidic conditions (Fig. 48A and 48B). We also detected an increase of the nuclear foci of SNAIL1 when cells were exposed for 24h to pH 6.5 (Fig. 48C). Noteworthy, SNAIL1 overexpression correlates with cortactin phosphorylation, which indicates that cortactin is activated in the invadopodia (Fig. 48D). Therefore, the results suggest that acute acidosis increases migration and invasion through SNAIL1 up-regulation.

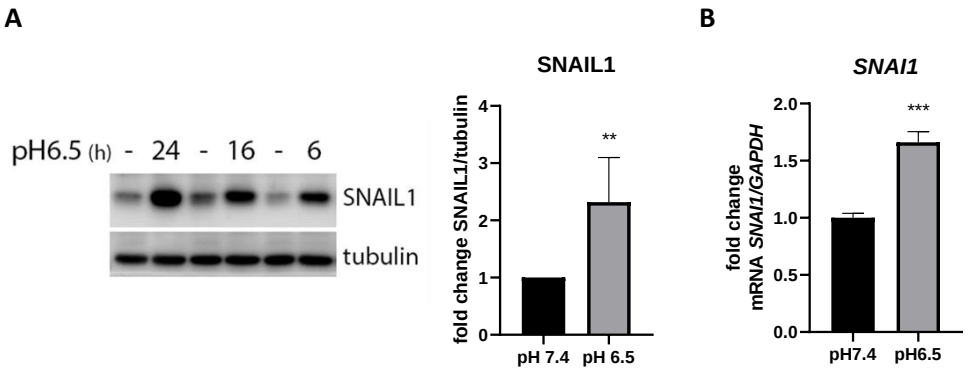

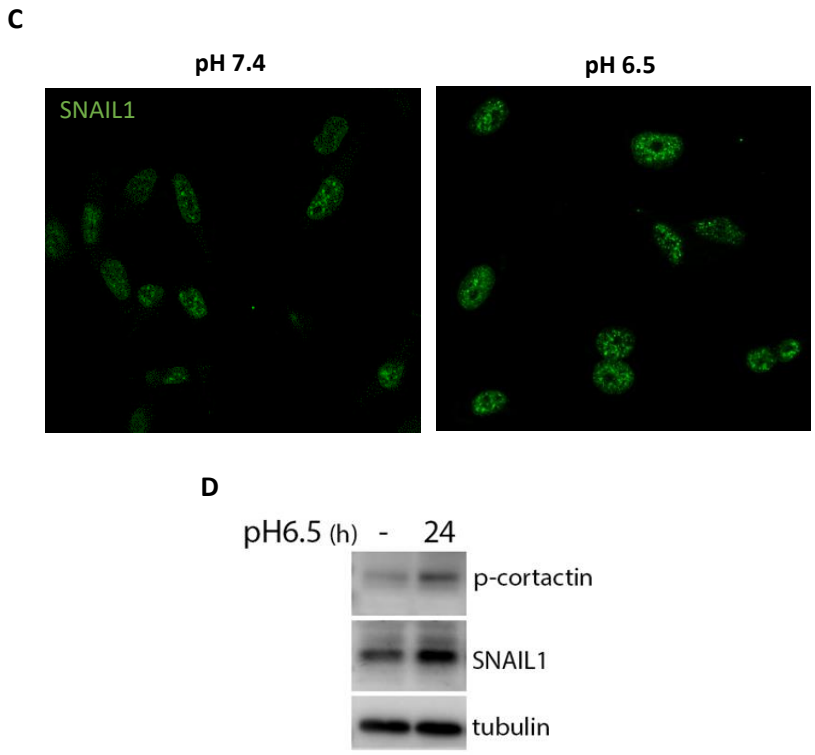

Figure 48. Acidosis increases SNAIL1 expression in MDA-MB-231 cells. (A) Expression of SNAIL1 in cells exposed 24h, 16h and 6h to acidosis. Quantification of SNAIL1 protein from different experiments of cells exposed 24h to pH 6.5. **(B)** Analysis of *SNAI1* mRNA expression in cells subjected 24h to acidic conditions. **(C)** Representative images of SNAIL1 immunofluorescence after 24h acidosis. **(D)** Detection of SNAIL1 and phosphor-cortactin expression from cells exposed 24h to acidosis. Results shown are the means for at least three independent experiments. Statistical analyses were done using unpaired t-test. **p<0.01 and ***p<0.001

After connecting the acidic microenvironment to SNAIL1 expression, we decided to study whether RAGE was involved in this process. First, we investigated the effect of acidosis in RAGE signaling pathways. The results showed that acidosis mostly activates ERK1/2 (Fig. 49A, line 4).

Then, we studied whether RAGE antagonists could inhibit the signaling, as well as SNAIL1 over-expression induced by acidosis. The results demonstrated that both RAGE antagonists (FPS-ZM1 and Azeliragon) reduce ERK1/2 phosphorylation during acidosis (Fig. 49A, line 5 and 6). However, the increase observed in NF-kB phosphorylation is not inhibited by RAGE antagonists. In addition, RAGE inhibition

with RAGE antagonists (Fig. 49B) or knockdown RAGE (Fig. 49C) reduce SNAIL1 expression induced by acidosis. Therefore, the RAGE-ERK1/2 signaling pathway is involved in SNAIL1 overexpression induced by acute acidosis.

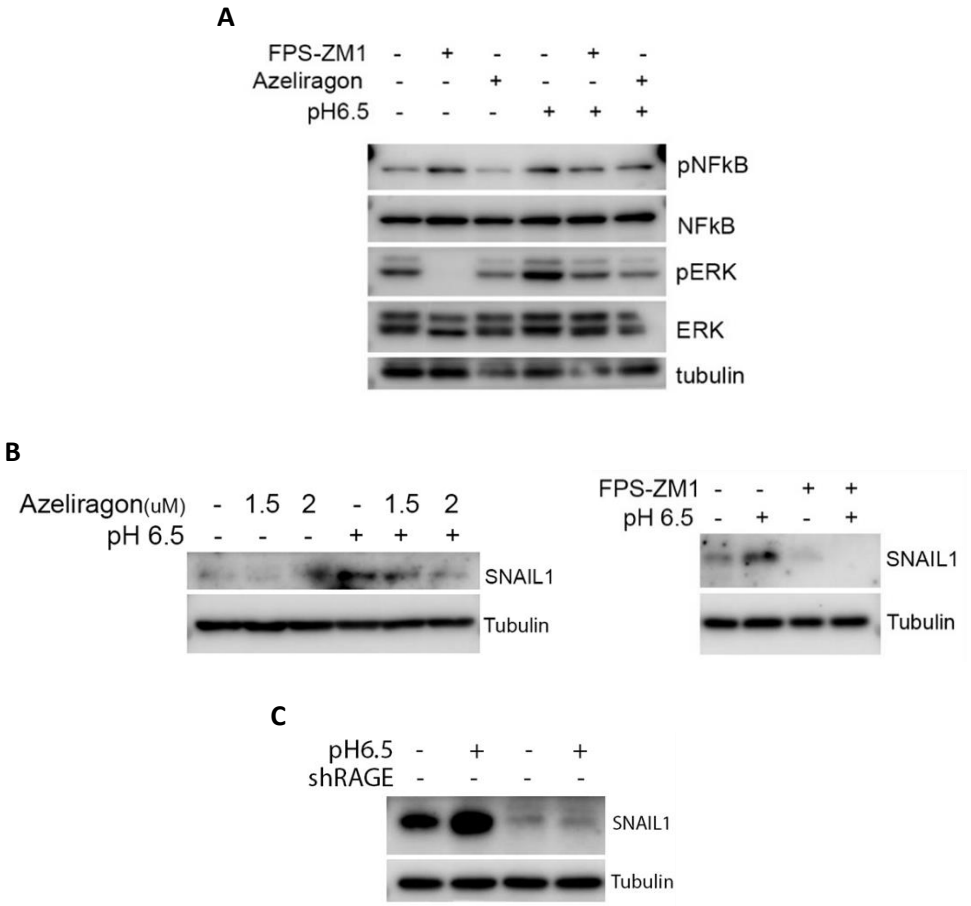

Figure 49. Acidosis activates ERK1/2 pathway inhibited by RAGE antagonists. (A) Effect of acute acidosis (2h) with or without RAGE antagonists (30µM FPS-ZM1 for 20min and 2µM Azeliragon for 1h) on RAGE pathway in MDA-MB-231 cells. **(B)** SNAIL1 expression in MDA-MB-231 cells pre-treated 48h with Azeliragon (left) or 30µM FPS-ZM1 (right) and then exposed 24h to acidosis keeping the RAGE antagonist' treatment. **(C)** Expression of SNAIL1 in shRAGE cells subjected 24h to pH 6.5. Tubulin was used as loading control.

SNAIL1 is an EMT-TF that plays a key role during EMT. We detected SNAIL1 overexpression in acidic conditions, whereas RAGE antagonists either at neutral and acidic conditions down-regulated it. Then, we decided to study the effect of RAGE antagonists on EMT under acidic conditions. We observed an increase of β-catenin

in the plasma membrane in cells treated with the two RAGE antagonists (Fig. 50A). This effect was maintained in acidic conditions (Fig. 50B) after treatment with the antagonists. Furthermore, IF analysis reinforced the results obtained previously by WB, confirming that RAGE antagonists inhibit RAGE oligomerization in the plasma membrane induced by acidic conditions (Fig. 50B). Although we previously did not detect a decrease in RAGE oligomerization with FPS-ZM1 by western blot (Fig. 47B), we did observe an effect by IF. This could be explained by the fact we used a different Ab in the WB and IF analyses, since one antibody recognizes the intracellular domain whereas the other recognizes the extracellular domain. Therefore, RAGE antagonists block the effects induced by acidosis and promote a partial MET.

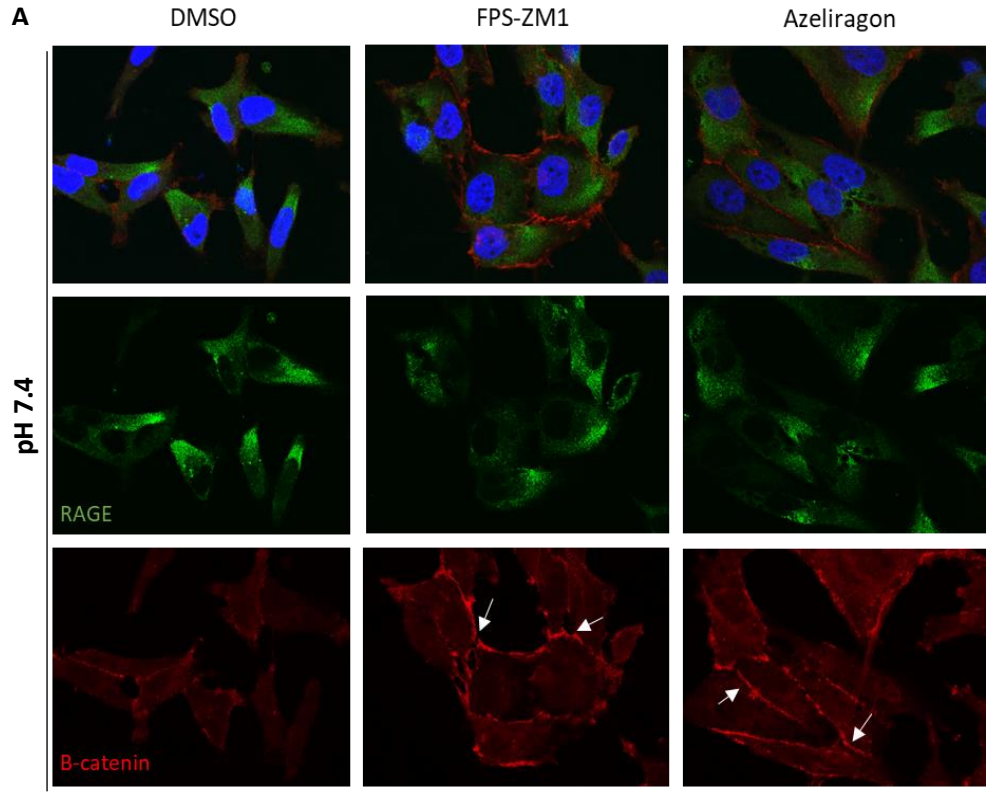

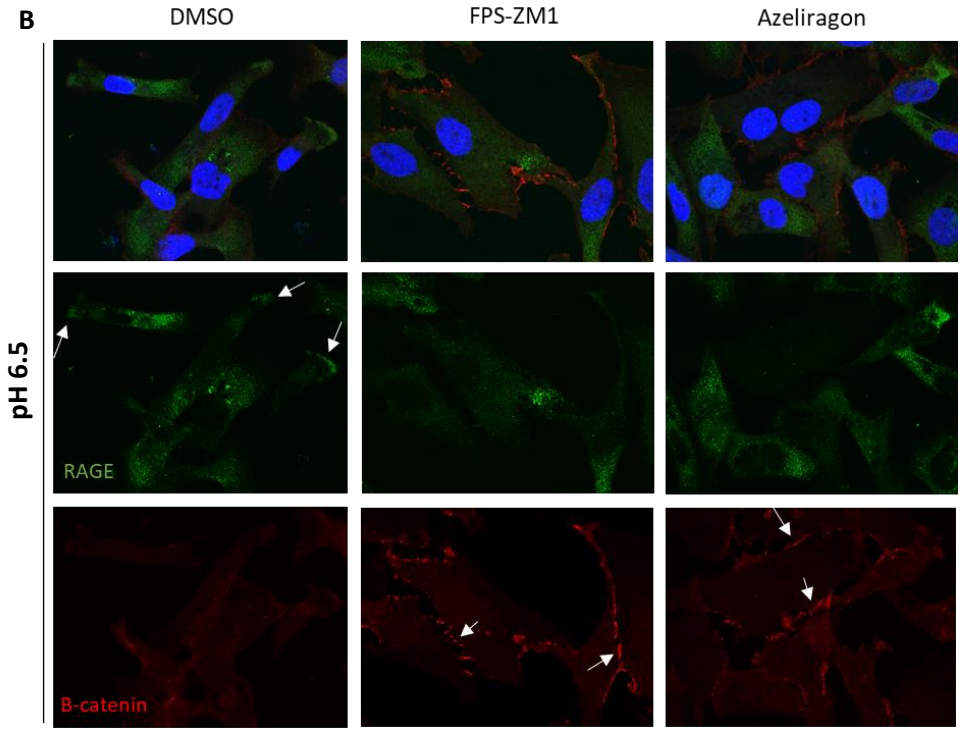

Figure 50. RAGE antagonists block the effect of acidosis inducing a partial MET. Representative images of β-catenin (red) and extracellular RAGE expression (green)in MDA-MB-231 cells (A) Cells were treated for 72h with 30μM FPS-ZM1 or 2μM Azeliragon. (B) Cells were pre-treated for 48h with both RAGE antagonists and then exposed 24h to acidosis keeping the antagonist treatment. Arrows indicate β-catenin expression and RAGE aggregates expression in the plasma membrane. For this purpose, RAGE staining was performed without permeabilization following permeabilization for β-catenin staining.

Finally, we decided to study whether RAGE plays a role in cell invasion induced by acidic conditions. Our previous results demonstrate that acidosis induces RAGE oligomerization in the plasma membrane and increases RAGE signaling pathway inducing SNAIL1 overexpression. These effects are blocked when RAGE is inhibited. Although we detected an increase in cortactin phosphorylation in acidosis, we did not know whether RAGE was involved in cell invasion caused by acidosis. To study that, we analyzed cell invasiveness by transwell assay in MDA-MB-231 cells subjected to acidosis treated with or without RAGE antagonist. As previously observed, acidosis increases cell invasion but this effect was significantly reduced by RAGE antagonist' treatment (Fig. 51).

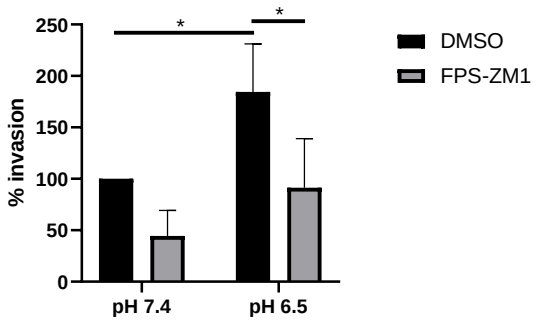

Figure 51. Acidosis increases cell invasion which is impaired by RAGE antagonist. MDA-MB-231 cells were pre-treated for 48h with 30μM FPS-ZM1 before doing transwell invasion assay 24h with or without acidosis. Statistical analyses were done using two-way ANOVA. *p<0.05

Altogether, these results revealed that acute acidosis induces RAGE oligomerization in the plasma membrane, an important step to activate the RAGE-ERK1/2-SNAIL1 pathway involved in cell migration and invasion. Besides, blocking RAGE oligomerization with RAGE antagonists reduce cell invasiveness by reversing the EMT.

5. CHARACTERIZING THE EFFECT OF AZELIRAGON DURING TUMORIGENESIS

Our *in vitro* results demonstrate that RAGE has a role in tumor cell invasion, and RAGE inhibition reduces cell aggressiveness inducing a partial MET in MDA-MB-231 cells. To validate the role of RAGE *in vivo*, MDA-MB-231 cells expressing the luciferase gen were orthotopically injected in the mammary fat pad of NOD-SCID mice treated with the vehicle or Azeliragon at 5mg/kg (see Materials and Methods section). We decided to use Azeliragon instead of FPS-ZM1, because although in 2D-culture there were no apparent differences among them related with cell invasion and EMT reversion, in 3D-culture the effect of Azeliragon in reducing tumoroids protrusions was higher than FPS-ZM1. Furthermore, Azeliragon is more soluble and its working concentration is lower, which is better for *in vivo* experiments. During the experiment, mice were treated 6 days a week with Azeliragon (5mg/kg) or vehicle and tumor volume and body weight were measured once a week. The

analysis in the primary tumor growth showed no statistical differences between Azeliragon and vehicle groups (Fig. 52A, B). Tumor volume results correlated well with our previous analysis on cell proliferation *in vitro* (Fig. 40), where no differences were detected on cell proliferation with Azeliragon treatment.

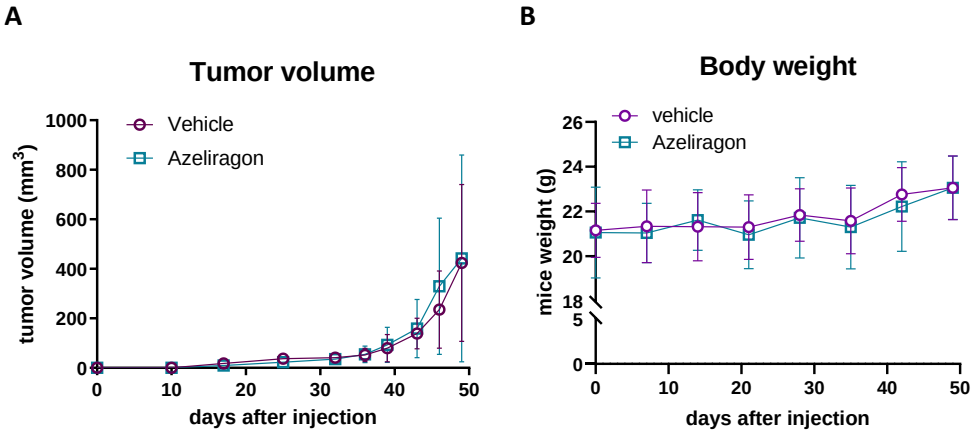

Figure 52. Tumorigenesis is not affected by Azeliragon. (A) Analysis of the primary tumor volume of mice xenograft after 5mg/kg Azeliragon treatment. **(B)** Body weight analysis of mice xenograft treated with 5mg/kg Azeliragon.

After the primary tumor was resected, treatment was kept until the experimental end point. During this time, metastases were controlled every week by luciferase signaling. Twelve days after the resection of the primary tumor, all mice of the vehicle group expressed bioluminescence signaling, whereas only two mice of the Azeliragon group expressed bioluminescence (Fig. 53).

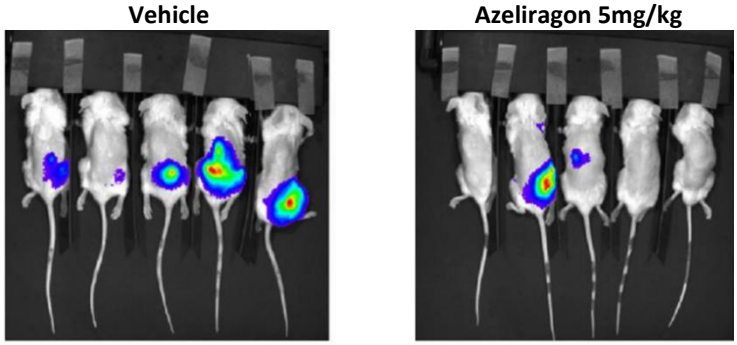

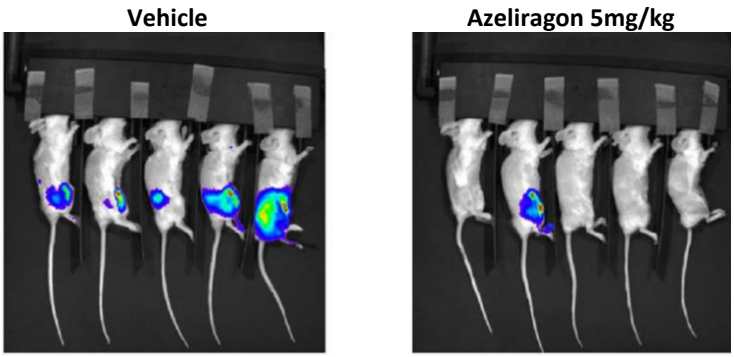

Figure 53. Azeliragon reduces metastases in vivo. Luciferase expression after 12 days of the primary tumor excision in mice treated with Azeliragon (right) or vehicle (left). Images acquired from the top (upper panel) or from the lateral (lower panel) perspective of mice xenograft.

Finally, when mice were sacrificed, metastases at different organs were quantified by bioluminescence imaging. The results showed a decreased relative luciferase units (RLU) in most of the organs of animals treated with Azeliragon (Fig. 54A). Even when the differences were not significant because the number of mice were too small, there was a tendency in the reduction of luciferase intensity in the organs from mice of the Azeliragon group. For example, in lung tissue, 4 of 5 animals of the Azeliragon group have lower levels of RLU compared to the vehicle group (Fig. 54B), presenting a smaller number of metastatic foci when they were analyzed by hematoxylin and eosin staining (Fig. 54B). Furthermore, the number of organs with metastases per mice was reduced with Azeliragon treatment (Fig. 54C). These differences were clearly reflected by an increase in the animal survival of the Azeliragon group (Fig. 54D). Although these results are encouraging, experiments should be repeated with more animals per group to improve the results and obtain better statistics.

A

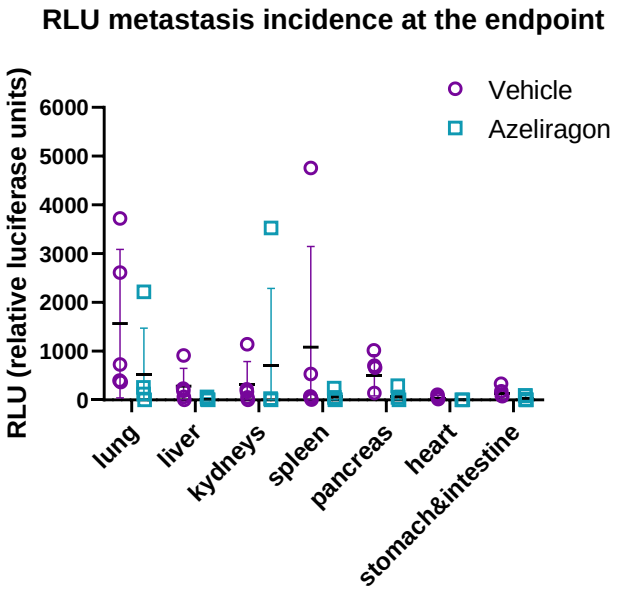

B

TREATMENT	ANIMALS	RLU
Vehicle	1	725,61
	2	2610,82
	3	367,55
	4	396,37
	5	3724,95
Azeliragon 5mg/kg	1	120,06
	2	256,97
	3	2217,32
	4	4,41
	5	5,27

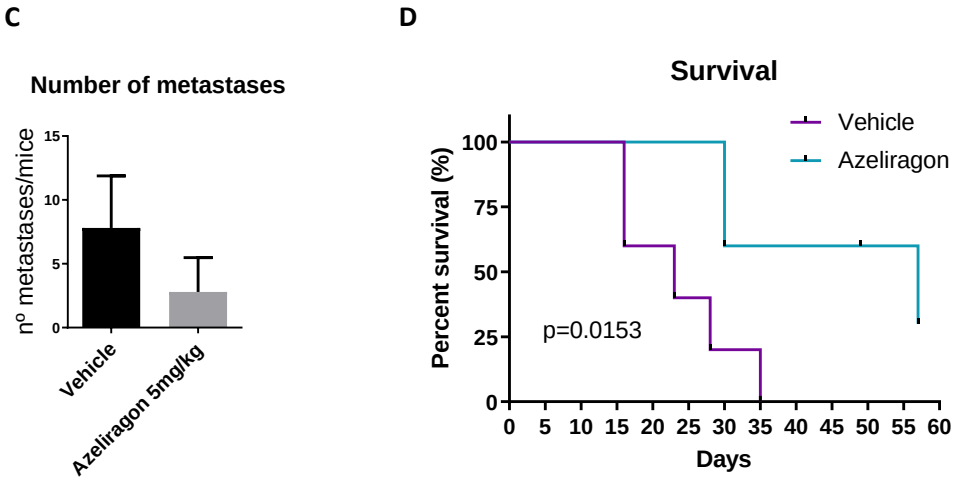

Figure 54. Azeliragon reduces metastases formation and increases survival rate in vivo. (A) Ex vivo relative luciferase units (RLU) of different organs from mice treated with Azeliragon compared to the vehicle. **(B)** (left) Table showing the RLU of lung tissue, and (right) a representative image of a hematoxylin and eosin staining of lung tissue from the vehicle and Azeliragon group. **(C)** Mean of the number of metastatic organs per mice. **(D)** Percentage survival of mice treated with 5mg/kg Azeliragon. Statistical significance of the animal survival was calculated using the Long-Rang (Mantel-Cox) test. P-value (p) is represented in the figure.

In summary, although Azeliragon does not affect primary tumor proliferation, it reduces metastasis incidence increasing overall survival *in vivo*.

DISCUSSION

In a tumor, the levels of oxygen are reduced due to the high proliferative rate of tumor cells and resulting poor blood perfusion. Under hypoxia, tumor cells switch their metabolism towards glycolysis. Due to the high glycolytic rate, the extracellular pH in tumors become more acidic than in healthy tissues. These microenvironmental stress conditions, which are known to promote tumorigenesis [83,236], are also associated to an increase in unconventional protein secretion [84,116,117]. In our studies, we confirmed that breast cancer cells become more invasive when exposed to hypoxia, acidosis or glucose starvation. Furthermore, acidosis promotes the secretion of selected unconventionally secreted proteins such as the family of High-mobility group (HMG).

Microenvironmental stress can fluctuate from acute to chronic, and from moderate to severe depending on stress duration and severity. In our work, we compared invasiveness between chronic and acute stresses conditions in breast cancer cells. The results demonstrated that acute stress promote cell invasion, whereas chronic stress reduce it. Additionally, chronic stressed cells increase cytoplasmic vacuoles, which has also been reported in cells adapted to extracellular stress conditions. These cells up-regulate autophagic and lysosomal activity as survival mechanisms [237–240]. In some of these studies, the authors correlate the increased lysosomal and autophagic activity with an increase in cell invasion and proliferation. We did not observe this correlation, although the experimental conditions that we used to generate the stressed subpopulation were somehow different. In their case, to generate for example acid adapted cells, cells were passaged directly into low pH and maintained for 2-3 months until cells regained their original proliferative rate. Instead, in our case cells were gradually conditioned, but once they reach the final pH conditions, we started the phenotypic experiments, without waiting for a cell proliferation recovery.

The acute microenvironmental stresses studied in this thesis are hypoxia, acidosis and glucose starvation, which increase cell migration and invasion in different cell lines (MDA-MB-231, MCF-7 and MCF10A). We have particularly focused on acute

acidosis, which induces quite a dramatic change in the secretome. Under acidic conditions, we detected an over-secretion of the unconventional secreted HMGs proteins. When secreted, HMGs proteins interact with cell surface receptors, including RAGE, toll-like receptors-4 (TLR-4) and −2 (TLR-2), CD24/Siglec-10 and CXCR4 [241–244]. In secretomes obtained from cells undergoing acute acidosis, we also detected other RAGE-ligands such as S100 proteins, although they were not significantly over-secreted. In the last year, Sadeghi *et al*., described that acid adapted cells over-secrete S100s proteins, which induce EMT and tumorigenesis [86]. Although in our cells we did not detect the over-secretion of S100s proteins, maybe because of different experimental conditions used, these results reinforce our hypothesis that RAGE ligands are over-secreted under tumor microenvironmental stresses, and could have a role in breast tumor aggressiveness.

Acute acidosis strongly increases the phosphorylation of ERK1/2 and the expression of SNAIL1 in TNBC cells. These changes are reversed when RAGE expression is ablated or when cells are treated with RAGE antagonists. In support to our results, other investigators also described that extracellular acidosis induces ERK1/2 activation in different cancer cells [41,245] (Riemann *et al.*, 2011; Chen *et al.*, 2016). Given the heterogeneity of tumor cells, it is likely that different types of tumor cells may have different intracellular signaling pathways regulated in response to acidosis. For example, other studies have reported the activation of AKT, NF-kB or p38 under acidic conditions [40,41,246].

Our results show that acute acidosis induces RAGE oligomers in the plasma membrane of breast cancer cells. These oligomers co-localize with cortactin in the invasive front of the plasma membrane and their formation is inhibited by RAGE antagonists and RAGE ablation. Therefore, RAGE oligomerization might be a required step for the signaling transduction mediated by RAGE. In fact, Zong et al. demonstrate that RAGE dimerization is essential for ligand recognition and RAGE pathway activation, and Xie J, *et al*. suggest that RAGE activation generates oligomers [141,247]. Therefore, we hypothesize that the RAGE-oligomers could reside in

the aggregates we detected in acidosis, which are linked to the activation of RAGE signaling. A possible explanation for these aggregates came from a recent report that linked the recruitment of RAGE into lipid rafts during inflammation [248]. Lipid rafts are cholesterol-enriched microdomains implicated in different physiological cellular processes including protein membrane trafficking and signal transduction [249,250]. Since lipid rafts are localized in invadopodia [251], the RAGE-oligomers in the plasma membrane could be RAGE being recruited into lipid rafts during cell migration/invasion.

Overall, our results suggest that acute acidosis induces an over-secretion or a stabilization of HMG proteins that activate ERK1/2 and increase SNAIL1 expression by the activation of RAGE through its oligomerization, promoting breast cancer cell migration and invasion. Despite we do not know whether there is a specific ligand responsible to enhance cell invasion in acidic conditions, RAGE antagonists interfere with RAGE oligomers formation in the plasma membrane reducing cell migration and invasion induced by acute acidosis.

RAGE-engagement by its ligands, activate multiple signaling pathways, some of them involved in cell migration and proliferation [204,208]. Existing literature suggest a large complexity of RAGE signaling pathway activation depending on cell type, the type of ligand and its concentration as well as RAGE oligomerization capacity [143,208]. In this thesis, after stimulating breast cancer cells with different RAGE ligands, we detected that NF-kB is activated by different S100 proteins and HMGA1, while ERK1/2 is induced by different HMGs proteins and methylglyoxal (MGO). However, RAGE-ligand activation is blocked with RAGE antagonists. Previous studies also detected ERK1/2 activation by MGO and AGEs, promoting cell migration, invasion and metastasis formation [129,158,168]. In the literature, S100 and HMGs proteins are associated to different RAGE-mediated pathways, especially NF-kB [150,200,232], and ERK1/2 [189,212,252], both of them pushing for tumor growth and metastasis. Moreover, in our studies, those ligands, as well as acidosis, induce cortactin relocation to the plasma membrane promoting cell motility. By contrast, cortactin is translocated

from the invadopodia to the cytoplasm in MDA-MB-231 and BT549 cells when RAGE activation is suppressed, reducing their migratory capacity. Cortactin participates in the cytoskeletal rearrangement that forms lamellipodia and invadopodia, playing an important role in cell migration and invasion [220,253,254].

RAGE activation has been previously related to cellular plasticity. In the kidneys, RAGE mediates the fibrosis that leads to renal disease [229]. RAGE is also associated to fibrosis in the lens epithelial cells inducing secondary cataracts [230,255], and in the lungs contributing to pulmonary fibrosis [231,256]. Although RAGE is not well studied in cancer, its activation has been associated to an increase in cell migration, invasion and EMT in some tumor cell types. For example, HMGB1 in pancreatic cancer and S100A8/A9 in breast cancer, have been reported to induce EMT through the RAGE-NF-kB signaling pathway [200,232]. EMT is a dynamic process in which epithelial cells undergo phenotypic changes. Epithelial cells lose their apical-basal polarity and cell-cell adhesions to allow them to gain motility, enhancing tumor invasion and metastasis dissemination [45]. Interestingly, in our work, both RAGE antagonists and the ablation of RAGE expression decreases the phosphorylation of ERK1/2 followed by SNAIL1 down-regulation, in different TNBC cells. The decrease in SNAIL1 expression, is accompanied by a shift in β-catenin and ZO-1 expression and relocation to the plasma membrane. The results highlight the importance of the RAGE-ERK1/2 signaling in TNBC cells to induce EMP.

Two different RAGE antagonists (FPS-ZM1 and Azeliragon) which bind to different regions of the V-domain were used to block RAGE signaling pathway. RAGE antagonists have been previously used to block the receptor in inflammatory diseases [176,177,230,257]. Since most of studies with FPS-ZM1 and Azeliragon have been done in Alzheimer's disease, little is known about the effect of RAGE antagonists in cancer. Furthermore, previous results obtained in cancer are related with cell proliferation and migration [139,258], while few studies analyze the effect on cell invasion, and none of them observe an effect on cell morphology, reversing the EMT phenotype.

In this thesis, we found that RAGE antagonists down-regulate SNAIL1 in breast cancer cell lines triggering a partial MET. Nevertheless, we did not observe an increase of E-cadherin expression in MDA-MB-231 cells treated with RAGE antagonists. MDA-MB-231 have a strong mesenchymal phenotype and they might not be able to re-express and localize E-Cadherin in the plasma membrane. Besides, other cadherins could be involved in the MET process. P-cadherin has been reported to maintain epithelial tissue [259]. Furthermore, P-cadherin down-regulation has been correlated with melanoma and hepatocellular carcinoma progression [260,261]. Despite the lack of E-cadherin up-regulation, other epithelial markers including β-catenin, ZO-1 and claudin-1 were over-expressed and located to the plasma membrane increasing cell adhesions. Furthermore, the localization of β-catenin to the plasma membrane implies its binding to a cadherin, perhaps P-cadherin or even N-cadherin.

In the last decade, some studies started to link RAGE and TGF-β pathways. Most of these studies were done in fibrosis developed in patients with diabetic complications [229,262,263]. In diabetes there is an increase in AGEs which play a role in EMT. Usually, the TGF-β pathway is considered a responsible mediator in tissue fibrosis, such as renal, pulmonary and hepatic fibrosis, by activating the SMAD signaling pathway [264–266]. However, it is reported that AGEs also trigger diabetic fibrosis by activating SMAD pathway independently of TGF-β [262]. Moreover, AGEs enhance CTGF via RAGE-ERK1/2/p38-SMAD3 pathway in renal fibrosis [263]. In our studies, we observed an increase in SNAIL1 expression upon TGF-β1 treatment in both MDA-MB-231 and NMuMG cells, which promotes EMT through the SMAD (SMAD2) and non-SMAD (ERK1/2) pathways. The induction of EMT mediated by TGF-β1-ERK1/2 pathway has been previously reported in NMuMG cells, although in this report they did not analyze the expression of any EMT-TF [267]. In our study, although both RAGE antagonists block SNAIL1 expression induced by TGF-β1, the effect on SNAIL1 was even higher when both pathways were inhibited at the same time. These results suggest a possible synergy between RAGE and TGF-β pathways to reinforce EMT. Indeed, FPS-ZM1 reduces both ERK1/2 and SMAD2 signaling in NMuMG cells treated

with TGF-β1, suggesting a possible interaction between the two pathways. Along this line, a study investigating fibrosis in lens epithelial cells also uncovered a link between RAGE and TGF-β pathway, by observing a decrease in phospho-SMAD2 when RAGE was inhibited [230,255]. Although the crosstalk between RAGE and TGF-β pathways has not been well studied in cancer, a recent study proposed that the TGF-β1-mediated EMT is regulated by the HMGB1-RAGE pathway in hypopharyngeal carcinoma cells [268].

SNAIL1 represses the expression of E-cadherin by binding directly to the E-box motif of the E-cadherin promoter [269,270]. Since E-cadherin plays a role in cell adhesion, the down-regulation of E-cadherin involves the loss of cell adhesions and an increase in cell mobility. Moreover, in cancer, SNAIL1 expression induces the epithelial-mesenchymal transition increasing cell invasion. SNAIL1 inhibition reverses EMT reducing cell invasiveness, and could have therapeutic implications [71]. EMT plays a key role in tumor progression and metastasis dissemination, and is an attractive therapeutic target for cancer. However, controversial opinions emerged after some studies showed that EMT reversion is important for macrometastasis formation. It is thought that the mesenchymal phenotype is required to invade and escape from the primary tumor and extravasate to a secondary site, although EMT reversion is also important to acquire epithelial characteristics for metastatic outgrowth [271–273]. However, when it comes to proliferation our results are mixed. The ablation of RAGE expression increases cell proliferation. By contrast, Azeliragon does not affect cell proliferation, whereas FPS-ZM1 antagonist reduces cell proliferation compared to non-treated cells. More research is needed to understand how three different interventions (knockdown and two drugs against RAGE) that induce a pMET reducing cell migration and invasion, can induce such a disparity of effects on cell proliferation. Additionally, it is described that EMT confers therapeutic resistance [274–278] Therefore, inhibition or reversion of mesenchymal transition is still considered a potential therapeutic treatment for cancer.

Here we investigated the impact of RAGE on tumor progression and metastasis formation in TNBC cells. We validated that RAGE drive EMT and tumor cell invasion in mesenchymal TNBC cells, while RAGE inhibition reduces cell invasiveness by reverting EMT. In 3D culture, we observed that breast cancer cells lose their branching phenotype when RAGE is blocked using RAGE antagonists or RAGE ablation, associated with a decrease in cell migration and invasion.

Despite RAGE has a role during embryonic development, RAGE null mice are viable, fertile and present a phenotype similar to wild-type mice [279,280], although they are more active and more sensitive to auditory stimuli [281]. Previous studies in cancer with RAGE knockout or knockdown mice, observe an increase in overall survival and a decrease in tumor progression [140,282,283]. In our *in vivo* experiment, MDA-MB-231 cells were orthotopically implanted in NOD-SCID mice and treated with or without Azeliragon. Since RAGE plays a role in many pathological disorders, it has become an attractive therapeutic target for the development of inhibitors. Azeliragon is a small-molecule RAGE inhibitor that was initially used in Alzheimer's disease. It has been used in phase III clinical trials in mild to moderate Alzheimer's disease slowing cognitive decline, although it did not meet the primary endpoint of the trial [177,284,285]. These studies established that Azeliragon has no toxic side effects. In our *in vivo* study, the results revealed that Azeliragon reduces the capacity of MDA-MB-231 cells to generate metastasis. Furthermore, mice treated with Azeliragon have an overall survival rate longer than vehicle group although no differences were detected in the primary tumor growth. Similar results were obtained by Kwak *et al*. in mice treated with FPS-ZM1 [140]. Overall, the results suggest that RAGE antagonists could offer a safe therapeutic approach to target EMT and therapeutic resistance in breast cancer.

In conclusion, RAGE is a key mediator of breast cancer metastasis by promoting EMT. RAGE ligands activate NF-kB or ERK1/2 signaling pathway increasing cell invasion and migration. However, RAGE antagonists block RAGE signaling reducing SNAIL1 expression reversing the mesenchymal phenotype. Furthermore, RAGE antagonists reduce the capacity of breast cancer cells to generate metastasis increasing overall

survival *in vivo* models. Therefore, RAGE could be a potential therapeutic target for breast cancer.

CONCLUSIONS

1. Tumor microenvironmental stress increases the migration and invasion of BC cells. Moreover, acute acidosis increases the secretion of RAGE ligands in BC cells.

2. RAGE drives EMT in mesenchymal TNBC cells through ERK1/2-SNAIL1 pathway, and mediates cell migration and invasion.

3. The inhibition and down-regulation of RAGE reverses EMT inducing a partial mesenchymal-epithelial transition (pMET) in TNBC cells, and decreases tumor cell adhesion, migration and invasion.

4. Acute acidosis induces the oligomerization of RAGE in the plasma membrane of TNBC cells, which correlates with cell migration and invasion.

5. Acute acidosis activates the RAGE-ERK1/2-SNAIL1 pathway and promotes breast cancer invasion. Furthermore, RAGE antagonists impair the acidosis effects by reversing EMT.

6. There is a cross-talk between RAGE and TGF-β pathways in the mediation of EMT through SMAD2/ERK1/2 and SNAIL1. Besides, RAGE antagonists interfere with the induction of EMT by TGF-β1.

7. RAGE antagonists impair branching morphogenesis in 3D-culture of TNBC cells. Furthermore, Azeliragon treatment of a TNBC *in vivo* model reduces metastasis incidence and increases overall survival.

8. RAGE is a candidate therapeutic target in TNBC.

REFERENCES

1. Foulkes W, Smith I, Reis-Filho J. Tripel-negatives Breast Cancer. *N Engl J Med*. 2010;363:1938-1948. doi:10.1159/000321918

2. Cardoso F. Global Status Metastatic Breast Cancer Report (2005-2015). *Glob Status Metastatic Breast Cancer Rep*. 2016;(March). http://www.breastcancervision.com.

3. Waks AG, Winer EP, Winer M. Breast Cancer Treatment: A Review. *JAMA - J Am Med Assoc*. 2019;321(3):288-300. doi:10.1001/jama.2018.19323

4. Núñez Abad M, Calabuig-Fariñas S, Lobo de Mena M, et al. Update on systemic treatment in early triple negative breast cancer. *Ther Adv Med Oncol*. 2021;13:1-18. doi:10.1177/1758835920986749

5. Lehmann B, Jovanović B, Chen X, et al. Refinement of Triple-Negative Breast Cancer Molecular Subtypes: Implications for Neoadjuvant Chemotherapy Selection. *PLoS One*. 2016;11(6):e0157368. doi:10.1371/JOURNAL.PONE.0157368

6. Burstein MD, Tsimelzon A, Poage GM, et al. Comprehensive genomic analysis identifies novel subtypes and targets of triple-negative breast cancer. *Clin Cancer Res*. 2015;21(7):1688-1698. doi:10.1158/1078-0432.CCR-14-0432

7. Kim C, Gao R, Sei E, et al. Chemoresistance Evolution in Triple-Negative Breast Cancer Delineated by Single-Cell Sequencing. *Cell*. 2018;173(4):879-893. doi:10.1016/j.cell.2018.03.041

8. Kim J, Yu D, Kwon Y, et al. Genomic Characteristics of Triple-Negative Breast Cancer Nominate Molecular Subtypes That Predict Chemotherapy Response. *Mol Cancer Res*. 2020;18(2):253-263. doi:10.1158/1541-7786.MCR-19-0453

9. Garrido-Castro AC, Lin NU, Polyak K. Insights into molecular classifications of triple-negative breast cancer: Improving patient selection for treatment. *Cancer Discov*. 2019;9(2):176-198. doi:10.1158/2159-8290.CD-18-1177

10. Criscitiello C, Morganti S, Curigliano G. Antibody–drug conjugates in solid tumors: a look into novel targets. *J Hematol Oncol 2021 141*. 2021;14(1):1-18. doi:10.1186/S13045-021-01035-Z

11. Ballinger T, Kremer J, Miller K. Triple negative breast cancer-review of current and emerging therapeutic strategies. *Eur Oncol Haematol*. 2016;12(2):112-117. doi:10.17925/OHR.2016.12.02.89

12. Liu Y, Teng L, Fu S, et al. Highly heterogeneous-related genes of triple-negative breast cancer: potential diagnostic and prognostic biomarkers. *BMC Cancer*. 2021;21(644):1-15. doi:10.1186/S12885-021-08318-1

13. Loibl S, O'Shaughnessy J, Untch M, et al. Addition of the PARP inhibitor veliparib plus carboplatin or carboplatin alone to standard neoadjuvant

chemotherapy in triple-negative breast cancer (BrighTNess): a randomised, phase 3 trial. *Lancet Oncol*. 2018;19(4):497-509. doi:10.1016/S1470-2045(18)30111-6

14. Schmid P, Abraham J, Chan S, et al. Capivasertib plus paclitaxel versus placebo plus paclitaxel as first-line therapy for metastatic triple-negative breast cancer: The PAKT trial. In: *Journal of Clinical Oncology*. Vol 38. J Clin Oncol; 2020:423-433. doi:10.1200/JCO.19.00368

15. Lee JS, Yost SE, Yuan Y. Neoadjuvant treatment for triple negative breast cancer: Recent progresses and challenges. *Cancers (Basel)*. 2020;12(6). doi:10.3390/cancers12061404

16. Cortes J, Cescon DW, Rugo HS, et al. Pembrolizumab plus chemotherapy versus placebo plus chemotherapy for previously untreated locally recurrent inoperable or metastatic triple-negative breast cancer (KEYNOTE-355): a randomised, placebo-controlled, double-blind, phase 3 clinical trial. *Lancet*. 2020;396(10265):1817-1828. doi:10.1016/S0140-6736(20)32531-9

17. Schmid P, Cortes J, Pusztai L, et al. Pembrolizumab for Early Triple-Negative Breast Cancer. *N Engl J Med*. 2020;382(9):810-821. doi:10.1056/nejmoa1910549

18. Hanahan D, Weinberg RA. Hallmarks of cancer: The next generation. *Cell*. 2011;144(5):646-674. doi:10.1016/j.cell.2011.02.013

19. Place AE, Jin Huh S, Polyak K. The microenvironment in breast cancer progression: Biology and implications for treatment. *Breast Cancer Res*. 2011;13(6). doi:10.1186/bcr2912

20. Mittal S, Brown NJ, Holen I. The breast tumor microenvironment: role in cancer development, progression and response to therapy. *Expert Rev Mol Diagn*. 2018;18(3):227-243. doi:10.1080/14737159.2018.1439382

21. Boedtkjer E, Pedersen SF. The Acidic Tumor Microenvironment as a Driver of Cancer. *Annu Rev Physiol*. 2020;82:103-126. doi:10.1146/annurev-physiol-021119-034627

22. Vaupel P. Tumor microenvironmental physiology and its implications for radiation oncology. *Semin Radiat Oncol*. 2004;14(3):198-206. doi:10.1016/j.semradonc.2004.04.008

23. Nelson DL, Cox MM. *Lehninger Principles of Biochemistry*. Vol 5th.; 2000. doi:10.1007/978-3-662-08289-8

24. Vander Heiden MG, Cantley LC, Thompson CB. Understanding the warburg effect: The metabolic requirements of cell proliferation. *Science (80-)*. 2009;324(5930):1029-1033. doi:10.1126/science.1160809

25. Chen JLY, Merl D, Peterson CW, et al. Lactic acidosis triggers starvation response with paradoxical induction of TXNIP through MondoA. *PLoS Genet*. 2010;6(9):e1001093. doi:10.1371/journal.pgen.1001093

26. Ihling A, Ihling CH, Sinz A, Gekle M. Acidosis-Induced Changes in Proteome Patterns of the Prostate Cancer-Derived Tumor Cell Line AT-1. *J Proteome Res*. 2015;14(9):150804111902001. doi:10.1021/acs.jproteome.5b00503

27. Zagzag D, Lukyanov Y, Lan L, et al. Hypoxia-inducible factor 1 and VEGF upregulate CXCR4 in glioblastoma: implications for angiogenesis and glioma cell invasion. *Lab Investig*. 2006;86:1221-1232. doi:10.1038/labinvest.3700482

28. Chiche J, Brahimi-Horn MC, Pouysségur J. Tumour hypoxia induces a metabolic shift causing acidosis: A common feature in cancer. *J Cell Mol Med*. 2010;14(4):771-794. doi:10.1111/j.1582-4934.2009.00994.x

29. Semenza GL. Oxygen Sensing, Hypoxia-Inducible Factors, and Disease Pathophysiology. *Annu Rev Pathol Mech Dis*. 2014;9(1):47-71. doi:10.1146/annurev-pathol-012513-104720

30. Majmundar AJ, Wong WJ, Simon MC. Hypoxia-Inducible Factors and the Response to Hypoxic Stress. *Mol Cell*. 2010;40(2):294-309. doi:10.1016/j.molcel.2010.09.022

31. Kato Y, Ozawa S, Miyamoto C, et al. Acidic extracellular microenvironment and cancer. *Cancer Cell Int*. 2013;13(1):1. doi:10.1186/1475-2867-13-89

32. Peppicelli S, Andreucci E, Ruzzolini J, et al. The acidic microenvironment as a possible niche of dormant tumor cells. *Cell Mol Life Sci*. 2017;74(15):2761-2771. doi:10.1007/s00018-017-2496-y

33. Koltai T. Cancer: Fundamentals behind pH targeting and the double-edged approach. *Onco Targets Ther*. 2016;9:6343-6360. doi:10.2147/OTT.S115438

34. Gatenby RA, Gillies RJ. Why do cancers have high aerobic glycolysis? *Nat Rev Cancer*. 2004;4(11):891-899. doi:10.1038/nrc1478

35. Pastorekova S, Gillies RJ. The role of carbonic anhydrase IX in cancer development: links to hypoxia, acidosis, and beyond. *Cancer Metastasis Rev*. 2019;38:65-77. doi:10.1007/s10555-019-09799-0

36. Federici C, Petrucci F, Caimi S, et al. Exosome release and low pH belong to a framework of resistance of human melanoma cells to cisplatin. *PLoS One*. 2014;9(2):e88193. doi:10.1371/journal.pone.0088193

37. Webster KA, Discher DJ, Kaiser S, Hernandez O, Sato B, Bishopric NH. Hypoxia-activated apoptosis of cardiac myocytes requires reoxygenation or a pH shift and is independent of p53. *J Clin Invest*. 1999;104(3):239-252.

doi:10.1172/jci5871

38. Suzuki A, Maeda T, Baba Y, Shimamura K, Kato Y. Acidic extracellular ph promotes epithelial mesenchymal transition in lewis lung carcinoma model. *Cancer Cell Int*. 2014;14(1):1-11. doi:10.1186/s12935-014-0129-1

39. Rohani N, Hao L, Alexis MS, et al. Acidification of tumor at stromal boundaries drives transcriptome alterations associated with aggressive phenotypes. *Cancer Res*. 2019;79(8):1952-1966. doi:10.1158/0008-5472.CAN-18-1604

40. Gupta SC, Singh R, Pochampally R, Watabe K, Mo Y-Y. Acidosis promotes invasiveness of breast cancer cells through ROS-AKT-NF-kB pathway. *Oncotarget*. 2014;5(23). doi:10.18632/oncotarget.2514

41. Chen B, Liu J, Ho TT, Ding X, Mo YY. Erk-mediated nf-κb activation through asic1 in response to acidosis. *Oncogenesis*. 2016;5(12):1-8. doi:10.1038/oncsis.2016.81

42. Palm W. Metabolic plasticity allows cancer cells to thrive under nutrient starvation. *Proc Natl Acad Sci U S A*. 2021;118(14):1-3. doi:10.1073/PNAS.2102057118

43. Pavlova NN, Thompson CB. The Emerging Hallmarks of Cancer Metabolism. *Cell Metab*. 2016;23(1):27-47. doi:10.1016/J.CMET.2015.12.006

44. Finicle BT, Jayashankar V, Edinger AL. Nutrient scavenging in cancer. *Nat Rev Cancer*. 2018;18(10):619-633. doi:10.1038/s41568-018-0048-x

45. Yang J, Antin P, Berx G, et al. Guidelines and definitions for research on epithelial–mesenchymal transition. *Nat Rev Mol Cell Biol*. 2020;21(6):341-352. doi:10.1038/s41580-020-0237-9

46. Thiery JP, Acloque H, Huang RYJ, Nieto MA. Epithelial-Mesenchymal Transitions in Development and Disease. *Cell*. 2009;139(5):871-890. doi:10.1016/j.cell.2009.11.007

47. Nieto MA, Huang RYYJ, Jackson RAA, Thiery JPP. Emt: 2016. *Cell*. 2016;166(1):21-45. doi:10.1016/j.cell.2016.06.028

48. Haensel D, Dai X. Epithelial-to-mesenchymal transition in cutaneous wound healing: Where we are and where we are heading. *Dev Dyn*. 2018;247(3):473-480. doi:10.1002/DVDY.24561

49. Williams ED, Gao D, Redfern A, Thompson EW. Controversies around epithelial–mesenchymal plasticity in cancer metastasis. *Nat Rev Cancer*. 2019;19(12):716-732. doi:10.1038/s41568-019-0213-x

50. Basu S, Cheriyamundath S, Ben-Ze'ev A. Cell–cell adhesion: Linking wnt/β-catenin signaling with partial emt and stemness traits in tumorigenesis. *F1000Research*. 2018;7:1488. doi:10.12688/F1000RESEARCH.15782.1

51. Jolly MK, Boareto M, Huang B, et al. Implications of the hybrid epithelial/mesenchymal phenotype in metastasis. *Front Oncol*. 2015;5:155. doi:10.3389/fonc.2015.00155

52. Grigore AD, Jolly MK, Jia D, Farach-Carson MC, Levine H. Tumor budding: The name is EMT. partial EMT. *J Clin Med*. 2016;5(5). doi:10.3390/jcm5050051

53. Pastushenko I, Blanpain C. EMT Transition States during Tumor Progression and Metastasis. *Trends Cell Biol*. 2019;29(3):212-226. doi:10.1016/j.tcb.2018.12.001

54. Pastushenko I, Brisebarre A, Sifrim A, et al. Identification of the tumour transition states occurring during EMT. *Nature*. 2018;556(7702):463-468. doi:10.1038/s41586-018-0040-3

55. Yu M, Bardia A, Wittner BS, et al. Circulating breast tumor cells exhibit dynamic changes in epithelial and mesenchymal composition. *Science (80-)*. 2013;339(6119):580-584. doi:10.1126/science.1228522

56. Friedl P, Mayor R. Tuning collective cell migration by cell-cell junction regulation. *Cold Spring Harb Perspect Biol*. 2017;9(4):1-17. doi:10.1101/cshperspect.a029199

57. Aiello NM, Kang Y. Context-dependent EMT programs in cancer metastasis. *J Exp Med*. 2019;216(5):1016-1026. doi:10.1084/jem.20181827

58. Huang RY-J, Wong MK, Tan TZ, et al. An EMT spectrum defines an anoikis-resistant and spheroidogenic intermediate mesenchymal state that is sensitive to e-cadherin restoration by a src-kinase inhibitor, saracatinib (AZD0530). *Cell Death Dis*. 2013;4:e915. doi:10.1038/cddis.2013.442

59. Thomas PA, Kirschmann DA, Cerhan JR, et al. Association between keratin and vimentin expression, malignant phenotype, and survival in postmenopausal breast cancer patients. *Clin Cancer Res*. 1999;5(10):2698-2703.

60. George JT, Jolly MK, Xu S, Somarelli JA, Levine H. Survival outcomes in cancer patients predicted by a partial EMT gene expression scoring metric. *Cancer Res*. 2017;77(22):6415-6428. doi:10.1158/0008-5472.CAN-16-3521

61. Grosse-Wilde A, D'Hérouël AF, McIntosh E, et al. Stemness of the hybrid epithelial/mesenchymal state in breast cancer and its association with poor survival. *PLoS One*. 2015;10(5):e0126522. doi:10.1371/journal.pone.0126522

62. Dmello C, Sawant S, Alam H, et al. Vimentin regulates differentiation switch via modulation of keratin 14 levels and their expression together correlates with poor prognosis in oral cancer patients. *PLoS One*. 2017;12(2):e0172559. doi:10.1371/journal.pone.0172559

63. Gheldof A, Berx G. *Cadherins and Epithelial-to-Mesenchymal Transition*. Vol

116. 1st ed. Elsevier Inc.; 2013. doi:10.1016/B978-0-12-394311-8.00014-5

64. Peinado H, Olmeda D, Cano A. Snail, ZEB and bHLH factors in tumour progression: An alliance against the epithelial phenotype? *Nat Rev Cancer*. 2007;7(6):415-428. doi:10.1038/nrc2131

65. Roy S, Sunkara RR, Parmar MY, Shaikh S, Waghmare SK. EMT imparts cancer stemness and plasticity: new perspectives and therapeutic potential. *Front Biosci - Landmark*. 2021;26(2):238-265. doi:10.2741/4893

66. Yang MH, Wu MZ, Chiou SH, et al. Direct regulation of TWIST by HIF-1α promotes metastasis. *Nat Cell Biol*. 2008;10(3):295-305. doi:10.1038/ncb1691

67. Stemmler MP, Eccles RL, Brabletz S, Brabletz T. Non-redundant functions of EMT-TFs. *Nat Cell Biol*. 2019;21(January):102-112. https://doi.org/10.1038/s41556-018-0196-y.

68. Dong C, Wu Y, Yao J, et al. G9a interacts with Snail and is critical for Snail-mediated E-cadherin repression in human breast cancer. *J Clin Invest*. 2012;122(4):1469-1486. doi:10.1172/JCI57349DS1

69. Shioiri M, Shida T, Koda K, et al. Slug expression is an independent prognostic parameter for poor survival in colorectal carcinoma patients. *Br J Cancer*. 2006;94(12):1816-1822. doi:10.1038/sj.bjc.6603193

70. Endo K, Ueda T, Ueyama J, Ohta T, Terada T. Immunoreactive E-cadherin, alpha-catenin, beta-catenin, and gamma- catenin proteins in hepatocellular carcinoma: Relationships with tumor grade, clinicopathologic parameters, and patients' survival. *Hum Pathol*. 2000;31(5):558-565. doi:10.1053/hp.2000.6683

71. Tran HD, Luitel K, Kim M, Zhang K, Longmore GD, Tran DD. Transient SNAIL1 expression is necessary for metastatic competence in breast cancer. *Cancer Res*. 2014;74(21):6330-6340. doi:10.1158/0008-5472.CAN-14-0923

72. Wang W die, Shang Y, Li Y, Chen S zhen. Honokiol inhibits breast cancer cell metastasis by blocking EMT through modulation of Snail/Slug protein translation. *Acta Pharmacol Sin*. 2019;40(9):1219-1227. doi:10.1038/s41401-019-0240-x

73. Karihtala P, Auvinen P, Kauppila S, Haapasaari KM, Jukkola-Vuorinen A, Soini Y. Vimentin, zeb1 and Sip1 are up-regulated in triple-negative and basal-like breast cancers: Association with an aggressive tumour phenotype. *Breast Cancer Res Treat*. 2013;138(1):81-90. doi:10.1007/s10549-013-2442-0

74. Krebs AM, Mitschke J, Losada ML, et al. The EMT-activator Zeb1 is a key factor for cell plasticity and promotes metastasis in pancreatic cancer. *Nat Cell Biol*. 2017;19(5):518-529. doi:10.1038/ncb3513

75. Cho H-J, Oh N, Park J-H, et al. ZEB1 Collaborates with ELK3 to Repress E-Cadherin Expression in Triple-Negative Breast Cancer Cells. *Mol Cancer Res*. 2019;17(11):2257-2266. doi:10.1158/1541-7786.MCR-19-0380

76. Wang F, Sun G, Peng C, et al. ZEB1 promotes colorectal cancer cell invasion and disease progression by enhanced LOXL2 transcription. *Int J Clin Exp Pathol*. 2021;14(1):9-23.

77. Bruneel K, Verstappe J, Vandamme N, Berx G. Intrinsic balance between zeb family members is important for melanocyte homeostasis and melanoma progression. *Cancers (Basel)*. 2020;12(8):1-25. doi:10.3390/cancers12082248

78. Lu W, Kang Y. Epithelial-Mesenchymal Plasticity in Cancer Progression and Metastasis. *Dev Cell*. 2019;49(3):361-374. doi:10.1016/j.devcel.2019.04.010

79. Lamouille S, Subramanyam D, Blelloch R, Derynck R. Regulation of epithelial—mesenchymal and mesenchymal— epithelial transitions by microRNAs. *Curr Opin Cell Biol*. 2013;25(2):200-207. doi:10.1016/j.ceb.2013.01.008.Regulation

80. Zhou BP, Deng J, Xia W, et al. Dual regulation of Snail by GSK-3β-mediated phosphorylation in control of epithelial-mesenchymal transition. *Nat Cell Biol*. 2004;6(10):931-940. doi:10.1038/ncb1173

81. Wu CY, Tsai YP, Wu MZ, Teng SC, Wu KJ. Epigenetic reprogramming and post-transcriptional regulation during the epithelial-mesenchymal transition. *Trends Genet*. 2012;28(9):454-463. doi:10.1016/j.tig.2012.05.005

82. Estrella V, Chen T, Lloyd M, et al. Acidity generated by the tumor microenvironment drives local invasion. *Cancer Res*. 2013;73(5):1524-1535. doi:10.1158/0008-5472.CAN-12-2796.Acidity

83. Damaghi M, Gillies R. Phenotypic changes of acid-adapted cancer cells push them toward aggressiveness in their evolution in the tumor microenvironment. *Cell Cycle*. 2017;16(19):1739-1743. doi:10.1080/15384101.2016.1231284

84. Park JE, Tan H Sen, Datta A, et al. Hypoxic tumor cell modulates its microenvironment to enhance angiogenic and metastatic potential by secretion of proteins and exosomes. *Mol Cell Proteomics*. 2010;9(6):1085-1099. doi:10.1074/mcp.M900381-MCP200

85. Peppicelli S, Bianchini F, Torre E, Calorini L. Contribution of acidic melanoma cells undergoing epithelial-to-mesenchymal transition to aggressiveness of non-acidic melanoma cells. *Clin Exp Metastasis*. 2014;31(4):423-433. doi:10.1007/s10585-014-9637-6

86. Sadeghi M, Ordway B, Rafiei I, et al. Integrative Analysis of Breast Cancer Cells Reveals an Epithelial-Mesenchymal Transition Role in Adaptation to Acidic

Microenvironment. *Front Oncol*. 2020;10:1-14. doi:10.3389/fonc.2020.00304

87. Liu Y, Liu Y, Yan X, et al. HIFs enhance the migratory and neoplastic capacities of hepatocellular carcinoma cells by promoting EMT. *Tumor Biol*. 2014;35(8):8103-8114. doi:10.1007/s13277-014-2056-0

88. Shaikh D, Zhou Q, Chen T, Ibe JCF, Raj JU, Zhou G. CAMP-dependent protein kinase is essential for hypoxia-mediated epithelial-mesenchymal transition, migration, and invasion in lung cancer cells. *Cell Signal*. 2012;24(12):2396-2406. doi:10.1016/j.cellsig.2012.08.007

89. Tang C, Tianjie LIU, Wang K, et al. Transcriptional regulation of FoxM1 by HIF-1α mediates hypoxia-induced EMT in prostate cancer. *Oncol Rep*. 2019;42(4):1307-1318. doi:10.3892/or.2019.7248

90. Du J, Sun B, Zhao X, et al. Hypoxia promotes vasculogenic mimicry formation by inducing epithelial-mesenchymal transition in ovarian carcinoma. *Gynecol Oncol*. 2014;133(3):575-583. doi:10.1016/j.ygyno.2014.02.034

91. Wang SS, Jiang J, Liang XH, Tang YL. Links between cancer stem cells and epithelial– mesenchymal transition. *Onco Targets Ther*. 2015;8:2973-2980. doi:10.2147/OTT.S91863

92. Cho E, Kang H, Kim N, Yook J. Therapeutic implications of cancer epithelial-mesenchymal transition (EMT). *Arch Pharm Res*. 2019;42:14-24. doi:10.1007/s12272-018-01108-7

93. Bhatia S, Monkman J, Toh AKL, Nagaraj SH, Thompson EW. Targeting epithelial-mesenchymal plasticity in cancer: Clinical and preclinical advances in therapy and monitoring. *Biochem J*. 2017;474(19):3269-3306. doi:10.1042/BCJ20160782

94. Ramesh V, Brabletz T, Ceppi P. Targeting EMT in Cancer with Repurposed Metabolic Inhibitors. *Trends in Cancer*. 2020;6(11):942-950. doi:10.1016/j.trecan.2020.06.005

95. Peppicelli S, Toti A, Giannoni E, et al. Metformin is also effective on lactic acidosis-exposed melanoma cells switched to oxidative phosphorylation. *Cell Cycle*. 2016;15(14):1908-1918. doi:10.1080/15384101.2016.1191706

96. Jiang Y, Zhan H. Communication between EMT and PD-L1 signaling: New insights into tumor immune evasion. *Cancer Lett*. 2020;468:72-81. doi:10.1016/j.canlet.2019.10.013

97. Lee MCS, Miller EA, Goldberg J, Orci L, Schekman R. Bi-directional protein transport between the ER and Golgi. *Annu Rev Cell Dev Biol*. 2004;20:87-123. doi:10.1146/annurev.cellbio.20.010403.105307

98. Rabouille C, Malhotra V, Nickel W. Diversity in unconventional protein

secretion. *J Cell Sci*. 2012;125(22):5251-5255. doi:10.1242/jcs.103630

99. Jiyoon K, Heon Yung G, Min Goo L. Unconventional protein secretion – new insights into the pathogenesis and therapeutic targets of human diseases. *J Cell Sci*. 2018;131(12). doi:10.1242/jcs.213686

100. Nickel W, Rabouille C. Unconventional protein secretion: Diversity and consensus. *Semin Cell Dev Biol*. 2018;83:1-2. doi:10.1016/j.semcdb.2018.03.007

101. Steringer JP, Lange S, Čujová S, et al. Key steps in unconventional secretion of fibroblast growth factor 2 reconstituted with purified components. *Elife*. 2017;6:1-36. doi:10.7554/eLife.28985

102. Michaelis S. STE6, the yeast a-factor transporter. *Semin Cell Dev Biol*. 1993;4(1):17-27. doi:10.1006/scel.1993.1003

103. Christensen PU, Davey J, Nielsen O. The Schizosaccharomyces pombe mam1 gene encodes an ABC transporter mediating secretion of M-factor. *Mol Gen Genet MGG*. 1997;255:226-236. doi:10.1007/s004380050493

104. Stahl PD, Raposo G. Extracellular Vesicles: Exosomes and Microvesicles, Integrators of Homeostasis. *Physiology*. 2019;34:169-177. doi:10.1152/physiol.00045.2018

105. D'Souza-Schorey Crislyn C, Clancy JW. Tumor-derived microvesicles: Shedding light on novel microenvironment modulators and prospective cancer biomarkers. *Genes Dev*. 2012;26(12):1287-1299. doi:10.1101/gad.192351.112

106. Kalluri R, LeBleu VS. The biology, function, and biomedical applications of exosomes. *Science (80-)*. 2020;367(6478). doi:10.1126/science.aau6977

107. Cabral M, Anjard C, Malhotra V, Loomis WF, Kuspa A. Unconventional secretion of AcbA in Dictyostelium discoideum through a vesicular intermediate. *Eukaryot Cell*. 2010;9(7):1009-1017. doi:10.1128/EC.00337-09

108. Duran JM, Anjard C, Stefan C, Loomis WF, Malhotra V. Unconventional secretion of Acb1 is mediated by autophagosomes. *J Cell Biol*. 2010;188(4):527-536. doi:10.1083/jcb.200911154

109. Grieve AG, Rabouille C. Golgi bypass: Skirting around the heart of classical secretion. *Cold Spring Harb Perspect Biol*. 2011;3(4):1-15. doi:10.1101/cshperspect.a005298

110. Nickel W, Rabouille C. Mechanisms of regulated unconventional protein secretion. *Nat Rev Mol Cell Biol*. 2008;10(FEBRUARy):148-155. doi:10.1038/nrm2645

111. Ogura Y, Sutterwala FS, Flavell RA. The Inflammasome: First Line of the

Immune Response to Cell Stress. *Cell*. 2006;126(4):659-662. doi:10.1016/J.CELL.2006.08.002

112. Hardaway AL, Podgorski I. IL-1β, RAGE and FABP4: Targeting the dynamic trio in metabolic inflammation and related pathologies. *Future Med Chem*. 2013;5(10):1089-1108. doi:10.4155/fmc.13.90

113. He Q, You H, Li X, Liu T, Wang P, Wang B. HMGB1 promotes the synthesis of pro-IL-1β and pro-IL-18 by activation of p38 MAPK and NF-κB through receptors for advanced glycation end-products in macrophages. *Asian Pac J Cancer Prev*. 2012;13(4):1365-1370. doi:10.7314/APJCP.2012.13.4.1365

114. Keller M, Rüegg A, Werner S, Beer HD. Active Caspase-1 Is a Regulator of Unconventional Protein Secretion. *Cell*. 2008;132(5):818-831. doi:10.1016/j.cell.2007.12.040

115. Martins VR, Dias MS, Hainaut P. Tumor-cell-derived microvesicles as carriers of molecular information in cancer. *Curr Opin Oncol*. 2013;25(1):66-75. doi:10.1097/CCO.0B013E32835B7C81

116. Abramowicz A, Widłak P, Pietrowska M. Different types of cellular stress affect the proteome composition of small extracellular vesicles: A mini review. *Proteomes*. 2019;7(23):1-10. doi:10.3390/proteomes7020023

117. King HW, Michael MZ, Gleadle JM. Hypoxic enhancement of exosome release by breast cancer cells. *BMC Cancer*. 2012;12(1):421. doi:10.1186/1471-2407-12-421

118. Butler GS, Overall CM. Proteomic identification of multitasking proteins in unexpected locations complicates drug targeting. *Nat Rev Drug Discov*. 2009;8(12):935-948. doi:10.1038/nrd2945

119. Méndez O, Pérez J, Soberino J, Racca F, Cortés J, Villanueva J. Clinical implications of extracellular HMGA1 in breast cancer. *Int J Mol Sci*. 2019;20(23):1-18. doi:10.3390/ijms20235950

120. Van Doormaal FF, Kleinjan A, Di Nisio M, Büller HR, Nieuwland R. Cell-derived microvesicles and cancer. *Neth J Med*. 2009;67(7):266-273.

121. Shimoda M, Khokha R. Metalloproteinases in extracellular vesicles. *Biochim Biophys Acta - Mol Cell Res*. 2017;1864(11):1989-2000. doi:10.1016/J.BBAMCR.2017.05.027

122. Hoshino D, Kirkbride KC, Costello K, et al. Exosome secretion is enhanced by invadopodia and drives invasive behavior. *Cell Rep*. 2013;5(5):1159-1168. doi:10.1016/j.celrep.2013.10.050

123. Neeper M, Schmidt AM, Brett J, et al. Cloning and expression of a cell surface receptor for advanced glycosylation end products of proteins. *J Biol Chem*.

1992;267(21):14998-15004.

124. Akirav EM, Preston-Hurlburt P, Garyu J, et al. RAGE expression in human T cells: A link between environmental factors and adaptive immune responses. *PLoS One*. 2012;7(4):e34698. doi:10.1371/journal.pone.0034698

125. Narumi K, Miyakawa R, Ueda R, et al. Proinflammatory Proteins S100A8/S100A9 Activate NK Cells via Interaction with RAGE. *J Immunol*. 2015;194(11):5539-5548. doi:10.4049/jimmunol.1402301

126. Schmidt AM. Receptor for advanced glycation endproducts and implications for the pathogenesis an treatment of cardiometabolic disorders: Spotlight on the macrophage. *Arterioscler Thromb Vasc Biol*. 2017;37(4):613-621. doi:10.1161/ATVBAHA.117.307263

127. Demling N, Ehrhardt C, Kasper M, Laue M, Knels L, Rieber EP. Promotion of cell adherence and spreading: A novel function of RAGE, the highly selective differentiation marker of human alveolar epithelial type I cells. *Cell Tissue Res*. 2006;323(3):475-488. doi:10.1007/s00441-005-0069-0

128. Bongarzone S, Savickas V, Luzi F, Gee AD. Targeting the Receptor for Advanced Glycation Endproducts (RAGE): A Medicinal Chemistry Perspective. *J Med Chem*. 2017;60(17):7213-7232. doi:10.1021/acs.jmedchem.7b00058

129. Ko S-Y, Ko H-A, Shieh T-M, et al. Cell migration is regulated by AGE-RAGE interaction in human oral cancer cells in vitro. *PLoS One*. 2014;9(10):e110542. doi:10.1371/journal.pone.0110542

130. Hori O, Brett J, Slattery T, et al. The receptor for advanced glycation end products (RAGE) is a cellular binding site for amphoterin. Mediation of neurite outgrowth and co-expression of RAGE and amphoterin in the developing nervous system. *J Biol Chem*. 1995;270(43):25752-25761. doi:10.1074/jbc.270.43.25752

131. Reynolds PR, Kasteler SD, Cosio MG, Sturrock A, Hueckstead T, Hoidal JR. RAGE: Developmental expression and positive feedback regulation by Egr-1 during cigarette smoke exposure in pulmonary epithelial cells. *Am J Physiol - Lung Cell Mol Physiol*. 2008;294(6):L1094-L1101. doi:10.1152/ajplung.00318.2007

132. Lizotte PP, Hanford LE, Enghild JJ, Nozik-Grayck E, Giles BL, Oury TD. Developmental expression of the receptor for advanced glycation end-products (RAGE) and its response to hyperoxia in the neonatal rat lung. *BMC Dev Biol*. 2007;7. doi:10.1186/1471-213X-7-15

133. Sparvero LJ, Asafu-Adjei D, Kang R, et al. RAGE (Receptor for advanced glycation endproducts), RAGE ligands, and their role in cancer and inflammation. *J Transl Med*. 2009;7:1-21. doi:10.1186/1479-5876-7-17

134. Leclerc E, Fritz G, Vetter SW, Heizmann CW. Binding of S100 proteins to RAGE: An update. *Biochim Biophys Acta - Mol Cell Res*. 2009;1793(6):993-1007. doi:10.1016/j.bbamcr.2008.11.016

135. Sessa L, Gatti E, Zeni F, et al. The Receptor for Advanced Glycation End-products (RAGE) is only present in mammals, and belongs to a family of Cell Adhesion Molecules (CAMs). *PLoS One*. 2014;9(1):e86903. doi:10.1371/journal.pone.0086903

136. Yan SF, Ramasamy R, Schmidt AM. The RAGE axis a fundamental mechanism signaling danger to the vulnerable vasculature. *Circ Res*. 2010;106(5):842-853. doi:10.1161/CIRCRESAHA.109.212217

137. Cai Z, Liu N, Wang C, et al. Role of RAGE in Alzheimer's Disease. *Cell Mol Neurobiol*. 2016;36(4):483-495. doi:10.1007/s10571-015-0233-3

138. Palanissami G, Paul SFD. RAGE and Its Ligands: Molecular Interplay Between Glycation, Inflammation, and Hallmarks of Cancer—a Review. *Horm Cancer*. 2018;9(5):295-325. doi:10.1007/s12672-018-0342-9

139. Swami P, Thiyagarajan S, Vetter SW, Leclerc E, Vidger A, Indurthi VSK. Rage up-regulation differently affects cell proliferation and migration in pancreatic cancer cells. *Int J Mol Sci*. 2020;21(20):1-19. doi:10.3390/ijms21207723

140. Kwak T, Drews-Elger K, Ergonul A, et al. Targeting of RAGE-ligand signaling impairs breast cancer cell invasion and metastasis. *Oncogene*. 2017;36(11):1559-1572. doi:10.1038/onc.2016.324

141. Xie J, Reverdatto S, Frolov A, Hoffmann R, Burz DS, Shekhtman A. Structural basis for pattern recognition by the receptor for advanced glycation end products (RAGE). *J Biol Chem*. 2008;283(40):27255-27269. doi:10.1074/JBC.M801622200

142. Koch M, Chitayat S, Dattilo BM, et al. Structural Basis for Ligand Recognition and Activation of RAGE. *Structure*. 2010;18(10):1342-1352. doi:10.1016/j.str.2010.05.017

143. Hudson BI, Lippman ME. Targeting RAGE Signaling in Inflammatory Disease. *Annu Rev Med*. 2018;69(1):24.1-24.16. doi:10.1146/annurev-med-041316-085215

144. Teissier T, Boulanger É. The receptor for advanced glycation end-products (RAGE) is an important pattern recognition receptor (PRR) for inflammaging. *Biogerontology*. 2019;20(3):279-301. doi:10.1007/s10522-019-09808-3

145. Leclerc E, Fritz G, Weibel M, Heizmann CW, Galichet A. S100B and S100A6 differentially modulate cell survival by interacting with distinct RAGE (receptor for advanced glycation end products) immunoglobulin domains. *J Biol Chem*. 2007;282(43):31317-31331. doi:10.1074/jbc.M703951200

146. Xie J, Burz DS, He W, Bronstein IB, Lednev I, Shekhtman A. Hexameric calgranulin C (S100A12) binds to the receptor for advanced glycated end products (RAGE) using symmetric hydrophobic target-binding patches. *J Biol Chem*. 2007;282(6):4218-4231. doi:10.1074/jbc.M608888200

147. Yatime L, Andersen GR. Structural insights into the oligomerization mode of the human receptor for advanced glycation end-products. *FEBS J*. 2013;280(24):6556-6568. doi:10.1111/febs.12556

148. Yamamoto KI, Murata H, Putranto EW, et al. DOCK7 is a critical regulator of the RAGE-Cdc42 signaling axis that induces formation of dendritic pseudopodia in human cancer cells. *Oncol Rep*. 2013;29(3):1073-1079. doi:10.3892/or.2012.2191

149. Ott C, Jacobs K, Haucke E, Navarrete Santos A, Grune T, Simm A. Role of advanced glycation end products in cellular signaling. *Redox Biol*. 2014;2(1):411-429. doi:10.1016/j.redox.2013.12.016

150. Chen RC, Yi PP, Zhou RR, et al. The role of HMGB1-RAGE axis in migration and invasion of hepatocellular carcinoma cell lines. *Mol Cell Biochem*. 2014;390(1-2):271-280. doi:10.1007/s11010-014-1978-6

151. Taguchi A, Blood DC, Del Toro G, et al. Blockade of RAGE-amphoterin signalling suppresses tumour growth and metastases. *Nature*. 2000;405(6784):354-360. doi:10.1038/35012626

152. Geroldi D, Falcone C, Emanuele E. Soluble Receptor for Advanced Glycation End Products: From Disease Marker to Potential Therapeutic Target. *Curr Med Chem*. 2006;13(17):1971-1978. doi:10.2174/092986706777585013

153. Santilli F, Vazzana N, Bucciarelli L, Davi G. Soluble Forms of RAGE in Human Diseases: Clinical and Therapeutical Implications. *Curr Med Chem*. 2009;16(8):940-952. doi:10.2174/092986709787581888

154. Koyama H, Yamamoto H, Nishizawa Y. RAGE and soluble RAGE: Potential therapeutic targets for cardiovascular diseases. *Mol Med*. 2007;13(11-12):625-635. doi:10.2119/2007-00087.Koyama

155. Tesařová P, Kalousová M, Jáchymová M, Mestek O, Petruzelka L, Zima T. Receptor for advanced glycation end products (RAGE) - Soluble form (sRAGE) and gene polymorphisms in patients with breast cancer. *Cancer Invest*. 2007;25(8):720-725. doi:10.1080/07357900701560521

156. Li T, Qin W, Liu Y, Li S, Qin X, Liu Z. Effect of RAGE gene polymorphisms and circulating sRAGE levels on susceptibility to gastric cancer: A case-control study. *Cancer Cell Int*. 2017;17(19):1-10. doi:10.1186/s12935-017-0391-0

157. Jing R, Cui M, Wang J, Wang H. Receptor for advanced glycation end products (RAGE) soluble form (sRAGE): A new biomarker for lung cancer. *Neoplasma*.

2010;57(1):55-61. doi:10.4149/neo_2010_01_055

158. Sharaf H, Matou-Nasri S, Wang Q, et al. Advanced glycation endproducts increase proliferation, migration and invasion of the breast cancer cell line MDA-MB-231. *Biochim Biophys Acta - Mol Basis Dis*. 2015;1852(3):429-441. doi:10.1016/j.bbadis.2014.12.009

159. Azizian-Farsani F, Abedpoor N, Hasan Sheikhha M, Gure AO, Nasr-Esfahani MH, Ghaedi K. Receptor for Advanced Glycation End Products Acts as a Fuel to Colorectal Cancer Development. *Front Oncol*. 2020;10:1-24. doi:10.3389/FONC.2020.552283

160. Singh R, Barden A, Mori T, Beilin L. Advanced glycation end-products: A review. *Diabetologia*. 2001;44(2):129-146. doi:10.1007/s001250051591

161. Maillard LC. Action des acides aminés sur les sucres: Formation des mélanoidines par voie méthodique. Réaction de Maillard. *C R Acad Sci*. 1912;154:66-68.

162. John WG, Lamb EJ. The maillard or browning reaction in diabetes. *Eye*. 1993;7(2):230-237. doi:10.1038/eye.1993.55

163. Luevano-Contreras C, Chapman-Novakofski K. Dietary advanced glycation end products and aging. *Nutrients*. 2010;2(12):1247-1265. doi:10.3390/nu2121247

164. Cerami C, Founds H, Nicholl I, et al. Tobacco smoke is a source of toxic reactive glycation products. *Proc Natl Acad Sci U S A*. 1997;94(25):13915-13920. doi:10.1073/pnas.94.25.13915

165. Jangde N, Ray R, Rai V. RAGE and its ligands: from pathogenesis to therapeutics. *Crit Rev Biochem Mol Biol*. 2020;55(6):555-575. doi:10.1080/10409238.2020.1819194

166. Schlkwijk C, Stehouwer C. Methylglyoxal, a Highly Reactive Dicarbonyl Compound, in Diabetes, Its Vascular Complications, and Other Age-Related Diseases. *Physiol Rev*. 2020;100:407-461. doi:10.1152/physrev.00001.2019

167. Maessen DEM, Stehouwer CDA, Schalkwijk CG. The role of methylglyoxal and the glyoxalase system in diabetes and other age-related diseases. *Clin Sci*. 2015;128(12):839-861. doi:10.1042/CS20140683

168. Nokin M-J, Bellier J, Durieux F, et al. Methylglyoxal, a glycolysis metabolite, triggers metastasis through MEK/ERK/SMAD1 pathway activation in breast cancer. *Breast Cancer Res*. 2019;21(11):1-19. doi:10.1186/s13058-018-1095-7

169. Bellier J, Nokin M-J, Caprasse M, et al. Methylglyoxal Scavengers Resensitize KRAS-Mutated Colorectal Tumors to Cetuximab. *Cell Rep*. 2020;30(5):1400-

1416.e6. doi:10.1016/j.celrep.2020.01.012

170. Nokin M-J, Durieux F, Bellier J, et al. Hormetic potential of methylglyoxal, a side-product of glycolysis, in switching tumours from growth to death. *Sci Rep*. 2017;7(1):1-14. doi:10.1038/s41598-017-12119-7

171. Chen GF, Xu TH, Yan Y, et al. Amyloid beta: Structure, biology and structure-based therapeutic development. *Acta Pharmacol Sin*. 2017;38:1205-1235. doi:10.1038/aps.2017.28

172. Yan S Du, Chen X, Fu J, et al. RAGE and amyloid-β peptide neurotoxicity in Alzheimer's disease. *Nature*. 1996;382(6593):685-691. doi:10.1038/382685a0

173. Deane R, Yan S Du, Submamaryan RK, et al. RAGE mediates amyloid-β peptide transport across the blood-brain barrier and accumulation in brain. *Nat Med*. 2003;9(7):907-913. doi:10.1038/nm890

174. Sun X, Chen WD, Wang YD. β-Amyloid: The key peptide in the pathogenesis of Alzheimer's disease. *Front Pharmacol*. 2015;6(221):1-9. doi:10.3389/fphar.2015.00221

175. Murphy MP, Levine H. Alzheimer's disease and the amyloid-β peptide. *J Alzheimer's Dis*. 2010;19(1):311-327. doi:10.3233/JAD-2010-1221

176. Deane R, Singh I, Sagare AP, et al. A multimodal RAGE-specific inhibitor reduces amyloid β-mediated brain disorder in a mouse model of Alzheimer disease. *J Clin Invest*. 2012;122(4):1377-1392. doi:10.1172/JCI58642

177. Burstein AH, Grimes I, Galasko DR, Aisen PS, Sabbagh M, Mjalli AMM. Effect of TTP488 in patients with mild to moderate Alzheimer's disease. *BMC Neurol*. 2014;14(12):1-8. doi:10.1186/1471-2377-14-12

178. Cummings JL, Tong G, Ballard C. Treatment Combinations for Alzheimer's Disease: Current and Future Pharmacotherapy Options. *J Alzheimer's Dis*. 2019;67(3):779-794. doi:10.3233/JAD-180766

179. Reeves R. Nuclear functions of the HMG proteins. *Biochim Biophys Acta - Gene Regul Mech*. 2010;1799(1-2):3-14. doi:10.1016/j.bbagrm.2009.09.001

180. Hock R, Furusawa T, Ueda T, Bustin M. HMG chromosomal proteins in development and disease. *Trends Cell Biol*. 2007;17(2):72-79. doi:10.1016/j.tcb.2006.12.001

181. Gerlitz G, Hock R, Ueda T, Bustin M. The dynamics of HMG protein-chromatin interactions in living cells. *Biochem Cell Biol*. 2009;87(1):127-137. doi:10.1139/O08-110

182. Geierstanger BH, Volkman BF, Kremer W, Wemmer DE. Short Peptide Fragments Derived from HMG-I/Y Proteins Bind Specifically to the Minor

Groove of DNA. *Biochemistry*. 1994;33(17):5347-5355. doi:10.1021/bi00183a043

183. Banks GC, Mohr B, Reeves R. The HMG-I(Y) A · T-hook peptide motif confers DNA-binding specificity to a structured chimeric protein. *J Biol Chem*. 1999;274(23):16536-16544. doi:10.1074/jbc.274.23.16536

184. Postnikov Y, Bustin M. Regulation of chromatin structure and function By HMGN proteins. *Biochim Biophys Acta - Gene Regul Mech*. 2010;1799(1-2):62-68. doi:10.1016/j.bbagrm.2009.11.016

185. Catez F, Brown DT, Misteli T, Bustin M. Competition between histone H1 and HMGN proteins for chromatin binding sites. *EMBO Rep*. 2002;3(8):760-766. doi:10.1093/embo-reports/kvf156

186. Lim JH, West KL, Rubinstein Y, Bergel M, Postnikov Y V, Bustin M. Chromosomal protein HMGN1 enhances the acetylation of lysine 14 in histone H3. *EMBO J*. 2005;24(17):3038-3048. doi:10.1038/sj.emboj.7600768

187. Arnoys EJ, Wang JL. Dual localization: Proteins in extracellular and intracellular compartments. *Acta Histochem*. 2007;109(2):89-110. doi:10.1016/j.acthis.2006.10.002

188. Park IA, Heo S-H, Song IH, et al. Endoplasmic reticulum stress induces secretion of high-mobility group proteins and is associated with tumor-infiltrating lymphocytes in triple-negative breast cancer. *Oncotarget*. 2016;7(37):59957-59964. doi:10.18632/oncotarget.11010

189. Mendez O, Peg V, Salvans C, et al. Extracellular HMGA1 promotes tumor invasion and metastasis in triple-negative breast cancer. *Clin Cancer Res*. 2018;24(24):6367-6382. doi:10.1158/1078-0432.CCR-18-0517

190. Srikrishna G, Hudson B. AGER (advanced glycosylation end product-specific receptor). *Atlas Genet Cytogenet Oncol Haematol*. 2011;15(3):239-243. doi:10.4267/2042/44975

191. Scaffidi P, Misteli T, Bianchi ME. Release of chromatin protein HMGB1 by necrotic cells triggers inflammation. *Nature*. 2002;418(6894):191-195. doi:10.1038/nature00858

192. Kim YH, Kwak MS, Lee B, et al. Secretory autophagy machinery and vesicular trafficking are involved in HMGB1 secretion. *Autophagy*. 2020. doi:10.1080/15548627.2020.1826690

193. Wang Z, Zhou H, Zheng H, et al. Autophagy-based unconventional secretion of HMGB1 by keratinocytes plays a pivotal role in psoriatic skin inflammation. *Autophagy*. 2021;17(2):529-552. doi:10.1080/15548627.2020.1725381

194. Kang R, Tang D, Schapiro NE, et al. The HMGB1/RAGE inflammatory pathway

promotes pancreatic tumor growth by regulating mitochondrial bioenergetics. *Oncogene*. 2014;33(5):567-577. doi:10.1038/onc.2012.631

195. Wang Y, Hu L, Zheng Y, Guo L. HMGA1 in cancer: Cancer classification by location. *J Cell Mol Med*. 2019;23(4):2293-2302. doi:10.1111/jcmm.14082

196. Hristov AC, Cope L, Di Cello F, et al. HMGA1 correlates with advanced tumor grade and decreased survival in pancreatic ductal adenocarcinoma. *Mod Pathol*. 2010;23(1):98-104. doi:10.1038/modpathol.2009.139

197. Roy S, Di Cello F, Kowalski J, et al. HMGA1 overexpression correlates with relapse in childhood B-lineage acute lymphoblastic leukemia. *Leuk Lymphoma*. 2013;54(11):2565-2567. doi:10.3109/10428194.2013.782610

198. Gorbounov M, Carleton NM, Asch-Kendrick RJ, et al. High mobility group A1 (HMGA1) protein and gene expression correlate with ER-negativity and poor outcomes in breast cancer. *Breast Cancer Res Treat*. 2020;179:25-35. doi:10.1007/s10549-019-05419-1

199. Silva IC de A da, Carneiro VC, Maciel R de M, et al. CK2 Phosphorylation of Schistosoma mansoni HMGB1 Protein Regulates Its Cellular Traffic and Secretion but Not Its DNA Transactions. *PLoS One*. 2011;6(8):e23572. doi:10.1371/JOURNAL.PONE.0023572

200. Yin C, Li H, Zhang B, et al. RAGE-binding S100A8/A9 promotes the migration and invasion of human breast cancer cells through actin polymerization and epithelial-mesenchymal transition. *Breast Cancer Res Treat*. 2013;142(2):297-309. doi:10.1007/s10549-013-2737-1

201. Ichikawa M, Williams R, Wang L, Vogl T, Srikrishna G. S100A8/A9 activate key genes and pathways in colon tumor progression. *Mol Cancer Res*. 2011;9(2):133-148. doi:10.1158/1541-7786.MCR-10-0394

202. Ishihara K, Tsutsumi K, Kawane S, Nakajima M, Kasaoka T. The receptor for advanced glycation end-products (RAGE) directly binds to ERK by a D-domain-like docking site. *FEBS Lett*. 2003;550(1-3):107-113. doi:10.1016/S0014-5793(03)00846-9

203. Rai V, Maldonado AY, Burz DS, Reverdatto S, Schmidt AM, Shekhtman A. Signal transduction in receptor for advanced glycation end products (RAGE): Solution structure of C-terminal rage (ctRAGE) and its binding to mDia1. *J Biol Chem*. 2012;287(7):5133-5144. doi:10.1074/jbc.M111.277731

204. Xie J, Méndez JD, Méndez-Valenzuela V, Aguilar-Hernández MM. Cellular signalling of the receptor for advanced glycation end products (RAGE). *Cell Signal*. 2013;25(11):2185-2197. doi:10.1016/j.cellsig.2013.06.013

205. Sakaguchi M, Murata H, Yamamoto K ichi, et al. TIRAP, an adaptor protein for TLR2/4, transduces a signal from RAGE phosphorylated upon ligand binding.

PLoS One. 2011;6(8):e23132. doi:10.1371/journal.pone.0023132

206. El-Far AH, Sroga G, Al Jaouni SK, Mousa SA. Role and mechanisms of rage-ligand complexes and rage-inhibitors in cancer progression. *Int J Mol Sci*. 2020;21(10):3613. doi:10.3390/ijms21103613

207. Kierdorf K, Fritz G. RAGE regulation and signaling in inflammation and beyond. *J Leukoc Biol*. 2013;94:55-68. doi:10.1189/jlb.1012519

208. Olaoba OT, Kadasah S, Vetter SW, Leclerc E. Rage signaling in melanoma tumors. *Int J Mol Sci*. 2020;21(23):1-32. doi:10.3390/ijms21238989

209. Riehl A, Németh J, Angel P, Hess J. The receptor RAGE: Bridging inflammation and cancer. *Cell Commun Signal*. 2009;7(12):1-7. doi:10.1186/1478-811X-7-12

210. Yan SF, Yan S Du, Ramasamy R, Schmidt AM. Tempering the wrath of RAGE: An emerging therapeutic strategy against diabetic complications, neurodegeneration, and inflammation. *Ann Med*. 2009;41(6):408-422. doi:10.1080/07853890902806576

211. Nankali M, Karimi J, Goodarzi MT, et al. Increased Expression of the Receptor for Advanced Glycation End-Products (RAGE) Is Associated with Advanced Breast Cancer Stage. *Oncol Res Treat*. 2016;39(10):622-628. doi:10.1159/000449326

212. Dahlmann M, Okhrimenko A, Marcinkowski P, et al. RAGE mediates S100A4-induced cell motility via MAPK/ERK and hypoxia signaling and is a prognostic biomarker for human colorectal cancer metastasis. *Oncotarget*. 2014;5(10). doi:10.18632/oncotarget.1908

213. Medapati MR, Dahlmann M, Ghavami S, et al. RAGE mediates the pro-migratory response of extracellular S100A4 in human thyroid cancer cells. *Thyroid*. 2015;25(5):514-527. doi:10.1089/thy.2014.0257

214. Nasser MW, Wani NA, Ahirwar DK, et al. RAGE mediates S100A7-induced breast cancer growth and metastasis by modulating the tumor microenvironment. *Cancer Res*. 2015;75(6):974-985. doi:10.1158/0008-5472.CAN-14-2161

215. Zhang QY, Wu LQ, Zhang T, Han YF, Lin X. Autophagy-mediated HMGB1 release promotes gastric cancer cell survival via RAGE activation of extracellular signal-regulated kinases 1/2. *Oncol Rep*. 2015;33(4):1630-1638. doi:10.3892/or.2015.3782

216. Leclerc E, Vetter SW. The role of S100 proteins and their receptor RAGE in pancreatic cancer. *Biochim Biophys Acta - Mol Basis Dis*. 2015;1852(12):2706-2711. doi:10.1016/j.bbadis.2015.09.022

217. Arumugam T, Ramachandran V, Gomez SB, Schmidt AM, Logsdon CD. S100P-derived RAGE antagonistic peptide reduces tumor growth and metastasis. *Clin Cancer Res*. 2012;18(16):4356-4364. doi:10.1158/1078-0432.CCR-12-0221

218. Schnoor M, Stradal TE, Rottner K. Cortactin : Cell Functions of A Multifaceted Actin-Binding Protein. *Trends Cell Biol*. 2017;28(2):79-98. doi:10.1016/j.tcb.2017.10.009

219. Hong Wu and J. Thomas Parsons. Cortactin, an 80/85-Kilodalton pp60 src Substrate, Is a Filamentous Actin-binding Protein Enriched in the Cell Cortex. *J Cell Biol*. 1993;120(6):1417-1426.

220. Yin M, Ma W, An L. Cortactin in cancer cell migration and invasion. *Oncotarget*. 2017;8(50):88232-88243..

221. Radisky DC, Stallings-Mann M, Hirai Y, Bissell MJ. Single proteins might have dual but related functions in intracellular and extracellular microenvironments. *Nat Rev Mol Cell Biol*. 2009;10(3):228-234. doi:10.1038/nrm2633

222. Gregori J, Villarreal L, Méndez O, Sánchez A, Baselga J, Villanueva J. Batch effects correction improves the sensitivity of significance tests in spectral counting-based comparative discovery proteomics. *J Proteomics*. 2012;75(13):3938-3951. doi:10.1016/j.jprot.2012.05.005

223. Sheppard D. Dominant negative mutants: tools for the study of protein function in vitro and in vivo. *Am J Respir Cell Mol Biol*. 1994;11(1):1-6. doi:10.1165/ajrcmb.11.1.8018332

224. Yokota E, Iwai M, Yukawa T, et al. Clinical application of a lung cancer organoid (tumoroid) culture system. *npj Precis Oncol*. 2021;5:1-29. doi:10.1038/s41698-021-00166-3

225. Moreno-Bueno G, Peinado H, Molina P, et al. The morphological and molecular features of the epithelial-to-mesenchymal transition. *Nat Protoc*. 2009;4(11):1591-1613. doi:10.1038/nprot.2009.152

226. Fu NY, Nolan E, Lindeman GJ, Visvader JE. Stem cells and the differentiation hierarchy in mammary gland development. *Physiol Rev*. 2020;100(2):489-523. doi:10.1152/physrev.00040.2018

227. Vamvakidou AP, Mondrinos MJ, Petushi SP, Garcia FU, Lelkes PI, Tozeren A. Heterogeneous breast tumoroids: An in vitro assay for investigating cellular heterogeneity and drug delivery. *J Biomol Screen*. 2007;12(1):13-20. doi:10.1177/1087057106296482

228. Schutgens F, Clevers H. Human Organoids: Tools for Understanding Biology and Treating Diseases. *Annu Rev Pathol Mech Dis*. 2020;15:211-234.

doi:10.1146/annurev-pathmechdis-.

229. Cheng M, Liu H, Zhang D, et al. HMGB1 enhances the AGE-induced expression of CTGF and TGF-β via RAGE-dependent signaling in renal tubular epithelial cells. *Am J Nephrol*. 2015;41(3):257-266. doi:10.1159/000381464

230. Nam MH, Pantcheva MB, Rankenberg J, Nagaraj RH. Transforming growth factor-β2-mediated mesenchymal transition in lens epithelial cells is repressed in the absence of RAGE. *Biochem J*. 2021;478(12):2285-2296. doi:10.1042/BCJ20210069

231. Chen YC, Statt S, Wu R, et al. High mobility group box 1-induced epithelial mesenchymal transition in human airway epithelial cells. *Sci Rep*. 2016;6:18815. doi:10.1038/srep18815

232. Zhang J, Shao S, Han D, et al. High mobility group box 1 promotes the epithelial-to-mesenchymal transition in prostate cancer PC3 cells via the RAGE/NF-KB signaling pathway. *Int J Oncol*. 2018;53(2):659-671. doi:10.3892/ijo.2018.4420

233. Valenta T, Hausmann G, Basler K. The many faces and functions of beta-catenin. *EMBO J*. 2012;31(12):2714-2736. doi:10.1038/emboj.2012.150

234. Zucchini-Pascal N, Peyre L, Rahmani R. Crosstalk between beta-catenin and snail in the induction of epithelial to mesenchymal transition in hepatocarcinoma: Role of the ERK1/2 pathway. *Int J Mol Sci*. 2013;14(10):20768-20792. doi:10.3390/ijms141020768

235. Zhang YE. Non-Smad signaling pathways of the TGF-β family. *Cold Spring Harb Perspect Biol*. 2017;9(2):1-18. doi:10.1101/cshperspect.a022129

236. Gatenby RA, Smallbone K, Maini PK, et al. Cellular adaptations to hypoxia and acidosis during somatic evolution of breast cancer. *Br J Cancer*. 2007;97(5):646-653. doi:10.1038/sj.bjc.6603922

237. Glunde K, Guggino SE, Solaiyappan M, Pathak AP, Ichikawa Y, Bhujwalla ZM. Extracellular Acidification Alters Lysosomal Trafficking in Human Breast Cancer Cells. *Neoplasia*. 2003;5(6):533-545. doi:10.1016/s1476-5586(03)80037-4

238. Wojtkowiak JW, Rothberg JM, Kumar V, et al. Chronic autophagy is a cellular adaptation to tumor acidic pH microenvironments. *Cancer Res*. 2012;72(16):3938-3947. doi:10.1158/0008-5472.CAN-11-3881

239. Damaghi M, Tafreshi NK, Lloyd MC, et al. Chronic acidosis in the tumour microenvironment selects for overexpression of LAMP2 in the plasma membrane. *Nat Commun*. 2015;6. doi:10.1038/ncomms9752

240. Corbet C, Feron O. Tumour acidosis: From the passenger to the driver's seat.

Nat Rev Cancer. 2017;17(10):577-593. doi:10.1038/nrc.2017.77

241. Yu M, Wang H, Ding A, et al. HMGB1 signals through toll-like receptor (TLR) 4 and TLR2. *Shock*. 2006;26(2):174-179. doi:10.1097/01.shk.0000225404.51320.82

242. Yang D, Tewary P, Rosa G de la, Wei F, Oppenheim JJ. The alarmin functions of high-mobility group proteins. *Physiol Behav*. 2010;1799(1-2):157-163. doi:10.1016/j.bbagrm.2009.11.002.The

243. Schiraldi M, Raucci A, Muñoz LM, et al. HMGB1 promotes recruitment of inflammatory cells to damaged tissues by forming a complex with CXCL12 and signaling via CXCR4. *J Exp Med*. 2012;209(3):551-563. doi:10.1084/JEM.20111739

244. Yang D, Bustin M. Harnessing the alarmin HMGN1 for anticancer therapy. 2015;7:1129-1131. doi:10.2217/imt.15.76

245. Riemann A, Schneider B, Ihling A, et al. Acidic environment leads to ROS-Induced MAPK signaling in cancer cells. *PLoS One*. 2011;6(7):e22445. doi:10.1371/journal.pone.0022445

246. Sauvant C, Nowak M, Wirth C, et al. Acidosis induces multi-drug resistance in rat prostate cancer cells (AT1) in vitro and in vivo by increasing the activity of the p-glycoprotein via activation of p38. *Int J Cancer*. 2008;123(11):2532-2542. doi:10.1002/ijc.23818

247. Zong H, Madden A, Ward M, Mooney M, Elliott C, Stitt A. Homodimerization is essential for the receptor for advanced glycation end products (RAGE)-mediated signal transduction. *J Biol Chem*. 2010;285(30):23137-23146. doi:10.1074/JBC.M110.133827

248. Lin HJ, Jiang ZP, Lo HR, et al. Coalescence of RAGE in lipid rafts in response to cytolethal distending toxin-induced inflammation. *Front Immunol*. 2019;10:109. doi:10.3389/fimmu.2019.00109

249. Hanzal-Bayer MF, Hancock JF. Lipid rafts and membrane traffic. *FEBS Lett*. 2007;581(11):2098-2104. doi:10.1016/j.febslet.2007.03.019

250. Simons K, Toomre D. Lipid rafts and signal transduction. *Nat Rev Mol Cell Biol*. 2000;1:31-41. doi:10.1002/jssc.201600295

251. Yamaguchi H, Takeo Y, Yoshida S, Kouchi Z, Nakamura Y, Fukami K. Lipid rafts and caveolin-1 are required for invadopodia formation and extracellular matrix degradation by human breast cancer cells. *Cancer Res*. 2009;69(22):8594-8602. doi:10.1158/0008-5472.CAN-09-2305

252. Tian T, Li X, Hua Z, et al. S100A7 promotes the migration, invasion and metastasis of human cervical cancer cells through epithelial-mesenchymal

transition. *Oncotarget*. 2017;8(15):24964-24977. doi:10.18632/oncotarget.15329

253. Mader CC, Oser M, Magalhaes MAO, et al. An EGFR-Src-Arg-cortactin pathway mediates functional maturation of invadopodia and breast cancer cell invasion. *Cancer Res*. 2011;71(5):1730-1741. doi:10.1158/0008-5472.CAN-10-1432

254. Stock K, Borrink R, Mikesch JH, et al. Overexpression and Tyr421-phosphorylation of cortactin is induced by three-dimensional spheroid culturing and contributes to migration and invasion of pancreatic ductal adenocarcinoma (PDAC) cells. *Cancer Cell Int*. 2019;19:77. doi:10.1186/s12935-019-0798-x

255. Raghavan CT, Nagaraj RH. AGE-RAGE interaction in the TGFβ2-mediated epithelial to mesenchymal transition of human lens epithelial cells. *Glycoconj J*. 2016;33(4):631-643. doi:10.1007/s10719-016-9686-y

256. He M, Kubo H, Ishizawa K, et al. The role of the receptor for advanced glycation end-products in lung fibrosis. *Am J Physiol - Lung Cell Mol Physiol*. 2007;293(6):1427-1436. doi:10.1152/ajplung.00075.2007

257. Kostura MJ, Kindy MS, Burstein A, et al. Efficacy of RAGE antagonists in murine models of Alzheimer's disease. *Alzheimer's Dement*. 2014;10(4):P638-P639. doi:10.1016/j.jalz.2014.05.1119

258. Zha C, Meng X, Li L, et al. Neutrophil extracellular traps mediate the crosstalk between glioma progression and the tumor microenvironment via the HMGB1/RAGE/IL-8 axis. *Cancer Biol Med*. 2020;17(1):154-168. doi:10.20892/j.issn.2095-3941.2019.0353

259. Yu W, Yang L, Li T, Zhang Y. Cadherin Signaling in Cancer: Its Functions and Role as a Therapeutic Target. *Front Oncol*. 2019;9(October). doi:10.3389/fonc.2019.00989

260. Jacobs K, Feys L, Vanhoecke B, Van Marck V, Bracke M. P-cadherin expression reduces melanoma growth, invasion, and responsiveness to growth factors in nude mice. *Eur J Cancer Prev*. 2011;20(3):207-216. doi:10.1097/CEJ.0b013e3283429e8b

261. Bauer R, Valletta D, Bauer K, et al. Downregulation of P-cadherin expression in hepatocellular carcinoma induces tumorigenicity. *Int J Clin Exp Pathol*. 2014;7(9):6125-6132. doi:10.1055/s-0032-1332048

262. Li JH, Huang XR, Zhu HJ, et al. Advanced glycation end products activate Smad signaling via TGF-beta-dependent and independent mechanisms: implications for diabetic renal and vascular disease. *FASEB J*. 2004;18(1):176-178. doi:10.1096/fj.02-1117fje

263. Chung ACK, Zhang H, Kong YZ, et al. Advanced glycation end-products induce tubular CTGF via TGF-β-independent Smad3 signaling. *J Am Soc Nephrol*. 2010;21(2):249-260. doi:10.1681/ASN.2009010018

264. Chen S, Jim B, Ziyadeh FN. Diabetic Nephropathy and Transforming Growth Factor-β: Transforming Our View of Glomerulosclerosis and Fibrosis Build-Up. *Semin Nephrol*. 2003;23(6):532-543. doi:10.1053/S0270-9295(03)00132-3

265. Hu HH, Chen DQ, Wang YN, et al. New insights into TGF-β/Smad signaling in tissue fibrosis. *Chem Biol Interact*. 2018;292:76-83. doi:10.1016/j.cbi.2018.07.008

266. Wang L, Wang HL, Liu TT, Lan HY. TGF-beta as a master regulator of diabetic nephropathy. *Int J Mol Sci*. 2021;22(15):1-18. doi:10.3390/ijms22157881

267. Xie L, Law BK, Chytil AM, Brown KA, Aakre ME, Moses HL. Activation of the Erk Pathway Is Required for TGF-b1 – Induced EMT In Vitro. *Neoplasia*. 2004;6(5):603-610. doi:10.1593/neo.04241

268. Li Y, Wang P, Zhao J, Li H, Liu D, Zhu W. HMGB1 attenuates TGF-β-induced epithelial–mesenchymal transition of FaDu hypopharyngeal carcinoma cells through regulation of RAGE expression. *Mol Cell Biochem*. 2017;431(1-2):1-10. doi:10.1007/s11010-017-2968-2

269. Batlle E, Sancho E, Francí C, et al. The transcription factor snail is a repressor of E-cadherin gene expression in epithelial tumour cells. *Nat Cell Biol*. 2000;2(2):84-89. doi:10.1038/35000034

270. Cano A, Pérez-Moreno MA, Rodrigo I, et al. The transcription factor Snail controls epithelial-mesenchymal transitions by repressing E-cadherin expression. *Nat Cell Biol*. 2000;2(2):76-83. doi:10.1038/35000025

271. Ocaña OH, Córcoles R, Fabra Á, et al. Metastatic Colonization Requires the Repression of the Epithelial-Mesenchymal Transition Inducer Prrx1. *Cancer Cell*. 2012;22:709-724. doi:10.1016/j.ccr.2012.10.012

272. Tsai JH, Donaher JL, Murphy DA, Chau S, Yang J. Spatiotemporal regulation of EMT is Essential for Squamous Cell Carcinoma Metastasis. *Changes*. 2012;29(6):997-1003. doi:10.1016/j.ccr.2012.09.022.Spatiotemporal

273. Nieto MA. Epithelial Plasticity: A Common Theme in Embryonic and Cancer Cells. *Science (80-)*. 2013;342. doi:10.1126/science.1234850

274. Marín-Aguilera M, Codony-Servat J, Reig Ò, et al. Epithelial-to-mesenchymal transition mediates docetaxel resistance and high risk of relapse in prostate cancer. *Mol Cancer Ther*. 2014;13(5):1270-1284. doi:10.1158/1535-7163.MCT-13-0775

275. Dongre A, Rashidian M, Reinhardt F, et al. Epithelial-to-mesenchymal

Transition contributes to Immunosuppression in Breast Carcinomas. *Cancer Res*. 2017;77(5):3982-3989. doi:10.1158/0008-5472.CAN-16-3292.Epithelial-to-mesenchymal

276. Papadaki MA, Stoupis G, Theodoropoulos PA, Mavroudis D, Georgoulias V, Agelaki S. Circulating tumor cells with stemness and epithelial-to-mesenchymal transition features are chemoresistant and predictive of poor outcome in metastatic breast cancer. *Mol Cancer Ther*. 2019;18(2):437-447. doi:10.1158/1535-7163.MCT-18-0584

277. Dudas J, Ladanyi A, Ingruber J, Steinbichler TB, Riechelmann H. Epithelial to Mesenchymal Transition: A Mechanism that Fuels Cancer Radio/Chemoresistance. *Cells*. 2020;9(428):1-25. doi:10.3390/cells9020428

278. Hill C, Wang Y. The importance of epithelial-mesenchymal transition and autophagy in cancer drug resistance. *Cancer Drug Resist*. 2020;3(1):38-47. doi:10.20517/cdr.2019.75

279. Sakaguchi T, Yan SF, Yan S Du, et al. Central role of RAGE-dependent neointimal expansion in arterial restenosis. *J Clin Invest*. 2003;111(7):959-972. doi:10.1172/JCI200317115

280. Wendt T, Tanji N, Guo J, et al. Glucose, glycation, and RAGE: Implications for amplification of cellular dysfunction in diabetic nephropathy. *J Am Soc Nephrol*. 2003;14(5):1383-1395. doi:10.1097/01.ASN.0000065100.17349.CA

281. Sakatani S, Yamada K, Homma C, et al. Deletion of RAGE causes hyperactivity and increased sensitivity to auditory stimuli in mice. *PLoS One*. 2009;4(12):e8309. doi:10.1371/journal.pone.0008309

282. Gebhardt C, Riehl A, Durchdewald M, et al. RAGE signaling sustains inflammation and promotes tumor development. *J Exp Med*. 2008;205(2):275-285. doi:10.1084/jem.20070679

283. Kang R, Tang D, Lotze MT, Zeh HJ. AGER/RAGE-mediated autophagy promotes pancreatic tumorigenesis and bioenergetics through the IL6-pSTAT3 pathway. *Autophagy*. 2012;8(6):989-991. doi:10.4161/auto.20258

284. Galasko D, Bell J, Mancuso JY, et al. Clinical trial of an inhibitor of RAGE-Ab interactions in Alzheimer disease. *Neurology*. 2014;82(17):1536-1542. doi:10.1212/WNL.0000000000000364

285. ClinicalTrials.gov. *Evaluation of the Efficacy and Safety of Azeliragon (TTP488) in Patients With Mild Alzheimer's Disease (STEADFAST).* Identifier (NCT number): NCT02080364(2014).